Two–Way Relaying Communications with OFDM and BICM/BICM-ID

A Thesis Submitted
to the College of Graduate Studies and Research
in Partial Fulfilment of the Requirements
for the Degree of Doctor of Philosophy
in the Department of Electrical and Computer Engineering
University of Saskatchewan
Saskatoon

by

Hongzhong Yan

Permission To Use

In presenting this thesis in partial fulfilment of the requirements for a Postgraduate degree from the University of Saskatchewan, it is agreed that the Libraries of this University may make it freely available for inspection. Permission for copying of this thesis in any manner, in whole or in part, for scholarly purposes may be granted by the professors who supervised this thesis work or, in their absence, by the Head of the Department of Electrical and Computer Engineering or the Dean of the College of Graduate Studies and Research at the University of Saskatchewan. Any copying, publication, or use of this thesis, or parts thereof, for financial gain without the written permission of the author is strictly prohibited. Proper recognition shall be given to the author and to the University of Saskatchewan in any scholarly use which may be made of any material in this thesis. Request for permission to copy or to make any other use of material in this thesis in whole or in part should be addressed to:

Head of the Department of Electrical and Computer Engineering
57 Campus Drive
University of Saskatchewan
Saskatoon SK S7N 5A9
Canada

Acknowledgements

This dissertation would not be possible without the help and support of many people during my studies in Saskatoon. These few lines are not enough to express my gratitude to all of them.

First and foremost, I would like to express my deepest gratitude toward my supervisor, Professor Ha H. Nguyen, for his criticism, patience, invaluable support and guidance through my research program at the University of Saskatchewan. It has truly been my honour and rewarding experience to work under his supervision. I have learnt several important lessons on the skills and values of conducting research.

I would also like to extend my gratitude to Professors Aryan S. Saadat-Mehr, Francis Bui and Moh Boulfiza from the University of Saskatchewan, and Professor Predeepa Yahampath from the University of Manitoba, for serving in my doctoral committee. Their insightful advice and comments have improved the quality of this thesis.

My special thanks go to Prof. Eric Salt who taught me three wonderful courses. I learned a lot from his precise attitude towards teaching and research. He also provides me many useful suggestions on my courses and future career.

I gratefully acknowledge the Natural Sciences and Engineering Research Council (NSERC) and the Department of Electrical and Computer Engineering at the University of Saskatchewan for their financial supports of my Ph.D. studies.

My deepest love and gratitude belong to my beloved wife Jian Su for her tremendous understanding, support and encouragement during this long term study. To her and our dearest daughter Christina, I dedicate this thesis.

Finally, I wish to express my appreciation to all of those who gave me help when I studied at the University of Saskatchewan.

Abstract

Relay-aided communication methods have gained strong interests in academic community and been applied in various wireless communication scenarios. Among different techniques in relay-aided communication system, two-way relaying communication (TWRC) achieves the highest spectral efficiency due to its bi-directional transmission capability. Nevertheless, different from the conventional point-to-point communication system, TWRC suffers from detection quality degradation caused by the multiple-access interference (MAI). In addition, because of the propagation characteristics of wireless channels, fading and multipath dispersion also contribute strongly to detection errors. Therefore, this thesis is mainly concerned with designing transmission and detection schemes to provide good detection quality of TWRC while taking into account the negative impacts of fading, multipath dispersion and multiple-access interference.

First, a TWRC system operating over multipath fading channels is considered and orthogonal frequency-division multiplexing (OFDM) is adopted to handle the inter-symbol interference (ISI) caused by the multipath dispersion. In particular, adaptive physical-layer network coding (PNC) is employed to address the MAI issue. By analyzing the detection error probability, various adaptive PNC schemes are discussed for using with OFDM and the scheme achieving the best trade-off among performance, overhead and complexity is suggested.

In the second part of the thesis, the design of distributed precoding in TWRC using OFDM under multipath fading channels is studied. The objective is to design a distributed precoding scheme which can alleviate MAI and achieve multipath diversity to combat fading. Specifically, three types of errors are introduced when analyzing the error probability in the multiple access (MA) phase. Through analysis and simulation, the scheme that performs precoding in both time and frequency domains is demonstrated to achieve the maximum diversity gains under all types of errors.

Finally, the last part of the thesis examines a communication system incorporating forward error correction (FEC) codes. Specifically, bit-interleaved code modulation (BICM) without and with iterative decoding (BICM-ID) are investigated in a TWRC system. Distributed linear constellation precoding (DLCP) is applied to handle MAI and the design of DLCP in a TWRC system using BICM/BICM-ID is discussed. Taking into account the multiple access channel from the terminal nodes to the relay node, decoding based on the quaternary code representation is introduced. Several error probability bounds are derived to aid in the design of DLCP. Based on these bounds, optimal parameters of DLCP are obtained through analysis and computer search. It is also found that, by combining XOR-based network coding with successful iterative decoding, the MAI is eliminated and thus DLCP is not required in a BICM-ID system.

Table of Contents

List of Abbreviations

AF	Amplify-and-Forward
ASK	Amplitude-Shift Keying
AWGN	Additive White Gaussian Noise
BC	Broadcast
BEP	Bit Error Probability
BER	Bit Error Rate
BICM	Bit-Interleaved Coded Modulation
BICM-ID	BICM with Iterative Decoding
CDMA	Code Division Multiple Access
CNC	Closest Neighbour Clustering
CP	Cyclic Prefix
DF	Decode-and-Forward
DFT	Discrete Fourier Transform
DLCP	Distributed Linear Constellation Precoding
DNF	Denoise-and-forward
DSTC	Distributed Space-time Coding
EF	Error Free
F-GLCP	Frequency-Grouped Linear Constellation Precoding
FEC	Forward Error Correction

FER	Frame Error Rate
FFT	Fast Fourier Transform
FT-GLCP	Frequency-Time Grouped Linear Constellation Precoding
IDFT	Inverse Discrete Fourier Transform
ISI	Inter-symbol Interference
LCP	Linear Constellation Precoding
LDPC	Low Density Parity Check
LOS	Line-of-Sight
MA	Multiple Access
MAC	Multiple Access Channel
MAI	Multiple Access Interference
MAP	Maximum a Posterior
MIMO	Multiple-Input Multiple-Output
ML	Maximum Likelihood
MMSE	Minimum Mean Square Error
MRC	Maximum Ratio Combing
NNC	Nearest Neighbour Clustering
OFDM	Orthogonal Frequency Division Multiplexing
OWRC	One-Way Relaying Communications
PDF	Partial Decode-and-forward
PEP	Pairwise Error Probability

PNC	Physical-layer Network Coding
PSK	Phase-Shift Keying
QAM	Quadrature Amplitude Modulation
QEP	Quaternary-Digit Error Probability
QER	Quaternary-Digit Error Rate
QPSK	Quadrature Phase Shift Keying
SER	Symbol Error Rate
SISO	Soft-Input Soft-Output
SNR	Signal-to-Noise Ratio
SSD	Signal Space Diversity
STC	Space Time Coding
TWRC	Two-Way Relaying Communications
XOR	Exclusive OR

List of Figures

List of Tables

1. Introduction

1.1 Introduction

Given the rapid growth in the use of wireless devices (e.g. smart phones, tablets) and increased variety of data services (e.g. social networks, cloud computing) in recent years, wireless communication systems require higher transmission rate and better quality of service. Specifically, higher data rate can be achieved by using larger bandwidth and increasing spectrum efficiency (data rate transmitted per unit bandwidth). To guarantee the quality of service, the design of a wireless communication system needs to consider the influence of two important factors of the wireless channels: fading and multipath dispersion.

Fading, the effect of the variation that signal level experiences due to the unique propagation characteristics of wireless channels, is the main challenge in wireless communications. In general, fading includes two types: large scale fading and small scale fading. Large scale fading is caused by the long distance the signal travels and blocking by large objects in the propagation path. The fading caused by the former is called pass loss, while that caused by the later is called shadowing. Path loss determines the region of coverage and shadowing causes coverage holes (regions of space at which the signal strength is very low). Because of the existence of large scale fading, the quality of service at the edge of coverage areas or in coverage holes cannot be guaranteed. To overcome the influence of large scale fading, the conventional approach is to increase the transmitted power. However, for power-limited devices, such as mobile phones, it is not economical or even realistic to increase the transmit power beyond a certain limit. To overcome such technical problems, relaying techniques have been studied extensively in recent years [1, 2].

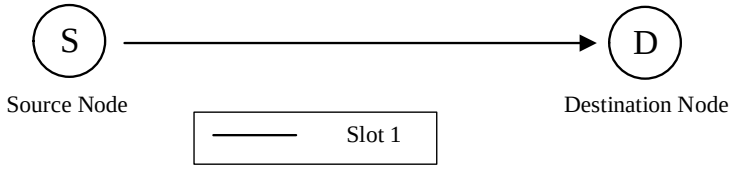

(a) Direct communications

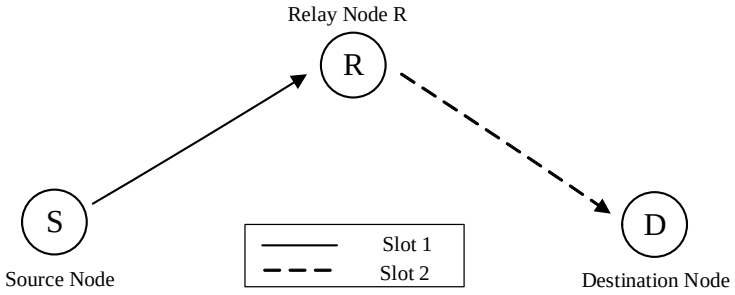

(b) Relay-aided communications

Figure 1.1 One-way communications: Direct and relay-aided transmissions.

A *relay*, as shown in Figure 1.1, is a node in a wireless network which is used to help the transmission of information from one node to another when those two nodes cannot directly communicate in a reliable manner. It has been shown that using relay is effective to alleviate the influence of large scale fading and thus increases the coverage and enhances the transmission reliability. In fact, relaying technology has been included in many advanced wireless communication systems [3, 4]. Since relays operate in half-duplex mode (i.e., they cannot transmit and receive at the same time), relay-aided communication requires one more time slot when compared to direct communication, as shown in Figure 1.1. Due to the scarcity of spectrum resource, more efficient relaying schemes need to be investigated to enhance the spectrum efficiency.

It is difficult to solve the problem that relay-aided communication needs one more time slot, especially when the communication is one-way, as shown in Figure 1.1. However, if the communication is conducted in two-way, as shown in Figure 1.2, in which two nodes exchange their information simultaneously, new protocols can be implemented so that the number of time slots required to complete the transmission is the same as communicating directly. In this scenario, the information exchange process aided by a relay is called two-way relay communications (TWRC).

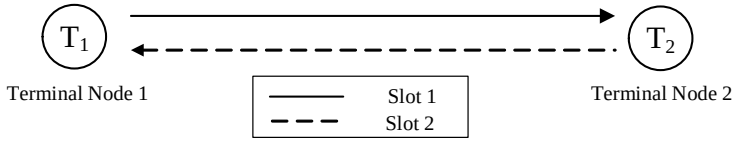

(a) Direct communications

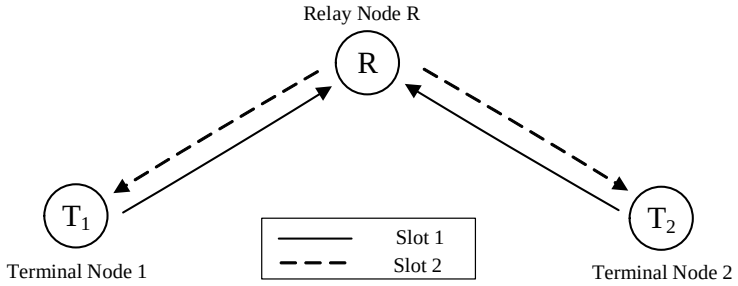

(b) Relay-aided communications

Figure 1.2 Two-way communications: Direct and relay-aided transmissions.

Small scale fading is caused by scattering, reflection and diffraction of the transmitted signal by surrounding objects in the propagation environment. The receiver obtains constructively or destructively superimposed copies of the transmitted signal. This causes the fluctuation of the power of the received signal. The fluctuation, especially when the power of the received signal is extremely low (which is also called *deep fade*), has the negative influence on the system reliability. To take into account signal fluctuation in system design, the wireless channel under small scale fading is usually modelled as a complex random variable whose distribution depends on the characteristics of the propagation environment. Typically, the channel coefficient h is modelled as a complex Gaussian random variable with mean μ and variance σ^2. If there is no line-of-sight (LOS) path between the transmitter and receiver, μ is set to zero and the magnitude of the channel gain $\eta = |h|$ follows a Rayleigh distribution as given in Equation (1.1). It is common to refer to h as a Rayleigh fading channel.

$$f_\eta(\eta) = \frac{\eta}{\sigma^2}\exp\left(-\frac{\eta^2}{2\sigma^2}\right), \quad \eta \geq 0. \tag{1.1}$$

If there is a LOS path between the transmitter and receiver, then η follows a Rician distribution as shown in Equation (1.2) and h is called a Rician fading channel.

$$f_\eta(\eta) = \frac{\eta}{\sigma^2} I_0\left(\frac{|\mu|\eta}{\sigma^2}\right)\exp\left(-\frac{\eta^2 + |\mu|^2}{2\sigma^2}\right), \quad \eta \geq 0. \tag{1.2}$$

In Equation (1.2), $I_0(\cdot)$ is the modified Bessel function of the first kind, given as

$$I_0(x) = \frac{1}{2\pi} \int_0^{2\pi} \exp(x \cos \varphi)\, d\varphi. \tag{1.3}$$

To alleviate the influence of small scale fading, a technique called *diversity* is widely used in modern wireless communication systems. Generally speaking, diversity is implemented by sending copies of a signal over independent resource dimensions to lower the probability of occurrence of a deep fade. The performance gain obtained by using diversity technique is usually called *diversity gain*. Depending on the system resource that can be used to supply the multiple signal copies, diversity can be categorized into the following types.

- *Time diversity*: Time diversity is implemented by sending the same signal over multiple time periods whose channel responses are independent. Specifically, time diversity can be implemented by simply repeating the same signal on different time periods, a method called *repetition code*. More efficient schemes include using rotation matrix which can guarantee that different errors are related to multiple independent channels.

- *Space diversity*: Space diversity is implemented by deploying multiple antennas at the receiver or transmitter. If the multiple antennas are installed at the receiver, the diversity gain is usually achieved by using a combining scheme such as the maximum ratio combing (MRC) and it is called *receive diversity*. If the transmitter is equipped with multiple antennas, space time coding (STC) is usually used to achieve the diversity gain and it is called *transmit diversity*.

- *Multipath diversity*: Multipath diversity gain can only be exploited in the system that has the bandwidth large enough so that different propagation paths can be distinguished. Typical schemes that exploit multipath diversity includes the Rake receiver used in code division multiple access (CDMA) systems, and performing rotation matrix in orthogonal frequency division multiplexing (OFDM) systems.

Multipath dispersion is another characteristic of the wireless channel which causes the signal to reach the receiver in more than one path. In a narrowband communication system, since most of the paths arrive within one symbol time, the equivalent channel is represented

by one tap (this is typically called *flat fading*). However, in a broadband system, the transmitted signal arrives over multiple symbol times and the equivalent channel is represented as a filter with several taps and inter-symbol interference (ISI) exists (this is called *frequency-selective fading*).

Equalization is a traditional method to deal with the ISI problem. In this method, the receiver uses a filter with several taps to eliminate the influence of ISI. However, as larger bandwidth is used in modern wireless communications, the number of taps for the equivalent channel is large and the complexity of equalization can be very high. The techinique of OFDM is proposed to combat ISI with reasonable complexity in [5, 6]. By using inverse fast Fourier transform (IFFT) at the transmitter and fast Fourier transform (FFT) at the receiver, OFDM converts the high-rate data stream into a set of parallel low-rate streams and transmits them over distinct carriers (also commonly called *subcarriers*). As illustrated in Figure 1.3, signal in each subcarrier experiences an equivalent narrowband channel. Therefore, the receiver only needs to handle multiple parallel flat fading channels and the complexity is much lower than using a long equalization filter to remove ISI. Owing to its effectiveness and simplicity, OFDM is widely adopted in modern broadband wireless communication systems [7–9]. In addition, since multipath is also the source of diversity, different techniques of exploiting multipath diversity gain in OFDM systems have been studied and proved to be effective [10–12].

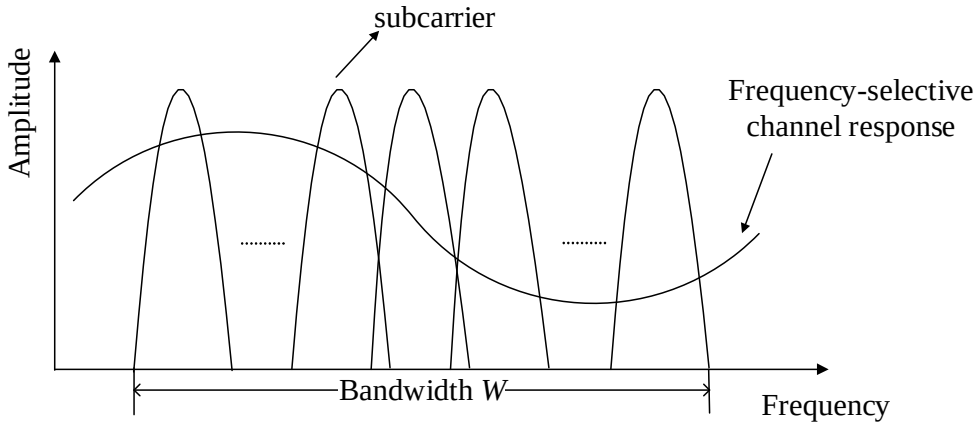

Figure 1.3 Multiple subcarriers in OFDM.

As listed above, techniques are developed to achieve the different types of diversity gains and all schemes are designed for system without considering forward error correction (FEC). Bit-interleaved coded modulation (BICM) is a technique first proposed in [13] which uses convolutional encoder/decoder and bit interleaver/de-interleaver to achieve potential diversity gains. Later, [14] gives an analytic framework of BICM and presents the design criterion which treats coding and modulation as separate components. By selecting the convolutional code with large free Hamming distance and designing interleaver with enough interleave depth, BICM is able to achieve any types of diversity gains. Specifically, references [13, 14] assume fast fading scenario where time diversity gains are achieved by using BICM. Then in [12, 15], BICM is combined with OFDM to obtain the multipath diversity gains. In multiple-input multiple-output (MIMO) systems, BICM is also able to exploit the space diversity gains [16, 17]. To further enhance the performance of BICM system, iterative processing is introduced in BICM systems and it is called BICM with iterative decoding (BICM-ID). Reference [18] first proposed the iterative processing between the demodulator and the decoder and shows that it can provide a significant performance gain over BICM systems.

1.2 Research Motivation and Objectives

Different from point-to-point communications, implementing two-way relaying communications in two time slots needs to consider the influence of multiple access interference (MAI). In other words, the relay node has to recover the signals of the two terminal nodes based on the superimposed signal. Recently, several schemes have been proposed to address the MAI problem. However, most of these schemes ignore the influence of small scale fading and multipath dispersion in wireless transmissions. Motivated from the above observations, this thesis is concerned with the design of TWRC which can effectively and efficiently handle the problems caused by MAI, fading and multipath dispersion. The main research objectives are elaborated below.

- To handle the poor detection performance caused by MAI, several references [19–22] propose to use adaptive transmission schemes at the relay node to broadcast the processed

signal to the terminal nodes. Specifically, the relay node uses different mapping rules or constellations under different channel conditions in order to minimize the detection error probability. Based on theoretical analysis and simulations, those adaptive schemes are demonstrated to solve the problem caused by MAI. However, all these references consider the wireless channels to be flat fading and the adaptive transmission schemes are designed according to this assumption. As discussed above, multipath dispersion is the unique characteristic of wireless channels, especially for a broadband communication system. Over multipath channels, the existing schemes may not be efficient or even valid. Therefore, the first objective of our research is to study the anti-MAI schemes designed for TWRC in multipath channels. Since OFDM has been widely used to combat multipath dispersion, the research focuses on how to combine OFDM with TWRC. To this end, a system model is developed for a TWRC-OFDM system. Then the detection error probability in different scenarios is analyzed. The analysis leads to a scheme which is able to achieve the trade-off among performance, overhead and processing complexity.

- Most of the existing studies on TWRC focus on designing the schemes which are able to effectively handle MAI. However, in most scenarios, fading is still the dominating factor which causes detection errors. Since the focus of our research is on TWRC systems, the influence of large scale fading can be ignored by assuming that the relay node is properly located. On the other hand, to handle small scale fading, the most effective technique is to achieve diversity gains as discussed in Section 1.1. Therefore, another objective of our research is to investigate how to achieve diversity gains in TWRC systems. Different from simply using existing diversity-achieving schemes in TWRC systems, a joint design to handle MAI and achieve diversity gains at the same time is proposed. Specifically, the multipath diversity gain is selected as the target diversity gain since it is easy to implement (spatial diversity requires deploying multiple antennas, while time diversity requires a large buffer to store samples collected for a long time, or high mobility speed of terminal nodes). Meanwhile, OFDM is still adopted to address the problem caused by multipath dispersion.

- FEC is an essential part in any modern wireless communication systems. However, most of the designs and analysis on TWRC systems do not explicitly consider FEC. Because

of the excellent ability of FEC to correct many types of errors (caused by noise, fading, interference, etc.), it is of interest to also consider TWRC system incorporating FEC. As mentioned in Section 1.1, BICM/BICM-ID is able to achieve diversity gains. Therefore, our research will focus on TWRC system employing BICM/BICM-ID and the design of precoding schemes to handle the problem caused by MAI. Specifically, due the existence of MAI, the decoding process of the FEC code needs to be devised. Furthermore, the error probability in a TWRC system employing BICM/BICM-ID is derived and used to aid the optimization of anti-MAI precoding schemes.

1.3 Organization of the Thesis

This thesis is organized in a manuscript-based style. The first part of the thesis provides some relevant background and knowledge of wireless communications. The main content and contributions of the thesis are included in the form of published or submitted manuscripts. The remainder of the thesis is organized as follows.

Chapter 2 first presents some background on relay-aided cooperative communications. Fundamental knowledge on one-way relaying communications (OWRC) and TWRC are introduced. The MAI problem faced in TWRC is analyzed and the existing solutions are discussed. Since our research makes use of OFDM and BICM/BICM-ID techniques, some basic concepts of OFDM and BICM/BICM-ID are also given in Chapter 2. In each of the following chapters, a brief introduction precedes each manuscript in order to connect the manuscript to the main context of the thesis.

The manuscript in Chapter 3 studies the adaptive physical-layer network coding (PNC) in a TWRC system with OFDM under multipath channels. Different error events under multiple access channels are analyzed and the corresponding error probabilities are derived. Several adaptive PNC schemes in OFDM are proposed and the candidate achieving the best trade-off among performance, overhead and complexity is selected. The manuscript in Chapter 4 is also concerned with TWRC-OFDM systems under multipath channels. Instead of PNC, distributed precoding is investigated to handle MAI and achieve the multipath

diversity gains. The proposed precoding, conducted in both time and frequency domains, is theoretically proved to achieve the maximum multipath diversity gains. Through computer search, the optimal parameter of precoding matrices is obtained to further enhance the performance of the proposed scheme. While Chapter 3 and 4 are concerned with TWRC systems without explicitly considering FEC, the manuscript in Chapter 5 considered a TWRC system using BICM with and without iterative decoding. The iterative demodulation and decoding process under the multiple access channel is developed by using the quaternary code representation. Error probability bounds are derived in order to help the design of distributed linear constellation precoding (DLCP) to combat MAI.

Finally, Chapter 6 summarizes the contributions of this thesis and suggests potential research problems for future studies.

Notation: The complex number $\sqrt{-1}$ is denoted by j. The conjugate of complex number a is denoted by a^*. The matrix containing elements from the ith to jth row , from the kth to the lth columns of $\boldsymbol{A}$ are denoted by $\boldsymbol{A}(i:j,k:l)$. The inverse, transpose, Hermitian, rank, and determinant of matrix $\boldsymbol{A}$ are denoted by $\boldsymbol{A}^{-1}$, $\boldsymbol{A}^T$, $\boldsymbol{A}^H$, $\mathrm{rank}(\boldsymbol{A})$ and $\det(\boldsymbol{A})$, respectively. $\mathbf{0}_M$ is the length-M zero vector, $\mathbf{0}_{M\times N}$ is the $M \times N$ zero matrix and $\mathbf{I}_N$ is the $N \times N$ identity matrix. $|a|$ denotes the magnitude value of a complex number a. $\mathrm{diag}(\boldsymbol{a})$ denotes a diagonal matrix whose diagonal elements are from vector $\boldsymbol{a}$ and $\|\boldsymbol{a}\|_2$ denotes the Euclidean norm of vector $\boldsymbol{a}$. $\mathcal{CN}(0, N_0)$ denotes complex Gaussian distribution wit zero mean and variance N_0.

2. Background

This chapter first discusses relay-aided communications which includes both OWRC and TWRC. Different transmission protocols are introduced. Specifically for TWRC, the MAI problem is explained and different schemes used to address the MAI issue are discussed. Next, in order to familiarize the reader with the subject matters of the manuscripts in Chapter 3 and Chapter 4, basic concepts of OFDM and schemes used to achieve diversity gains in point-point communications are described. Finally, some basic knowledge of BICM/BICM-ID is introduced to establish a foundation for the manuscript in Chapter 5.

2.1 Relay-Aided Communications

As mentioned before, relay-aided communications have gained strong interests in research and industry communities. Depending on factors such as the number of relays deployed in a network, the number of antennas equipped in each relay, and whether fixed or mobile relays are employed, the topology of a relay-aided system can be very complicated. For example, considering multiple relays, references [23–27] focus on the optimization of resource allocations. References [28,29] examine scenarios that mobile stations are used as relays and analyze the influence of the mobility speed. Assuming multiple antennas are equipped at relays, references [30–34] focus on space-time signal processing to achieve higher diversity gains or to mitigate the interference. It is pointed out that, all research works conducted on complicated scenarios are extensions of the simplest system having one fixed relay node and two terminal nodes. As such, this section restricts the discussion on a communication system having two terminal nodes and one relay node. Furthermore, it is assumed that the relay node is fixed, equipped with one antenna and operates in a half-duplex mode.

2.1.1 One-Way Relaying Communications (OWRC)

The transmission/reception process of OWRC requires two time slots as illustrated in Fig. 2.1. The terminal node sending out information is called the source node, while the terminal node receiving information is referred to as the destination node. In the first time slot, the channel from source node $\mathbb{S}$ to relay node $\mathbb{R}$ is represented by h_{sr}, which is a complex Gaussian random variable with mean $\mu_{h_{sr}}$ and variance $\sigma^2_{h_{sr}}$.

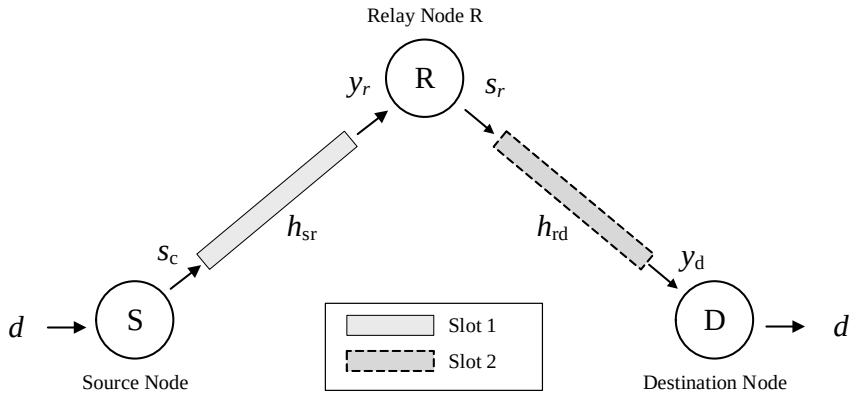

Figure 2.1 One-way relaying communcations without a direct link

The binary information bits d are mapped into symbols s_c. The information bits can be mapped into amplitude levels of a sinusoidal carrier such as with amplitude-shift keying (ASK), or into phases such as with phase-shift keying (PSK), or into both amplitude levels and phases such as with quadrature amplitude modulation (QAM). If each symbol carries m information bits, then there are $M = 2^m$ symbols in the symbol set and this set is called *constellation* $\mathcal{S}$. Figure 2.2 illustrates the constellation of 16-QAM and a mapping rule from 4 information bits into 16 symbols. In the figure, $d_{\min}$ is defined as the minimum Euclidean distance between any two symbols in the constellation. This is an important parameter of the constellation because it strongly influences the overall performance of the communication system.

At the relay node, the received signal is:

$$y_r = h_{sr} s_c + \omega_r, \tag{2.1}$$

where $\omega_r \sim \mathcal{CN}(0, \sigma_r^2)$ represents the additive white Gaussian noise (AWGN) at the relay.

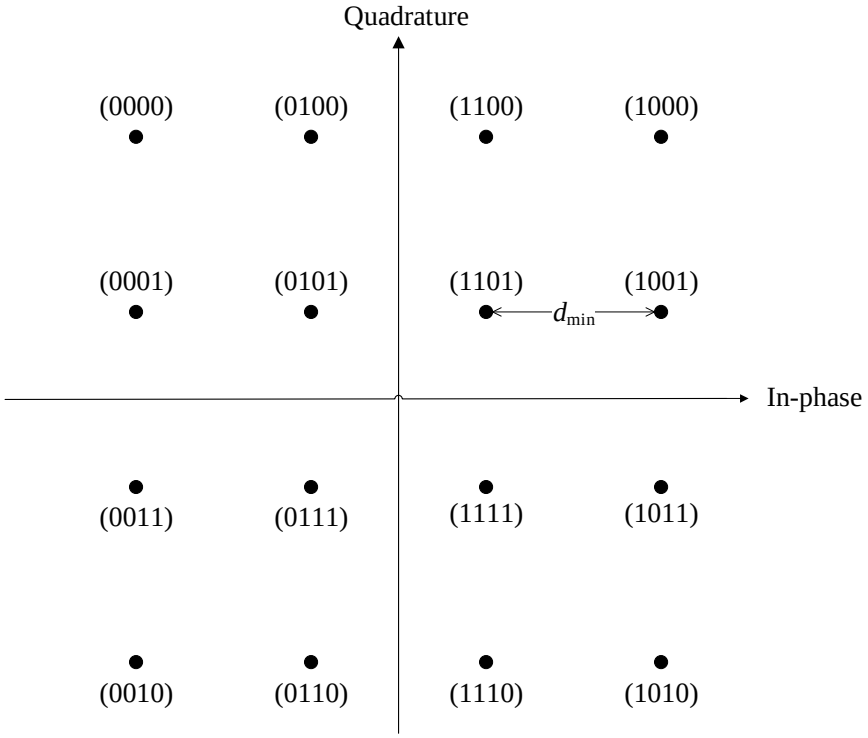

Figure 2.2 Constellation and mapping of 16-QAM.

In the second time slot, the relay generates new signal s_r from the received signal y_r and transmits it through channel h_{rd}, which is medelled as a complex Gaussian variable with mean $\mu_{h_{rd}}$ and variance $\sigma^2_{h_{rd}}$. The received signal at destination node $\mathbb{D}$ is:

$$y_d = h_{rd}s_r + \omega_d, \tag{2.2}$$

where $\omega_d \sim \mathcal{CN}(0, \sigma_d^2)$ is AWGN at destination node $\mathbb{D}$. Using the received signal y_d, the destination node tries to detect the transmitted information bits.

To implement the transmission described above, the most important design problem is how to generate s_r at the relay node. Depending on the type of signal processing used at the relay node, two types of forwarding strategies are usually considered. A simple strategy is amplify-and-forward (AF). In AF, the relay simply adjusts the power and re-transmits the received signal y_r. Assuming that all nodes have the same transmitted power, the AF signal is:

$$s_r = \sqrt{\frac{1}{|h_{sr}|^2 + \sigma_r^2}} y_r. \tag{2.3}$$

Using (2.1) and (2.3), the received signal at the destination node in (2.2) can be expressed as:

$$y_d = \frac{h_{sr}h_{rd}}{\sqrt{|h_{sr}|^2 + \sigma_r^2}}s_c + \left(\frac{h_{rd}}{\sqrt{|h_{sr}|^2 + \sigma_r^2}}\omega_r + \omega_d\right). \tag{2.4}$$

It can be observed from (2.4) that the noise component ω_r at the relay is also amplified. Therefore, although AF is easy to implement, it suffers from a performance degradation caused by noise amplification.

Another strategy is decode-and-forward (DF). Different from AF, the relay first detects the signal transmitted from the source node as $\hat{s}_c$ and use $\hat{s}_c$ as the forward signal s_r. The DF technique eliminates the influence of noise generated at the relay and is preferred in the case that noise is the dominant factor causing errors. However, there are two disadvantages of using DF. First, the signal processing needed for detection is much more complicated than simply amplifying the received signal. Therefore, the relay using DF strategy requires more computation resources than that using AF. Another problem is that, since erroneous detection is unavoidable, this leads to a error propagation phenomenon due to forwarding erroneous signals.

2.1.2 Two-Way Relaying Communications (TWRC)

Different from OWRC, a relay node, $\mathbb{R}$, is used in TWRC to help the information exchange between two terminal nodes $\mathbb{T}_1$ and $\mathbb{T}_2$. Depending on how many time slots are required to complete the communication process, three types of transmission protocols are considered as illustrated in Fig. 2.3.

Comparing Fig. 2.3(a) with Fig. 2.1, it can be seen that the four-slots protocol can be viewed as a concatenation of two OWRC transmissions. In time slot 1 and time slot 2, $\mathbb{T}_1$ acts as the source node and $\mathbb{T}_2$ acts as the destination node, while in time slot 3 and time slot 4, the roles of $\mathbb{T}_1$ and $\mathbb{T}_2$ are reversed. Under this protocol, all transmission techniques designed for OWRC can be applied directly. However, this protocol has the lowest spectral efficiency. In the three-slots protocol, instead of allocating different time slots for each terminal node, relay node $\mathbb{R}$ broadcasts the processed signal in only one time slot and that time slot is

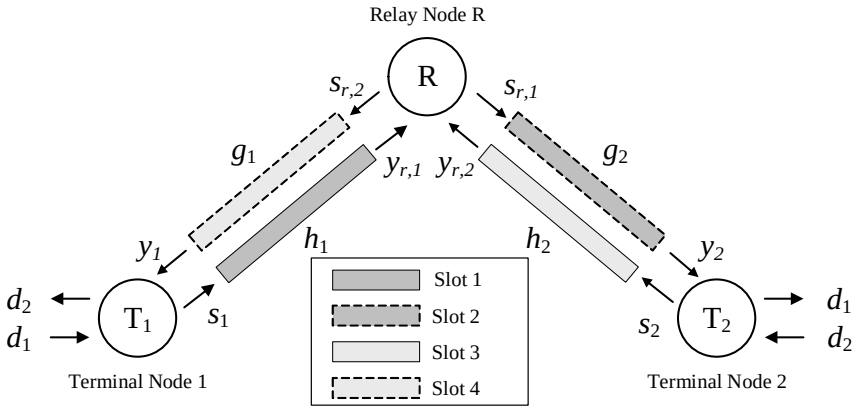

(a) Four-slots protocol

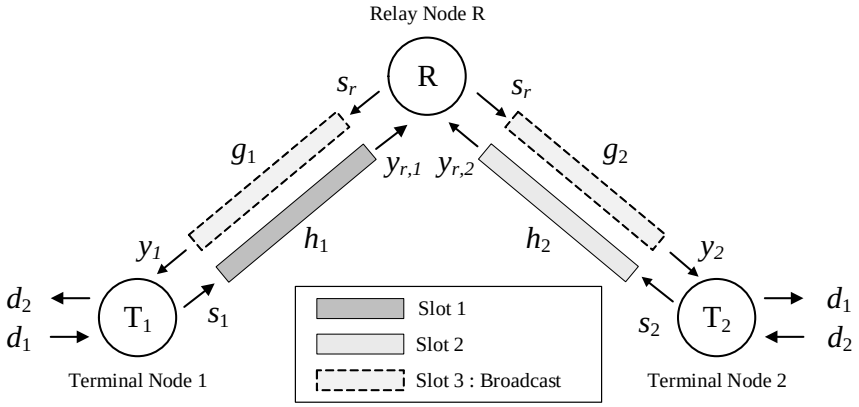

(b) Three-slots protocol

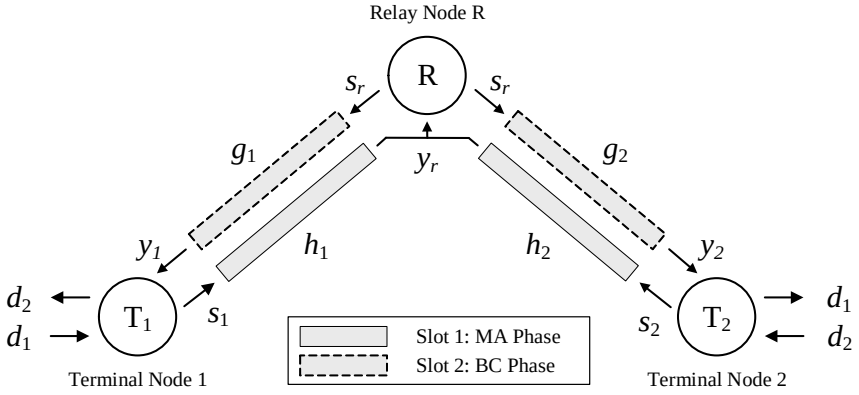

(c) Two-slots protocol

Figure 2.3 Two-way relaying communications without a direct link.

usually called the broadcasting (BC) phase. The main design problem in this protocol is how to generate the broadcast signal so that both terminal nodes can recover the intended

information from a received version of the broadcast signal. The solution of this problem is discussed later in this section.

As an extension of the three-slots protocol, by allowing the two terminal nodes to send their signals to the relay node in the same time slot, the resulting two-slots protocol further eliminates one time slot in the whole transmission process. Besides the problem of generating a proper signal for the BC phase, the relay used in the two-slots protocol needs to detect signals of the two terminal nodes based on one superimposed signal it receives. Since the transmission conducted in the first time slot is under a multiple access channel, it is called the multiple access (MA) phase. Although it is most challenging to implement, the two-slots protocol achieves the highest spectral efficiency (as high as in direct transmission). In the remaining of this section, a system model based on the two-slots protocol is presented and the related problems with existing solutions are discussed.

In the MA phase, the channel from terminal node $\mathbb{T}_i$ to relay node $\mathbb{R}$ is represented by $h_i\,(i \in \{1,2\})$ which is modeled as a complex Gaussian random variable with mean μ_{h_i} and variance $\sigma_{h_i}^2$. The binary information bits d_1 and d_2 are modulated into symbols s_1 and s_2, respectively. The symbols s_1 and s_2 are then simultaneously transmitted from two terminal nodes over channels h_1 and h_2. At the relay, the received signal is:

$$y_r = h_1 s_1 + h_2 s_2 + \omega_r, \tag{2.5}$$

where $\omega_r \sim \mathcal{CN}\,(0, \sigma_r^2)$ is additive white Gaussian noise (AWGN) at the relay.

In the BC phase, the relay generates a new signal s_r from the received signal y_r and transmits it over channels $g_i\,(i \in \{1,2\})$, which is modelled as a complex Gaussian random variable with mean μ_{g_i} and variance $\sigma_{g_i}^2$. The received signal at terminal node $\mathbb{T}_i$ is:

$$y_i = g_i s_r + \omega_i, \quad i \in \{1,2\} \tag{2.6}$$

where $\omega_i \sim \mathcal{CN}\,(0, \sigma_i^2)$ is AWGN at terminal node $\mathbb{T}_i$. Based on the self information d_1 and received signal y_1, terminal node $\mathbb{T}_1$ can detect the information d_2 and vice versa.

Similar to the processing in OWRC, the strategies to generate s_r can also be classified as AF and DF. Like the AF process in OWRC, the relay using AF in TWRC also adjusts

the power and re-transmits a scaled version of y_r. Because y_r is a superimposed signal from the two terminal nodes, the amplification factor needs to consider the amplitudes of both h_1 and h_2. Assuming all nodes have the same transmitted power, the amplified signal s_r can be expressed as:

$$s_r = \sqrt{\frac{1}{|h_1|^2 + |h_2|^2 + \sigma_r^2}} y_r. \tag{2.7}$$

It is can be observed that AF in TWRC also suffers from the problem of noise amplification.

Different from the DF strategy in OWRC, to implement DF in TWRC, the relay node first detects signals transmitted from the two terminal nodes, then generates a broadcast signal according to the detected symbols $\hat{s}_1$ and $\hat{s}_2$. Depending on how to combine these two detected symbols, at symbol level or bit level, DF can be implemented in different ways. In [35], the broadcast signal s_r is generated as:

$$s_r = h_1 \hat{s}_1 + h_2 \hat{s}_2. \tag{2.8}$$

Since s_r generated using this scheme incorporates the channel effect, it is named a partial decode-and-forward (PDF) strategy. Compared to AF, PDF avoids the problem of noise amplification. However, the broadcast signal generated by PDF may exceed the peak power constrain for some specific h_1 and h_2. To keep the transmit power constant, another DF scheme introduced in [36] generates s_r as a linear combination of the detected symbols:

$$s_r = \sqrt{p}\hat{s}_1 + \sqrt{1-p}\hat{s}_2 \tag{2.9}$$

where p is the power allocation coefficient.

The two DF schemes discussed above perform signal combinations at the symbol level. Alternatively, the signal processing to generate the broadcast symbol can operate at the bit level. For example, [21] proposes a joint modulation-based DF scheme in which s_r is expresses as:

$$s_r = \mathcal{M}\left(\hat{d}_1 \;\; \hat{d}_2\right) \tag{2.10}$$

where $\mathcal{M}$ denotes the function that maps bits to a constellation symbol and $\hat{d}_i$ denotes the bits demodulated from $\hat{s}_i$. It can be observed from (2.9) that the joint modulation-based DF

scheme requires a high-order modulation in the BC phase than in the MA phase. A more efficient bit-level DF scheme is proposed in [37], which generates s_r as:

$$s_r = \mathcal{M}\left(\hat{d}_1 \oplus \hat{d}_1\right). \tag{2.11}$$

In this scheme, the same modulation used in the MA phase can be used in the BC phase by conducting the exclusive-or (XOR) on the bits of two detected symbols. In [37], this XOR-based DF scheme is called *network coding* and it is adopted in most of research works on TWRC.

It is clear that no matter what the combination method is employed in the DF scheme, the most important task is to achieve a good performance in detecting $(\hat{s}_1, \hat{s}_2)$. However, this task is more difficult for a multiple access channel (MAC) than for the conventional point-to-point channel. For a point-to-point channel, the detection quality is determined by the signal-to-noise ratio (SNR) and the distance property of the employed constellation. For a MAC, besides the influence of noise, multiple access interference (MAI) could also lead to detection errors. To elaborate the influence of MAI, (2.5) can be rewritten as:

$$y_r = h_1(s_1 + \gamma e^{j\theta} s_2) + \omega_r \tag{2.12}$$

where $\gamma e^{j\theta} = h_2/h_1$ is the fade state of the MAC according to the definition in [38]. In some specific fade states, the relay may not be able to distinguish different symbol pairs (s_1, s_2) even if there is no noise. For example, under the scenario of $\gamma e^{j\theta} = -1$, all symbol pairs satisfying $s_1 = s_2$ would lead to the same received signal and thus cause detection ambiguity. Any fade state causing detection ambiguity is called a *singular fade state* whose distribution in the complex plane is related to the modulation type that the terminal nodes use.

Figure 2.4 gives examples of distribution of the singular fade states for the cases of quadrature phase-shift keying (QPSK) and 8-ary phase-shift keying (8-PSK). In practice, the probability of $\gamma e^{j\theta}$ equalling to a singular fade state is zero. However, if the value of $\gamma e^{j\theta}$ is close to a singular fade state, it would lead to the phenomenon of *distance shortening* and this is illustrated in Fig. 2.5. In the example of Fig. 2.5, QPSK is employed by the two terminal nodes and its constellation is given in Fig. 2.5(a). For simplicity, the decimal

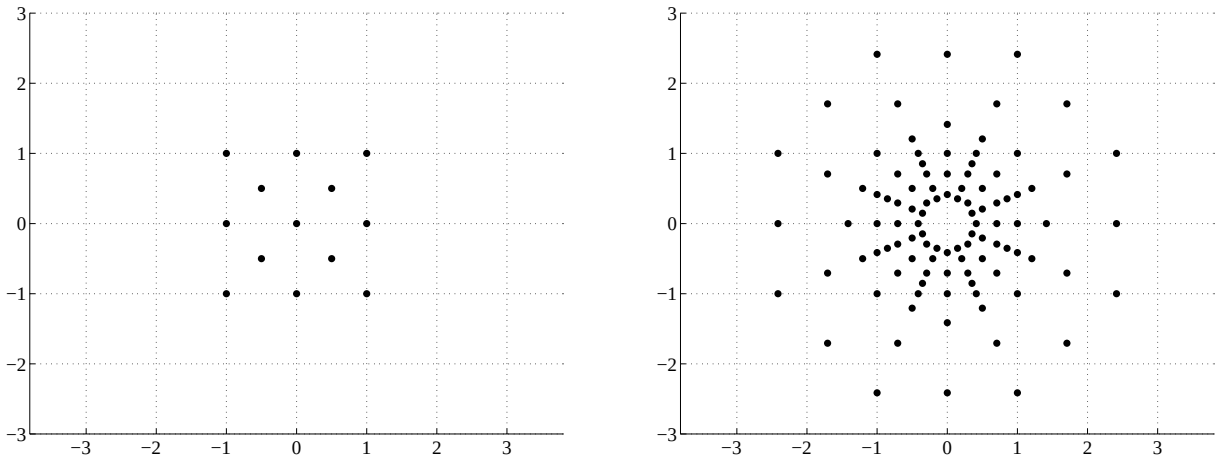

(a) (b)

Figure 2.4 Distribution of singular fade states: (a) QPSK; (b) 8-PSK.

number is used to denote the corresponding bits (e.g., 01 $\rightarrow$ 1). Figure 2.5(b) illustrates the constellation of the received signal y_r when the channel coefficients are assumed to be $h_1 = 1$, $h_2 \approx 1$. For each point in Fig. 2.5(b), the corresponding label denotes the pair of transmitted symbols: the first number denotes the information bits of s_1, while the second number represents the information bits of s_2. From Fig. 2.5, it can be seen that under specific channel conditions, some constellation points representing different symbol pairs may be very close to each other (e.g., those included in the same circle). This distance shortening deteriorates the detection quality in the MA phase.

In [19, 20], a denoise-and-forward (DNF) scheme is proposed to solve the problem of distance shortening. Specifically, DNF maps the closest symbol pairs to the same symbol in a (possibly new) constellation to be broadcast in the BC phase. By doing so, the detection error due to symbol pairs which are mapped to the same broadcast symbol can be eliminated at the terminal nodes by exploiting their self-information. To make such a scheme work, the mapping function needs to satisfy the *exclusive law*. Specifically, suppose $\mathcal{M}_2$ is the mapping function that generates the broadcast signal $s_r = \mathcal{M}_2(\hat{s}_1, \hat{s}_2)$. The exclusive law is as follows:

$$\begin{aligned} \mathcal{M}_2(s_1, s_2) &\neq \mathcal{M}_2(s_1', s_2) \text{ where } s_1 \neq s_2', \\ \mathcal{M}_2(s_1, s_2) &\neq \mathcal{M}_2(s_1, s_2') \text{ where } s_1 \neq s_2'. \end{aligned} \tag{2.13}$$

According to (2.13), different fade states $\gamma e^{j\theta}$ lead to different symbol pair profiles. Fig-

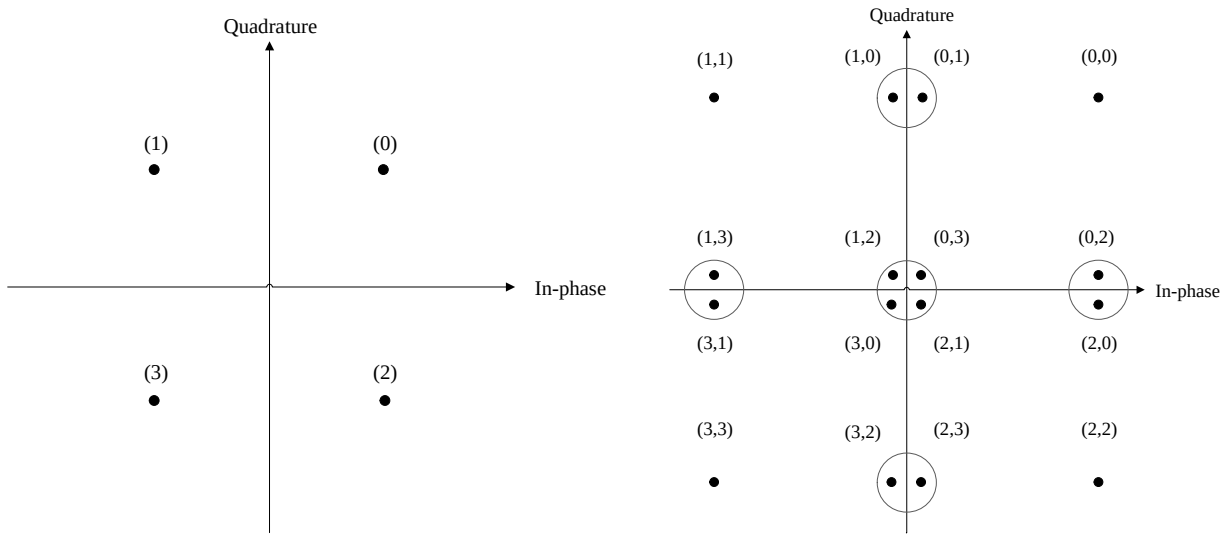

(a) (b)

Figure 2.5 Illustration of distance shortening: (a) constellation of transmitted QPSK; (b) constellation of the received signal at the relay with $h_1 = 1$, $h_2 \approx 1$.

ure 2.6 gives an example explaining how DNF operates under different channel conditions in which the symbols pairs covered with the same shape are grouped and mapped to the same symbol in the BC phase. As shown in Fig. 2.6, following the criteria of DNF, different mapping functions are used in different channel conditions. These mapping functions are called *denoising maps*. Because the mapping rule is adaptively changed according to the fade state, this scheme is also called *adaptive physical-layer network coding*. To aid the detection at terminal nodes, information of the denoising maps needs to be sent to terminal nodes in the BC phase. In fact, the main disadvantage of DNF is this extra overhead required to convey the denoising maps. Another observation concerning the example illustrated in Fig. 2.6(b) is that that there are five different shapes used to group different symbols. This means that, in the BC phase, one needs to use a constellation with five symbols. Requiring irregular modulation such as 5-QAM [20] in the BC phase for specific channel conditions is another disadvantage of DNF.

More recently, to overcome the disadvantages of DNF, reference [39] proposes another scheme called distributed space-time coding (DSTC) to alleviate the distance shortening

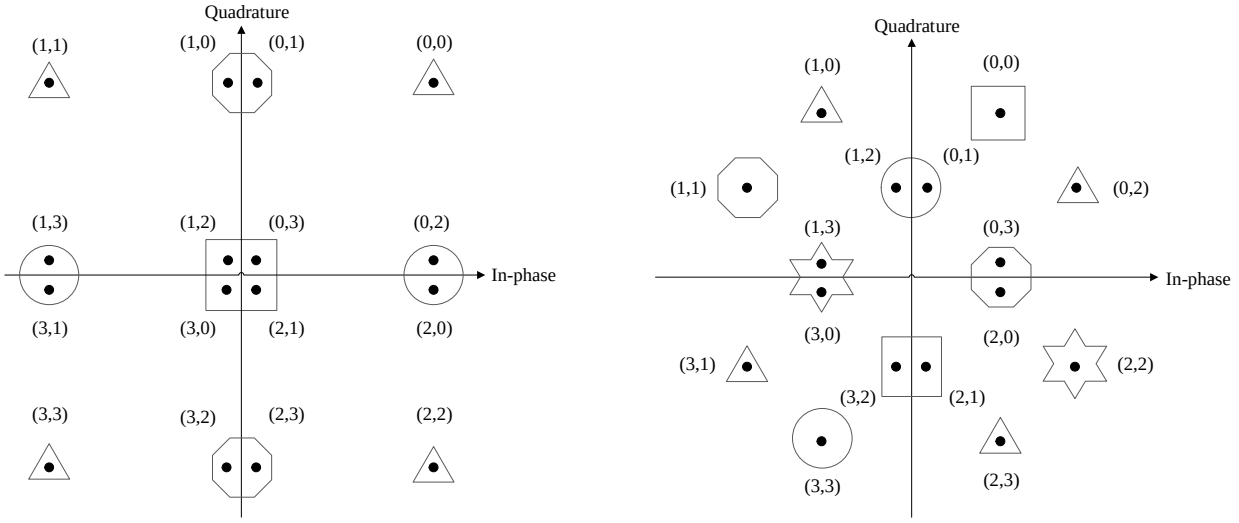

(a) (b)

Figure 2.6 Denoising map for different fade states with QPSK: (a) $\gamma e^{j\theta} \approx 1$; (b) $\gamma e^{j\theta} \approx (1+j)/2$.

problem. As illustrated in Fig. 2.7, information bits d_i are first modulated to two constellation symbols represented as $\boldsymbol{s}_i$. Suppose $\boldsymbol{s}_i(n) = [s_i(2n-1)\ s_i(2n)]^T$ is the nth symbol vector including symbols in adjacent time units from terminal node $\mathbb{T}_i$. Then the precoded symbol vector is:

$$\boldsymbol{x}_i(n) = \boldsymbol{\Theta}_i \boldsymbol{s}_i(n), \quad i \in \{1, 2\} \tag{2.14}$$

where $\boldsymbol{\Theta}_i$ is the 2×2 precoding matrix for terminal node $\mathbb{T}_i$. Instead of sending symbols in constellation $\mathcal{S}$, the precoded symbols are transmitted in the MA phase. The precoding matrices used in both terminal nodes are jointly designed to lower the probability of distance shortening in the MA phase. An example for jointly-designed precoding matrices given in reference [39] is as follows:

$$\boldsymbol{\Theta}_1 = \frac{1}{\sqrt{5}} \begin{pmatrix} a & a\theta \\ \bar{a} & \bar{a}\bar{\theta} \end{pmatrix}, \quad \boldsymbol{\Theta}_2 = \frac{1}{\sqrt{5}} \begin{pmatrix} ja & ja\theta \\ \bar{a} & \bar{a}\bar{\theta} \end{pmatrix},$$

with $\theta = \frac{1+\sqrt{5}}{2}$, $\bar{\theta} = \frac{1-\sqrt{5}}{2}$, $a = 1 + j - j\theta$ and $\bar{a} = 1 + j - j\bar{\theta}$.

Compared to DNF, DSTC does not require any overhead in the BC phase and all nodes can use the same modulation scheme. In addition, according to the simulation results given

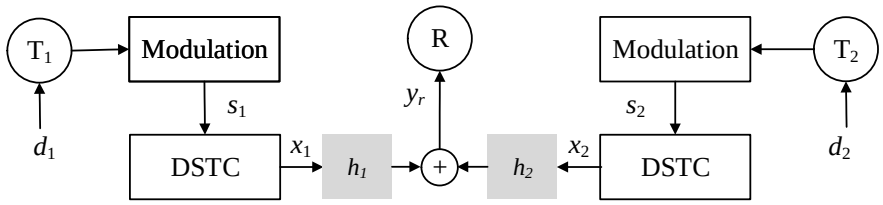

Figure 2.7 DSTC in a TWRC system.

in [39], DSTC shows better performance than DNF in the high SNR region.

Due to their effectiveness in handling the MAI problem, both the techniques of adaptive PNC and DSTC are investigated in our research for frequency-selective fading channels. Specifically, Chapter 3 examines the design of novel adaptive PNC schemes to lower the overhead in the BC phase. On the other other hand, Chapter 4 designs DSTC in a more general form so that it can achieve diversity gains and alleviate MAI at the same time.

2.2 Orthogonal Frequency-Division Multiplexing (OFDM)

As mentioned in Chapter 1, OFDM is an effective and widely used technique to combat multipath dispersion encountered in frequency-selective fading channels. As such, OFDM is also considered in our research when it is concerned with frequency-selective fading channels. In this section, the basic OFDM system model is first introduced. Then, a linear constellation precoding technique to achieve multipath diversity gains in OFDM is discussed.

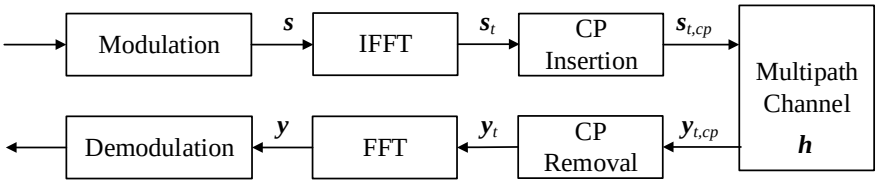

Figure 2.8 Block diagram of an OFDM system.

The block diagram of an OFDM system is shown in Fig. 2.8. The input bits are first modulated to a symbol vector $\boldsymbol{s} = [s(0)\ s(1)\ \cdots\ s(N-1)]^T$ whose elements belong to constellation $\mathcal{S}$. Then $\boldsymbol{s}_t = [s_t(0)\ s_t(1)\ \cdots\ s_t(N-1)]^T$ is generated by performing the inverse

discrete Fourier transform (IDFT)[1] on $\boldsymbol{s}$ where the nth element of $\boldsymbol{s}_t$ can be expressed as:

$$s_t(n) = \frac{1}{\sqrt{N}} \sum_{k=0}^{N-1} s(k) \mathrm{e}^{j2\pi nk/N}, \;\; 0 \leq n \leq N-1. \tag{2.15}$$

After that, a cyclic prefix (CP) is generated by copying the last P samples in $\boldsymbol{s}_t$ and inserting them to the beginning of $\boldsymbol{s}_t$, generating $\boldsymbol{s}_{t,\mathrm{CP}} = [s_t(N-P) \; \cdots \; s_t(N-1) \; s_t(0) \; s_t(1) \; \cdots \; s_t(N-1)]^T$. The multipath channel is represented by vector $\boldsymbol{h} = [h(0) \; h(1) \; \cdots \; h(L-1)]^T$, where L is the number of channel taps. For the case of Rayleigh fading, the components of the channel vector are i.i.d. zero-mean complex Gaussian random variables with unit variance. The received signal $\boldsymbol{y}_{t,\mathrm{CP}}$ is a convolution between $\boldsymbol{s}_{t,\mathrm{CP}}$ and $\boldsymbol{h}$ and added with noise. If the CP length is longer than the number of the channel taps, the symbols that are interfered by the previous OFDM symbol can be discarded by removing the first P symbols of $\boldsymbol{y}_{t,\mathrm{CP}}$ to obtain $\boldsymbol{y}_t$. Furthermore, $\boldsymbol{y}_t$ can be shown to be given as:

$$\boldsymbol{y}_t = \boldsymbol{H}\boldsymbol{s}_{t,\mathrm{CP}} + \boldsymbol{\omega} \tag{2.16}$$

where $\boldsymbol{\omega} = [\omega(0) \; \omega(1) \; \cdots \; \omega(N-1)]^T$ is an AWGN vector with $\boldsymbol{\omega} \sim \mathcal{CN}(\mathbf{0}_N, N_0\mathbf{I}_N)$, and $\boldsymbol{H}$ is a convolution matrix, expressed as:

$$\boldsymbol{H} = \begin{pmatrix} h(L-1) & h(L-2) & \cdots & h(0) & 0 & \cdots & 0 \\ 0 & h(L-1) & \cdots & h(1) & h(0) & \cdots & 0 \\ \vdots & \vdots & \ddots & \ddots & \ddots & \ddots & \vdots \\ 0 & \cdots & 0 & h(L-1) & \cdots & h(1) & h(0) \end{pmatrix} \tag{2.17}$$

Due the cyclic property of CP, (2.16) can also be expressed as:

$$\boldsymbol{y}_t = \tilde{\boldsymbol{H}}\boldsymbol{s}_t + \boldsymbol{\omega}, \tag{2.18}$$

[1]If N is a power of 2, then the DFT and IDFT can be efficiently implemented with fast Fourier transform (FFT) and inverse FFT (IFFT), respectively.

where

$$\tilde{\boldsymbol{H}} = \begin{pmatrix} h(0) & 0 & \cdots & h(L-2) & \cdots & h(2) & h(1) \\ h(1) & h(0) & \cdots & h(L-3) & \cdots & h(3) & h(2) \\ \vdots & \vdots & \ddots & \ddots & \ddots & \ddots & \vdots \\ h(L-1) & h(L-2) & \cdots & h(0) & 0 & \cdots 0 & \\ \vdots & \vdots & \ddots & \ddots & \ddots & \ddots & \vdots \\ 0 & \cdot & h(L-1) & h(L-2) & \cdots & h(0) & 0 \\ 0 & \cdot & 0 & h(L-1) & \cdots & h(1) & h(0) \end{pmatrix}. \tag{2.19}$$

Since $\tilde{\boldsymbol{H}}$ is a circulant convolution matrix, it has the eigenvalue decomposition as:

$$\tilde{\boldsymbol{H}} = \boldsymbol{W}^H \boldsymbol{\Gamma} \boldsymbol{W}, \tag{2.20}$$

where $\boldsymbol{W}$ is a DFT matrix whose elements are $\boldsymbol{W}(n,k) = \mathrm{e}^{-j2\pi nk/N}$ and $\boldsymbol{W}^H$ is the corresponding IDFT matrix. $\boldsymbol{\Gamma}$ is a diagonal matrix of the eigenvalues of $\tilde{\boldsymbol{H}}$. Applying DFT on $\boldsymbol{y}_t$ is equivalent to multiplying with a DFT matrix. One has:

$$\begin{aligned} \boldsymbol{y} &= \boldsymbol{W}\boldsymbol{y}_t \\ &= \boldsymbol{W}\boldsymbol{W}^H\boldsymbol{\Gamma}\boldsymbol{W}\boldsymbol{s}_t + \boldsymbol{W}\boldsymbol{\omega} \\ &= \boldsymbol{\Gamma}\boldsymbol{s} + \tilde{\boldsymbol{\omega}}. \end{aligned} \tag{2.21}$$

Because $\boldsymbol{W}$ is a unitary matrix, $\tilde{\boldsymbol{\omega}}$ has the same statistical property as $\boldsymbol{\omega}$. From (2.21), one can see that by using IFFT/FFT and CP operation, OFDM successfully converts a multipath channel into N parallel flat fading channels. For the convenience of further discussion, by writing $\boldsymbol{\Gamma} = \mathrm{diag}\,(\boldsymbol{W}_T\boldsymbol{h})$, (2.21) can be expressed as:

$$\boldsymbol{y} = \boldsymbol{S}\boldsymbol{W}_T\boldsymbol{h} + \tilde{\boldsymbol{\omega}} \tag{2.22}$$

where $\boldsymbol{S} = \mathrm{diag}(\boldsymbol{s})$ and $\boldsymbol{W}_T$ is a truncated DFT matrix with $\boldsymbol{W}_T = \boldsymbol{W}(1:N, 1:L)$.

Although OFDM successfully eliminates the ISI, it still suffers from the channel fading. In fact, the channel response magnitude in each subcarrier significantly varies over a multipath channel. For the symbols allocated in the subcarriers experiencing a deep fade, the error

probability of detection can be very high. To overcome this problem, linear constellation precoding (LCP) was proposed for OFDM system to achieve multipath diversity gains.

LCP, which is also known as signal space diversity (SSD), is proposed in [40, 41] for point-to-point communications. In LCP, the transmitted symbols are partitioned into several groups and each group contains symbols which are from conventional constellation (such as QPSK, 16-QAM). Then an LCP matrix is multiplied to each group to create the precoded symbols and all the symbols in each group are assigned to interleaved subcarriers. The LCP matrix is designed using algebraic number theory to achieve the maximum diversity gain. In [10], LCP is extended to OFDM systems and shown to be able to achieve the maximum multipath diversity gain.

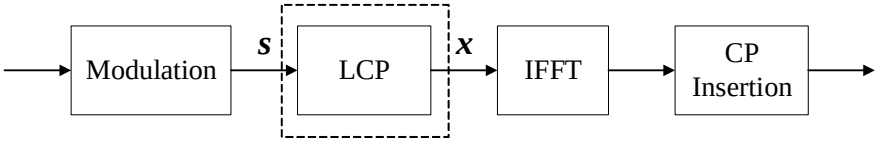

Figure 2.9 Block diagram of an LCP-OFDM system.

Using the same notations for the traditional OFDM system model described above, LCP is applied on $\boldsymbol{s}$ to produce

$$\boldsymbol{x} = \boldsymbol{\Theta}\boldsymbol{s}, \tag{2.23}$$

where $\boldsymbol{x} = [x(0)\ x(1)\ \cdots\ x(N-1)]^T$ is the symbol vector after precoding and $\boldsymbol{\Theta}$ is the LCP matrix. Then the received signal can be expressed as:

$$\boldsymbol{y} = \boldsymbol{X}\boldsymbol{W}_T\boldsymbol{h} + \tilde{\boldsymbol{\omega}}, \tag{2.24}$$

where $\boldsymbol{X} = \mathrm{diag}\,(\boldsymbol{x})$.

To establish the connection between the LCP matrix and system performance, the pairwise error probability (PEP) under the maximum likelihood (ML) detection is analyzed. First the pairwise error event $\{\boldsymbol{s} \to \boldsymbol{s}'\}$ where $\boldsymbol{s} \neq \boldsymbol{s}'$ is defined by assuming $\boldsymbol{s}$ was transmitted but it is erroneously detected to $\boldsymbol{s}'$. Letting $\boldsymbol{X}' = \mathrm{diag}\,(\boldsymbol{\Theta}\boldsymbol{s}')$, the conditional PEP can be bounded as [42]

$$P\left(\boldsymbol{s} \to \boldsymbol{s}'|\boldsymbol{h}\right) \leq \exp\left[-\frac{\left\|\left(\boldsymbol{X}-\boldsymbol{X}'\right)\boldsymbol{W}_T\boldsymbol{h}\right\|_2^{\,2}}{4N_0}\right] \tag{2.25}$$

Further, let $\boldsymbol{\Lambda} = \boldsymbol{X} - \boldsymbol{X}'$. Then (2.25) can be expressed as:

$$P\left(\boldsymbol{s} \to \boldsymbol{s}'|\boldsymbol{h}\right) \leq \exp\left[-\frac{\boldsymbol{h}^H \boldsymbol{W}_T^H \boldsymbol{\Lambda}^H \boldsymbol{\Lambda} \boldsymbol{W}_T \boldsymbol{h}}{4N_0}\right] = \exp\left[-\frac{\boldsymbol{h}^H \boldsymbol{\Psi} \boldsymbol{h}}{4N_0}\right], \tag{2.26}$$

where the $L \times L$ matrix $\boldsymbol{\Psi}$ is $\boldsymbol{\Psi} = \boldsymbol{W}_T^H \boldsymbol{\Lambda}^H \boldsymbol{\Lambda} \boldsymbol{W}_T$. Averaging the conditional PEP with respect to the distribution of $\boldsymbol{h}$, one obtains the following upper bound on the average PEP:

$$P\left(\boldsymbol{s} \to \boldsymbol{s}'\right) \leq \left(\delta_c \frac{1}{4N_0}\right)^{-\delta_d}, \tag{2.27}$$

where $\delta_d = \operatorname{rank}\left(\boldsymbol{\Psi}\right)$ and $\delta_c = \left(\prod_{l=0}^{\operatorname{rank}(\boldsymbol{\Psi})-1} \lambda_l\right)^{\frac{1}{\operatorname{rank}(\boldsymbol{\Psi})}}$ with λ_l, $l = 0, \ldots, \operatorname{rank}\left(\boldsymbol{\Psi}\right) - 1$, are the nonzero eigenvalues of $\boldsymbol{\Psi}$. The *diversity gain* is defined as:

$$G_d = \min_{\forall \boldsymbol{s} \neq \boldsymbol{s}'} \delta_d \tag{2.28}$$

The criterion to design the LCP matrix is to find the matrix that maximizes G_d. Based on algebraic number theory, the $Q \times Q$ optimal LCP matrix is constructed as:

$$\boldsymbol{\Theta} = \frac{1}{\beta} \begin{pmatrix} 1 & \alpha_1 & \ldots & \alpha_1^{Q-1} \\ \vdots & \vdots & \ddots & \vdots \\ 1 & \alpha_Q & \ldots & \alpha_Q^{Q-1} \end{pmatrix}, \tag{2.29}$$

where β is the normalization factor such that $\operatorname{tr}\left(\boldsymbol{\Theta}\boldsymbol{\Theta}^H\right) = Q$. The rules on choosing the parameters $\{\alpha_q\}$, $1 \leq q \leq Q$, are given in [10]. This form of matrix can guarantee that $\boldsymbol{\Psi}$ is full rank under all error events and therefore $G_d = \min\{L, Q\}$.

According to the above analysis, as long as Q is equal or larger than the number of channel taps, the maximum multipath diversity gain is achieved by using LCP.

In our research, when OFDM is incorporated in a TWRC system, the problem of how to effectively combine OFDM with adaptive PNC is analyzed and a few solutions are investigated. On the other hand, when LCP is applied (in a distributed manner) to a TWRC system, it is designed not only to achieve the diversity gain, but also to handle the MAI problem in both uncoded and coded systems.

2.3 Bit-Interleaved Coded Modulation and Iterative Decoding

Due to its ability to achieve many types of diversity gain, BICM and its "iterative" version, BICM-ID (which is BICM equipped with a iterative decoding process at the receiver) is also considered in our research. In this section, the system model, decoding procedure and performance analysis are presented for BICM and BICM-ID. Since BICM can be treated as BICM-ID with only one iteration, the presentation is mainly given for BICM-ID.

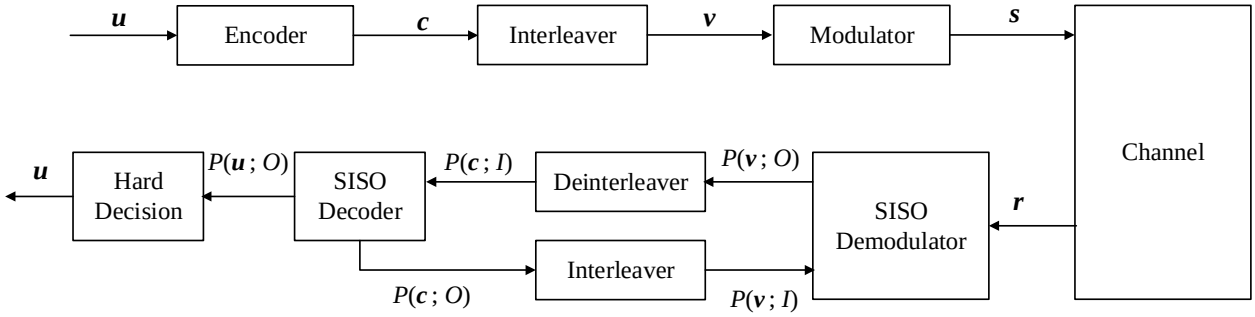

Figure 2.10 Block diagram of a BICM-ID system.

The block diagram of a BICM-ID system is shown in Fig. 2.10. At the transmitter, the L-bit vector $\boldsymbol{u} = [u(1) \ \cdots \ u(L)]^T$ is first encoded into a coded vector $\boldsymbol{c} = [c(1) \ \cdots \ c(M)]^T$. The coded vector $\boldsymbol{c}$ is then interleaved by a bit-wise interleaver to become the interleaved vector $\boldsymbol{v}$. Then each group of K coded bits in $\boldsymbol{v} = [v(1) \ \cdots \ v(M)]^T$ is mapped to a complex constellation symbol. The vector consists of N constellation symbols, $\boldsymbol{s} = [s(1) \ \cdots \ s(N)]^T$, is sent to the receiver.

Let $\boldsymbol{r} = [r(1) \ \cdots \ r(N)]^T$ denote the received symbol vector at the relay node. It can be expressed as:

$$\boldsymbol{r} = \boldsymbol{H}\boldsymbol{s} + \boldsymbol{\omega}, \tag{2.30}$$

where $\boldsymbol{H} = \text{diag}\left([h(1) \ \cdots \ h(N)]\right)$ is the $N \times N$ diagonal matrix whose components are i.i.d. zero-mean complex Gaussian random variables with unit variance and $\boldsymbol{\omega} = [\omega(0) \ \cdots \omega(N-1)]^T$ is an AWGN vector with $\boldsymbol{\omega} \sim \mathcal{CN}\left(\mathbf{0}_N, N_0\mathbf{I}_N\right)$. Based on $\boldsymbol{r}$, the receiver performs iterative decoding to obtain $\boldsymbol{u}$. As illustrated in Fig. 2.10, iterative decoding involves two blocks: the soft-input soft-output (SISO) demodulator and the SISO decoder, which uses the *maximum a posterior* (MAP) algorithm.

To elaborate the process of iterative decoding, the nth element of $\boldsymbol{r}$ can be expressed as:

$$r(n) = h(n)s(n) + \omega(n). \tag{2.31}$$

Let $\mathcal{M}$ be a function that maps K bits into a constellation symbol, i.e., $s(n) = \mathcal{M}(\boldsymbol{v}_n)$ where $\boldsymbol{v}_n = [v((n-1)K+1) \cdots v(nK)]$. Using the same notations as in [43], the *a priori* information and the *extrinsic* information of a random variable z are denoted by $P(z;I)$ and $P(z;O)$, respectively. In the first iteration, the *a priori* information sent to the deinterleaver is the *a posteriori* probability. Given the received signal $r(n)$, the *a posteriori* probability for K coded bits $\boldsymbol{v}_n(k)$, $1 \leq k \leq K$, is computed as follows:

$$P(\boldsymbol{v}_n(k) = q|r(n)) = \sum_{s(n)\in\mathcal{S}_q^k} P(s(n)|r(n)). \tag{2.32}$$

In (2.32), $P(s(n)|r(n))$ is the *a posteriori* probability of the transmitted signal $s(n)$ given the received signal $r(n)$. The set $\mathcal{S}_q^k$, $q \in \{0,1\}$, denotes the subset of $\mathcal{S}$ that contains all signals whose labels have the value q at the kth position, $1 \leq k \leq K$. Using Bayes' rule, $P(\boldsymbol{v}_n(k) = q|r(n))$ can be determined as follows:

$$P(\boldsymbol{v}_n(k) = q|r(n)) = \sum_{s(n)\in\mathcal{S}_q^k} \frac{P(r(n)|s(n))P(s(n))}{P(r(n))} \propto \sum_{s(n)\in\mathcal{S}_q^k} P(r(n)|s(n))P(s(n)) \tag{2.33}$$

where $P(s(n))$ is the *a priori* probability of the transmitted $s(n)$. For the first iteration, the transmitted signal can be assumed to be equally likely, i.e., $P(s(n))$ can be set to $1/2^K$.

From the second iteration, the *extrinsic* information $P(\boldsymbol{c};O)$ of coded bits produced by the SISO decoder is sent to the interleaver. After being interleaved, it becomes the *a priori* information $P(\boldsymbol{v};I)$ to enter the SISO demodulator. Thanks to interleaving, K bits corresponding to each vector $s(n)$ are assumed to be independent. Hence the *a priori* information $P(s(n))$ of $s(n) \in \mathcal{S}$ can be obtained as:

$$P(s(n)) = P(\boldsymbol{v}_n(1|s(n)), \cdots, \boldsymbol{v}_n(K|s(n))) = \prod_{k=1}^{K} P(\boldsymbol{v}_n(k) = \boldsymbol{v}_n(k|s(n));I) \tag{2.34}$$

where $\boldsymbol{v}_n(k|s(n)) \in \{0,1\}$ is the value of the kth bit in the label of $s(n)$. Using (2.33) and

(2.34), the *extrinsic* information from the second iteration can be computed as:

$$\begin{aligned} P\left(\boldsymbol{v}_n(k)=q;O\right) &= \frac{P\left(\boldsymbol{v}_n(k)=q|r(n)\right)}{P\left(\boldsymbol{v}_n(k)=q;I\right)} \propto \frac{\sum_{s(n)\in\mathcal{S}_q^k} P\left(r(n)|s(n)\right)P\left(s(n)\right)}{P\left(\boldsymbol{v}_n(k)=q;I\right)} \\ &= \sum_{s(n)\in\mathcal{S}_q^k}\left[P\left(r(n)|s(n)\right)\prod_{j\neq k}P\left(\boldsymbol{v}_n(j)=\boldsymbol{v}_n(j|s(n));I\right)\right]. \end{aligned} \tag{2.35}$$

The *extrinsic* information is then deinterleaved to become *a priori* information and delivered to the SISO decoder. At any iteration, the hard-decisions of bits $\boldsymbol{u}$ can be obtained based on the corresponding *extrinsic* information $P\left(\boldsymbol{u};O\right)$.

To evaluate the performance of a BICM system (with or without iterative decoding), the bit error probability (BEP) is usually used [14, 44, 45]. Suppose a rate-k_c/n_c convolutional code is adopted. The corresponding BEP is calculated as:

$$P_e \leq \frac{1}{k_c}\sum_{d=d_H}^{\infty}\rho_d f\left(d,\mathcal{S},\mathcal{M}\right) \tag{2.36}$$

where ρ_d is the total information weight of all error events at Hamming distance d and d_H is the free Hamming distance of the code. The function $f\left(d,\mathcal{S},\mathcal{M}\right)$ is the average PEP, which depends on the Hamming distance d, the constellation $\mathcal{S}$ and the mapping rule $\mathcal{M}$. Let $\boldsymbol{c}$ and $\hat{\boldsymbol{c}}$ denote the transmitted and decoded vectors, respectively, with Hamming distance d between them. The function $f\left(d,\mathcal{S},\mathcal{M}\right)$ is computed from the PEP $P\left(\boldsymbol{s}\rightarrow\hat{\boldsymbol{s}}\right)$ by averaging over all possible vectors $\boldsymbol{s}$ and $\hat{\boldsymbol{s}}$. The calculation of $P\left(\boldsymbol{s}\rightarrow\hat{\boldsymbol{s}}\right)$ is as follows.

Without loss of generality, assume that $\boldsymbol{c}$ and $\hat{\boldsymbol{c}}$ differ in the first d consecutive bits. Hence, $\boldsymbol{s}$ and $\hat{\boldsymbol{s}}$ can be redefined as $\boldsymbol{s}=[s(1),\cdots,s(d)]$ and $\hat{\boldsymbol{s}}=[\hat{s}(1),\cdots,\hat{s}(d)]$. Also let $\boldsymbol{h}_d=[h(1),\cdots,h(d)]$, the PEP conditioned on $\boldsymbol{h}_d$ can be computed as follows:

$$P\left(\boldsymbol{s}\rightarrow\hat{\boldsymbol{s}}|\boldsymbol{h}_d\right)=Q\left(\sqrt{\frac{1}{2N_0}\sum_{n=1}^{d}\left|h(n)\right|^2\left|s(n)-\hat{s}(n)\right|^2}\right). \tag{2.37}$$

By using the Gaussian probability integral $Q\left(\sqrt{2\gamma}\right)=\frac{1}{\pi}\int_0^{\pi/2}\exp\left(-\frac{\gamma}{\sin^2\theta}\right)\mathrm{d}\theta$ and averaging (2.37) over $\boldsymbol{h}_d$ of d i.i.d. Rayleigh random variables, it can be shown that [45]

$$P\left(\boldsymbol{s}\rightarrow\hat{\boldsymbol{s}}\right)=\frac{1}{\pi}\int_0^{\pi/2}\sum_{n=1}^{d}\left(1+\frac{1}{4N_0}\frac{\left|s(n)-\hat{s}(n)\right|^2}{\sin^2\theta}\right)^{-1}\mathrm{d}\theta \tag{2.38}$$

Then take the average of $P(\boldsymbol{s} \to \hat{\boldsymbol{s}})$ over all possible $\boldsymbol{s}$ and $\hat{\boldsymbol{s}}$, $f(d, \mathcal{S}, \mathcal{M})$ can be calculated as follows:

$$f(d, \mathcal{S}, \mathcal{M}) \leq \frac{1}{\pi} \int_0^{\pi/2} E\left\{ \left(1 + \frac{1}{4N_0} \frac{|s(n) - \hat{s}(n)|^2}{\sin^2 \theta} \right)^{-1} \right\}^d \mathrm{d}\theta. \tag{2.39}$$

For BICM without iterative decoding, the union bound is usually used [14] and the expectation in (2.39) can be expressed as:

$$E\left\{ \left(1 + \frac{1}{4N_0} \frac{|s(n) - \hat{s}(n)|^2}{\sin^2 \theta} \right)^{-1} \right\} = \frac{1}{K 2^K} \sum_{s(n) \in \mathcal{S}} \sum_{k=1}^{K} \frac{1}{2^{K-1}} \sum_{\hat{s}(n) \in \bar{\mathcal{S}}_{s(n)}^k} \left(1 + \frac{1}{4N_0} \frac{|s(n) - \hat{s}(n)|^2}{\sin^2 \theta} \right)^{-1} \tag{2.40}$$

where $\bar{\mathcal{S}}_{s(n)}^k$ denotes the subset of $\mathcal{S}$ which contains all the symbols whose labels differ at position k compared to $s(n)$.

For BICM-ID with enough number of iterations, the error-free feedback bound (EF bound) is used [44] and the expectation (2.39) can be expressed as:

$$E\left\{ \left(1 + \frac{1}{4N_0} \frac{|s(n) - \hat{s}(n)|^2}{\sin^2 \theta} \right)^{-1} \right\} = \frac{1}{K 2^K} \sum_{s(n) \in \mathcal{S}} \sum_{k=1}^{K} \left(1 + \frac{1}{4N_0} \frac{|s(n) - \hat{s}(n)|^2}{\sin^2 \theta} \right)^{-1} \tag{2.41}$$

where $\hat{s}(n)$ is the symbol whose label only differs at position k compared to the label of $s(n)$.

In our research, BICM/BICM-ID techniques are investigated for TWRC systems. Specifically, the receiver with and without iterative decoding are developed that takes into account the unique feature of the MAC in a TWRC system. Furthermore, distributed LCP schemes are also designed to be used with BICM/BICM-ID and the performance advantage obtained through iterative decoding is analyzed for TWRC.

3. Adaptive Physical-Layer Network Coding in Two-Way Relaying with OFDM

In the previous chapter, the transmission protocols of two-way relaying communications have been discussed. In particular, it was shown that to implement the two-slots protocol, which achieves the highest spectrum efficiency, the relay node has to handle the *distance shortening* problem caused by multiple access interference (MAI) in the MA phase. On the other hand, adaptive physical-layer network coding (PNC), which is also known as denoise-and-forward (DNF), is able to effectively combat MAI in a flat fading channel at the cost of requiring extra overhead and the use of irregular modulation in the BC phase [20].

The manuscript in this chapter studies adaptive PNC over the multipath fading channels with OFDM. First, the system model under flat fading channels in the MA phase, which corresponds to information transmission over one subcarrier, is established. Then the concept of *singular fade state* is introduced to explain the the distance shortening problem. Furthermore, following the *exclusive law*, two clustering criteria, closest-neighbour clustering (CNC) and nearest neighbour clustering (NNC) are discussed. Given the low complexity of NNC, one objective of this manuscript is to examine the error performance of adaptive PNC under the NNC criterion. For this purpose, the minimum distances in three different cases and the corresponding symbol error probabilities are analyzed.

Another objective of this manuscript is to design a clustering scheme when OFDM is adopted since different subcarriers have different channel responses. Applying different clusterings in different subcarriers is the simple method and it has no performance loss. However, this method has the disadvantage of high overhead in the BC phase, especially when the

number of subcarriers is very large. Selecting one clustering for all subcarriers is more realistic although it suffers from the performance loss. Based on the analysis of the symbol error probability, three clustering methods are proposed in this manuscript with different trade-offs between performance and complexity. Simulation results of all methods using different modulation and under different channel scenarios are provided. Comparing the obtained results, the clustering method considering the singular fade state which causes largest symbol error probability is shown to achieve the best performance-complexity trade-off.

The results of our study on adaptive PNC in TWRC with OFDM are reported in the below manuscript.

[Ch3-1] H. Yan and Ha H. Nguyen, "Adaptive Physical-Layer Network Coding in Two-Way Relaying with OFDM", *IEEE Global Telecommun. Conf.*, Atlanta, GA, USA, pp. 4244–4249, Dec. 2013.

Adaptive Physical-Layer Network Coding in Two-Way Relaying with OFDM

Hongzhong Yan and Ha H. Nguyen

Abstract

Adaptive physical layer network coding (PNC) has been shown to be effective in two-way relay communications (TWRC). Given that the existing PNC methods were developed for frequency-flat fading channels, this paper studies adaptive PNC in OFDM systems operating over frequency-selective fading channels. Proposed and investigated are three methods to determine a common clustering for all subcarriers in order to reduce the overhead information required in the broadcast phase. The "Min-SER" method is given based on the analysis of the error event in the multiple access phase, while the "Max-fade-SER" and "Min-fade-distance" methods are recommended to further reduce the computational complexity in determining the common clustering. Considering the trade-off among performance, overhead and complexity, the "Max-fade-SER" method is the most attractive clustering method for applying adaptive PNC in OFDM systems.

Index terms

Two-way relaying, OFDM, physical layer network coding, singular fade state.

3.1 Introduction

With the bi-directional transmission capability, two-way relay communication (TWRC) has recently gained a strong interest in research community. Many new techniques have been presented concerning the design of relaying protocols and signal processing methods at the relay and/or the terminal nodes [36, 46, 47]. Among them, physical-layer network coding (PNC) [47] is an important technique that extends the traditional network coding into the field of wireless communications.

The transmission protocol of TWRC has two phases. In the first phase, the terminal nodes send their information to the relay node. This is also known as the multiple access (MA) phase. In the second phase, which is also called the broadcast (BC) phase, the relay transmits the processed information back to the terminal nodes. If the traditional network coding is used, two time slots would be needed in the MA phase in order to provide orthogonal channels for the two terminal nodes. In contrast, the PNC assigns only one time slot for the MA phase by allowing the two terminal nodes send their information over the same channel. Such a MA scheme significantly enhances the spectrum efficiency of the network. With the PNC approach, the signals from the two terminal nodes are superimposed at the relay and it is challenging to process the superimposed signal at the relay so that the desired information can be detected and re-encoded in the relay node.

Several signal processing strategies have been proposed [19, 47, 48]. One solution is *denoise-and-forward* (DNF), which is described in [19] together with the optimal detection and coding scheme for BPSK. Reference [20] extends the DNF technique to QPSK and 16-QAM. Since the DNF technique needs to change the clustering (a mapping rule from detected signal pairs in the MA phase to a single signal in the BC phase) and even the modulation type according to the channel condition, it is also called *adaptive* PNC. Recently, the authors in [49] and [50] perform a detailed analysis of the relationship between the clustering and channel condition. Compared to the conventional XOR network coding, the adaptive PNC is able to significantly lower the error probability and thus improve transmission efficiency.

To date, most of the research studies concerning TWRC only consider frequency-flat fading channels. Given the effectiveness of TWRC and the fact that orthogonal frequency-division multiplexing (OFDM) is a popular and efficient approach to combat frequency-selective channels, it is natural to combine adaptive PNC with OFDM in TWRC when designing communication systems that operate over frequency-selective fading channels. For a frequency-selective fading channel, the gains in different subcarrriers of the OFDM system are different and thus generally require different clusterings. This would cause a large overhead in the BC phase if the clustering information needs to be conveyed to the terminal nodes in subcarrier-by-subcarrier manner. To reduce overhead information, this paper

proposes sub-optimal clustering methods that determine one common clustering for all the subcarriers in a given OFDM frame. It is shown that the proposed methods have better performance when compared to the pure XOR method and offer a good trade-off among performance, computational complexity and the amount of overhead bits when compared to the optimal method that is based on subcarrier-by-subcarrier clustering.

The rest of the paper is organized as follows. Section 3.2 presents the system model and summarizes the important details of the adaptive PNC technique. Section 3.3 analyzes the error probability in different channel conditions. Different clustering selection strategies are investigated in Section 3.4. Section 3.5 provides the simulation results for performance comparison. Section 3.6 draws conclusions.

3.2 System Model and Adaptive PNC

The TWRC system under consideration has two terminal nodes, denoted as node $\mathbb{T}_1$ and node $\mathbb{T}_2$, which exchange their information by the help of the relay node $\mathbb{R}$. Both the terminal nodes use the same modulation type. Let $\mathcal{S}$ denote the set of the constellation points, whose average energy is normalized to unity. The channel of each communication link is assumed to be block fading. The discussion in this section focuses on flat-fading channels, while frequency-selective channels and the use of OFDM will be discussed in Section 3.4.

In the MA phase, the relay node receives the combined signal from nodes $\mathbb{T}_1$ and $\mathbb{T}_2$. That is

$$Y_R = H_1 X_1 + H_2 X_2 + \omega_R, \tag{3.1}$$

where $X_1, X_2 \in \mathcal{S}$, H_1 and H_2 are the coefficients of the $\mathbb{T}_1$-$\mathbb{R}$ and $\mathbb{T}_2$-$\mathbb{R}$ channels, respectively, and ω_R is the additive Gaussian noise, modeled as $\mathcal{CN}(0, N_0)$. By defining $H_2/H_1 = \gamma e^{j\theta}$ as a *fade state* [50], one has

$$Y_R = H_1 \left(X_1 + \gamma e^{j\theta} X_2\right) + \omega_R. \tag{3.2}$$

It follows that the effective constellation at the relay during the MA phase, $S_R(\gamma, \theta)$ is related to the fade state:

$$S_R(\gamma, \theta) = \left\{X_i + \gamma e^{j\theta} X_j | X_i, X_j \in \mathcal{S}\right\}. \tag{3.3}$$

Let $D_{\min}(\gamma,\theta)$ be the minimum distance of the constellation $S_R(\gamma,\theta)$, which is calculated as:

$$D_{\min}(\gamma,\theta) = \min_{\substack{(X_1,X_2),(X_1',X_2')\in\mathcal{S}\times\mathcal{S} \\ (X_1,X_2)\neq(X_1',X_2')}} \left|(X_1 - X_1') + \gamma e^{j\theta}(X_2 - X_2')\right|. \tag{3.4}$$

It can be seen from (3.4) that there exists particular fade state $\gamma e^{j\theta}$ that causes the minimum distance to be zero. Following the definition in [50], such a fade state is called *singular fade state* and the set of singular fade states is $\mathcal{F} = \left\{\gamma e^{j\theta} | D_{\min}(\gamma,\theta) = 0\right\}$. It should be noted that although the singular fade states happen with an extremely low probability, the fade states near them cause short minimum distance (although not zero), and this phenomenon is called *distance shortening* [20].

At the relay, the maximum likelihood (ML) detection is performed to obtain the estimates $\hat{X}_1$ and $\hat{X}_2$ as follows:

$$\left(\hat{X}_1,\hat{X}_2\right) = \arg\min_{(X_1',X_2')\in\mathcal{S}\times\mathcal{S}} |Y_R - H_1X_1' - H_2X_2'|. \tag{3.5}$$

After obtaining the ML estimates, the relay node would map the pair $\left(\hat{X}_1,\hat{X}_2\right)$ into one signal. This mapping process is described as $\mathcal{M}:\mathcal{S}\times\mathcal{S}\to\mathcal{S}'$. In general, the constellation $\mathcal{S}'$ can be different from the constellation used by the two terminal nodes. In the conventional network coding, the XOR operation is used at the bit level and $\mathcal{S}'$ would be the same as $\mathcal{S}$. However, in adaptive network coding [20], to handle the problem of distance shortening, the mapping is determined by the value of the fade state $\gamma e^{j\theta}$ and it is explicitly written as $\mathcal{M}^{\gamma,\theta}$. The elements in $\mathcal{S}\times\mathcal{S}$ which are mapped to the same element in $\mathcal{S}'$ by $\mathcal{M}^{\gamma,\theta}$ are said to form a cluster and the formation of clusters under the fade state $\gamma e^{j\theta}$ is called *clustering* and denoted by $\mathcal{C}^{\gamma,\theta}$ [50].

When designing the clustering, the exclusive law [19] should be followed to ensure the successful decoding at the terminal nodes in the BC phase. The exclusive law is a follows:

$$\begin{aligned} &\mathcal{M}^{\gamma,\theta}(X_1,X_2) \neq \mathcal{M}^{\gamma,\theta}(X_1',X_2) \text{ where } X_1\neq X_1', \\ &\mathcal{M}^{\gamma,\theta}(X_1,X_2) \neq \mathcal{M}^{\gamma,\theta}(X_1,X_2') \text{ where } X_2\neq X_2'. \end{aligned} \tag{3.6}$$

Based on the above exclusive law, reference [20] performs exhaustive computer search to find the clustering that gives the optimal distance profile, which is called the closest-neighbor clustering (CNC). However, this method is very computationally intensive and also requires a large overhead in the BC phase. A simpler criterion, called the nearest neighbor clustering (NNC), is also proposed in [20] and shown to achieve performance very close to that of the CNC. The NNC method simply maximizes the minimum cluster distance instead of taking into account the whole distance profile as in the CNC method. The minimum cluster distance is computed as [49]:

$$d_{\min}\left(\mathcal{C}^{\gamma,\theta}\right) = \min_{\substack{(X_1,X_2),\left(X_1',X_2'\right)\in\mathcal{S}\times\mathcal{S} \\ \mathcal{M}^{\gamma,\theta}(X_1,X_2)\neq\mathcal{M}^{\gamma,\theta}\left(X_1',X_2'\right)}} \left|(X_1 - X_1') + \gamma e^{j\theta}\left(X_2 - X_2'\right)\right|. \tag{3.7}$$

More recently, the authors in [49] and [50] present an analytical approach to find clustering under the NNC criterion instead of relying on computer search. According to their analysis, the whole complex plane representing $\gamma e^{j\theta}$ can be partitioned into the singularity-free and singularity regions. If the fade state is in the singularity-free region, any clustering that satisfies the exclusive law achieves the upper bound of the minimum cluster distance. However, if the fade state is in the singularity region, the clustering needs to be carefully chosen according to the value of fade state $\gamma e^{j\theta}$. Reference [50] further quantizes the singularity region into a finite number of sub-regions, each centered by a singular fade state. The authors also point out that in each sub-region, there exists one optimal clustering under the NNC criterion which can remove the distance shortening effect caused by the fade states in that sub-region.

In the BC phase, nodes A and B receive the following signals:

$$Y_1 = H_1' X_R + \omega_1, \quad Y_2 = H_2' X_R + \omega_2, \tag{3.8}$$

where $X_R = \mathcal{M}^{\gamma,\theta}\left(\hat{X}_1, \hat{X}_2\right) \in \mathcal{S}'$, H_1' and H_2' are coefficients of the $\mathbb{R}$-$\mathbb{T}_1$ and $\mathbb{R}$-$\mathbb{T}_2$ channels, and ω_1 and ω_2 represent additive Gaussian noise components, which are modeled as $\mathcal{CN}(0, N_0)$. After receiving the signal broadcast from the relay, each terminal node finds $\hat{X}_R$ using the ML detection rule. Thanks to the exclusive law, with the knowledge of $\hat{X}_R$ each node can decode the information of its partner.

3.3 Analysis of the Error Event in The MA Phase

This paper also adopts the NNC criterion to find the clustering when OFDM is used for frequency-selective fading channels. The notations Φ_{F} and Φ_{S} are used to denote the singularity-free and singularity regions, respectively. When OFDM is used, different subcarriers experience different gains (i.e., frequency responses) and thus different fade states. It is unlikely that all the fade states belong to the same sub-region of Φ_{S} and share the same clustering. Our objective is to come up with one clustering that can be used for all subcarriers. However, this also means that some subcarriers have to use a clustering which is non-optimal (in the sense of the NNC criterion) with respect to their current fade states. To analyze the impact of an unmatched clustering on the error performance, $\overline{\mathcal{C}}$ and $\overline{\mathcal{M}}$ shall be used to denote some arbitrary clustering and the corresponding mapping in the following analysis.

Let E_1, E_2, and E_{MA} respectively, denote the error events of detections at nodes $\mathbb{T}_1$, $\mathbb{T}_2$, and in the MA phase. Also let $\mathcal{H} = (H_1, H_2)$ and $\mathcal{H}' = (H_1', H_2')$. Reference [51] gives the conditional terminal-to-terminal symbol error rate (SER) expression as follows:

$$\begin{aligned} P_{\mathcal{H},\mathcal{H}'}\left\{E_1 \cup E_2\right\} = {} & P_{\mathcal{H}'}\left\{E_1 \cup E_2 | E_{\mathrm{MA}}\right\} P_{\mathcal{H}}\left\{E_{\mathrm{MA}}\right\} \\ & + P_{\mathcal{H}'}\left\{E_1 \cup E_2 | \overline{E_{\mathrm{MA}}}\right\}\left(1 - P_{\mathcal{H}}\left\{E_{\mathrm{MA}}\right\}\right), \end{aligned} \tag{3.9}$$

where

$$P_{\mathcal{H}}\left\{E_{\mathrm{MA}}\right\} = P_{\mathcal{H}}\left\{\overline{\mathcal{M}}\left(\hat{X}_1, \hat{X}_2\right) \neq \overline{\mathcal{M}}\left(X_1, X_2\right)\right\}. \tag{3.10}$$

Since the performance bottleneck of TWRC is in the MA phase, we shall focus on the error probability in (3.10). It is important to recognize that the error event happens when the transmitted signal pair (X_1, X_2) is incorrectly determined to another pair which is not included in the same cluster under clustering $\overline{\mathcal{C}}$, i.e., the error event is influenced by both the ML detection rule in (3.5) and the employed clustering $\overline{\mathcal{C}}$.

Using the nearest-neighbor approximation [52], the error probability associated with the transmission of (X_1, X_2) under clustering $\overline{\mathcal{C}}$ can be written as:

$$P_{\mathcal{H}}^{(\mathrm{MA})}(X_1, X_2 | \overline{\mathcal{C}}, \gamma \mathrm{e}^{j\theta}) \approx \kappa_{d_{\min}} Q\left(\frac{|H_1|\, d_{\min}\left(X_1, X_2 | \overline{\mathcal{C}}, \gamma \mathrm{e}^{j\theta}\right)}{\sqrt{2N_0}}\right) \tag{3.11}$$

where $\kappa_{d_{\min}}$ is the number of nearest-neighbor pairs (X_1', X_2') which are not included in the same cluster of (X_1, X_2). The corresponding minimum distance is computed and bounded as [50]:

$$\begin{aligned} d_{\min}\left(X_1, X_2|\overline{\mathcal{C}}, \gamma \mathrm{e}^{j\theta}\right) &= \min_{\substack{\left(X_1', X_2'\right)\in\mathcal{S}\times\mathcal{S} \\ \overline{\mathcal{M}}(X_1,X_2)\neq\overline{\mathcal{M}}\left(X_1', X_2'\right)}} \left|\left(X_1 - X_1'\right) + \gamma \mathrm{e}^{j\theta}\left(X_2 - X_2'\right)\right| \\ &\leq \min\left(D_{\min}^{(\mathcal{S})}, \gamma D_{\min}^{(\mathcal{S})}\right), \end{aligned} \tag{3.12}$$

where $D_{\min}^{(\mathcal{S})}$ is the minimum distance of constellation $\mathcal{S}$ employed at the terminal nodes.

The above minimum distance can be further analyzed in three different cases as follows:

Case 1: If $\gamma \mathrm{e}^{j\theta}$ is in the singularity-free region, every clustering satisfying the exclusive law achieves the upper bound, i.e.,

$$d_{\min}\left(X_1, X_2|\overline{\mathcal{C}}, \gamma \mathrm{e}^{j\theta} \in \Phi_{\mathrm{F}}\right) = \min\left(D_{\min}^{(\mathcal{S})}, \gamma D_{\min}^{(\mathcal{S})}\right). \tag{3.13}$$

Case 2: If $\gamma \mathrm{e}^{j\theta}$ is in the singularity region, Φ_{S}, and $\overline{\mathcal{C}}$ is the optimal clustering, the closest pairs are included in the same cluster. It follows that the upper bound can be very close to the actual minimum distance and one can use the following approximation:

$$d_{\min}\left(X_1, X_2|\overline{\mathcal{C}} = \mathcal{C}^{\gamma,\theta}, \gamma \mathrm{e}^{j\theta} \in \Phi_{\mathrm{S}}\right) \approx \min\left(D_{\min}^{(\mathcal{S})}, \gamma D_{\min}^{(\mathcal{S})}\right). \tag{3.14}$$

Case 3: If $\gamma \mathrm{e}^{j\theta}$ is in Φ_{S} and $\overline{\mathcal{C}}$ is a non-optimal clustering, the minimum distance is calculated as:

$$d_{\min}\big(X_1, X_2|\overline{\mathcal{C}} \neq \mathcal{C}^{\gamma,\theta}, \gamma \mathrm{e}^{j\theta} \in \Phi_{\mathrm{S}}\big) = \left|\Delta X_A\right| \left|1 + \gamma \mathrm{e}^{j\theta} \frac{\Delta X_2}{\Delta X_1}\right|, \tag{3.15}$$

where $\Delta X_1 = X_1 - X_1'$, $\Delta X_2 = X_2 - X_2'$ and the pair (X_1', X_2') is the one that is nearest to the transmitted pair (X_1, X_2). Because $\overline{\mathcal{C}}$ is a non-optimal clustering, the problem of distance shortening is not solved and the shortened distance cannot be approximated by the upper bound in (3.13). With a slight abuse of notation, let $\mathcal{F}_{\min}^{\gamma,\theta}$ be the singular fade state that makes $\left(1 + \mathcal{F}_{\min}^{\gamma,\theta} \frac{\Delta X_2}{\Delta X_1}\right) = 0$. Then (3.15) can also be expressed as:

$$d_{\min}\big(X_1, X_2|\overline{\mathcal{C}} \neq \mathcal{C}^{\gamma,\theta}, \gamma \mathrm{e}^{j\theta} \in \Phi_{\mathrm{S}}\big) = \left|\Delta X_1\right| \left|1 - \frac{\gamma \mathrm{e}^{j\theta}}{\mathcal{F}_{\min}^{\gamma,\theta}}\right|, \tag{3.16}$$

In fact, among all the singular fade states of the set $\mathcal{F}$, $\mathcal{F}_{\min}^{\gamma,\theta}$ is the singular fade state that is closest to the fade state $\gamma e^{j\theta}$. Furthermore, one can conclude that the closer to $\mathcal{F}_{\min}^{\gamma,\theta}$ the fade state $\gamma e^{j\theta}$ is, the smaller the minimum distance in (3.16) becomes.

For simplicity in the following analysis, we use a general expression $d_{\min}^{\gamma,\theta}(X_1, X_2)$ to denote the minimum distance in all these three cases under the fade state $\gamma e^{j\theta}$ and eliminate the explicit dependence on clustering $\overline{\mathcal{C}}$. With this simplification, (3.11) can be rewritten as

$$P_{\mathcal{H}}^{(\mathrm{MA})}(X_1, X_2) \approx \kappa_{d_{\min}} Q\left(\frac{|H_A|\, d_{\min}^{\gamma,\theta}(X_1, X_2)}{\sqrt{2N_0}}\right). \tag{3.17}$$

Therefore, the average error probability under the specific channel pair $\mathcal{H}$ is:

$$P_{\mathcal{H}}(E_{\mathrm{MA}}) = \sum_{(X_1,X_2)\in\mathcal{S}\times\mathcal{S}} P(X_1, X_2)\, P_{\mathcal{H}}^{(\mathrm{MA})}(X_1, X_2), \tag{3.18}$$

where $P(X_1, X_2) = 1/M^2$ with equally-likely symbols for M-ary transmission in the MAC phase.

To obtain a more explicit expression for $P_{\mathcal{H}}(E_{\mathrm{MA}})$, one not only needs to examine the three different cases as discussed before, but also to specify the constellation $\mathcal{S}$. For illustration purpose, we take $\mathcal{S}$ to be QPSK, which has $\kappa_{d_{\min}} = 2$. For Case 1 and Case 2, $d_{\min}^{\gamma,\theta}(X_1, X_2)$ is the upper bound in (3.13). When multiplied with the channel magnitude $|H_1|$, it would equal to the minimum distance of the constellation multiplied with the magnitude of the weaker channel, i.e.,

$$|H_1|\, d_{\min}^{\gamma,\theta}(X_1, X_2) = \lambda_{\mathcal{H}} D_{\min}^{(\mathcal{S})}, \tag{3.19}$$

where $\lambda_{\mathcal{H}} = \min(|H_1|, |H_2|)$. Thus for the first two cases, (3.17) is simply $2Q\left(\frac{D_{\min}^{(\mathcal{S})}\lambda_{\mathcal{H}}}{\sqrt{2N_0}}\right)$.

The tricky case is Case 3, when $\gamma e^{j\theta} \in \Phi_{\mathrm{S}}$ and $\overline{\mathcal{C}}$ is a non-optimal clustering. In this case, the number of nearest neighbor pairs would be different for different signal pairs and it depends on the value of $\gamma e^{j\theta}$. Besides, the minimum distance also varies according to $\left|1 - \frac{\gamma e^{j\theta}}{\mathcal{F}_{\min}^{\gamma,\theta}}\right|$. As described in [20], there are two types of fade states that cause distance shortening for QPSK. One type is shown in Fig. 3.1 where the correct clustering is equivalent to XOR (or modified XOR) rule. We use Φ_{X} to denote the region of such fade states and call it "XOR type". The other situation is shown in Fig. 3.2 and it is called singular point

in [20] for which 5QAM should be used in the BC phase. We use $\Phi_{\rm SP}$ to denote the region of such fade states and call it "SP type". It can be concluded that $\Phi_{\rm X}$ and $\Phi_{\rm SP}$ form the partitions of $\Phi_{\rm S}$.

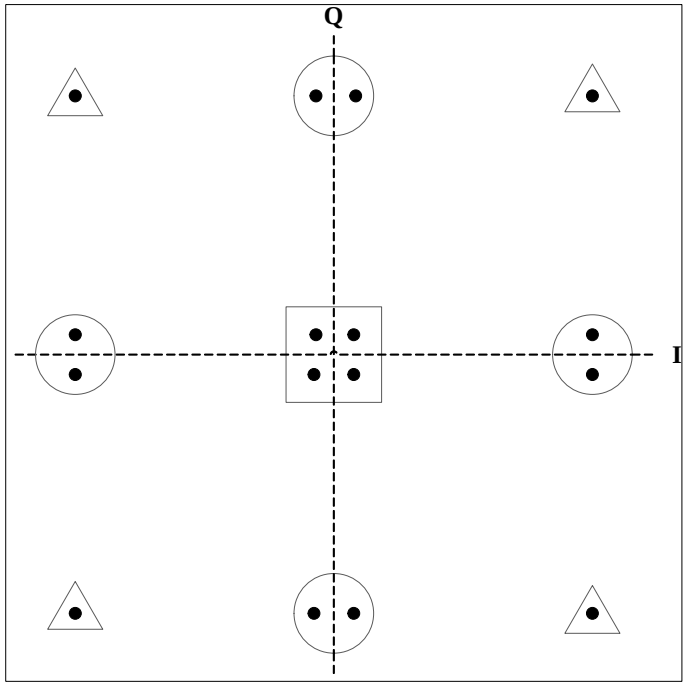

Figure 3.1 Constellation $S_R(\gamma,\theta)$ when $H_2/H_1 \approx 1$: Fade state of XOR type.

Fig. 3.1 shows that there are three types of signal pairs: (i) those covered by triangles (whose set is expressed as $\mathcal{X}_1$) that are not affected by distance shortening and have the same error probability as in the case of singularity-free region, (ii) those covered by circles (whose set is expressed as $\mathcal{X}_2$) that have 1 nearest neighbor pair, and (iii) those covered by rectangles (whose set is expressed as $\mathcal{X}_3$) that have 2 nearest neighbor pairs. For simplicity, we use $P^{(\rm MA)}_{\mathcal{H},\Phi_{\rm X}}(\mathcal{X}_i)$ to denote the probability $P^{(\rm MA)}_{\mathcal{H},\Phi_{\rm X}}((X_1,X_2)|(X_1,X_2)\in\mathcal{X}_i)$. It follows that

$$P^{(\rm MA)}_{\mathcal{H},\Phi_{\rm X}}(\mathcal{X}_1) \approx 2Q\left(\frac{D^{(\mathcal{S})}_{\min}\lambda_{\mathcal{H}}}{\sqrt{2N_0}}\right), \tag{3.20}$$

$$P^{(\rm MA)}_{\mathcal{H},\Phi_{\rm X}}(\mathcal{X}_2) \approx Q\left(\frac{D^{(\mathcal{S})}_{\min}|H_1|\left|1-\frac{\gamma e^{j\theta}}{\mathcal{F}^{\gamma,\theta}_{\min}}\right|}{\sqrt{2N_0}}\right), \tag{3.21}$$

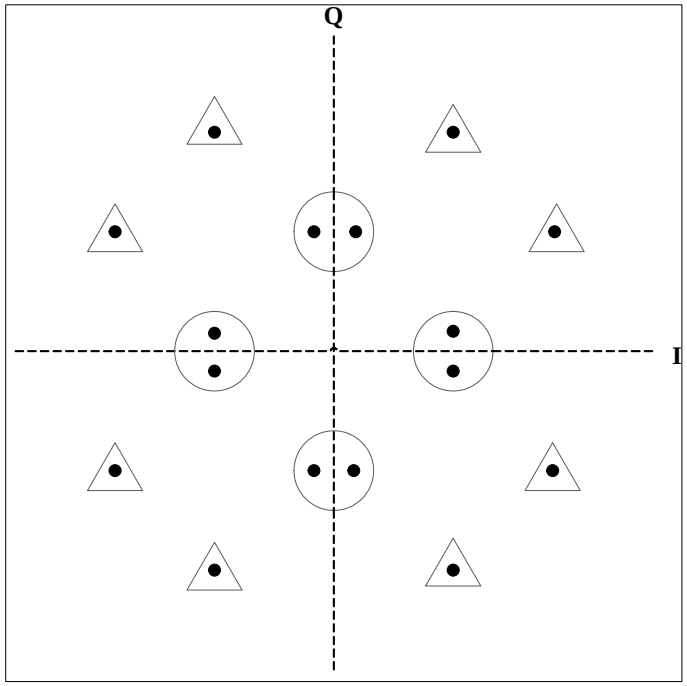

Figure 3.2 Constellation $S_R(\gamma,\theta)$ when $H_2/H_1 \approx (1+j)/2$: Fade state of singular point (SP) type.

$$P^{(\mathrm{MA})}_{\mathcal{H},\Phi_{\mathrm{X}}}(\mathcal{X}_3) \approx 2Q\left(\frac{D^{(\mathcal{S})}_{\min}|H_1|\left|1-\frac{\gamma e^{j\theta}}{\mathcal{F}^{\gamma,\theta}_{\min}}\right|}{\sqrt{2N_0}}\right), \tag{3.22}$$

Considering different types of pairs, one has the overall error probability under the fade states of XOR type as:

$$P^{(\mathrm{MA})}_{\mathcal{H},\Phi_{\mathrm{X}}} \approx \frac{1}{4}P^{(\mathrm{MA})}_{\mathcal{H},\Phi_{\mathrm{X}}}(\mathcal{X}_1) + \frac{1}{2}P^{(\mathrm{MA})}_{\mathcal{H},\Phi_{\mathrm{X}}}((\mathcal{X}_2) + \frac{1}{4}P^{(\mathrm{MA})}_{\mathcal{H},\Phi_{\mathrm{X}}}(\mathcal{X}_3)\,. \tag{3.23}$$

Similar for Fig. 3.2, those signal pairs covered by triangles (whose set is expressed as $\mathcal{Z}_1$) are not affected by distance shortening, whereas those covered by circles (whose set is expressed as $\mathcal{Z}_2$) have 1 nearest neighbor pair. Thus one has

$$P^{(\mathrm{MA})}_{\mathcal{H},\Phi_{\mathrm{SP}}}(\mathcal{Z}_1) \approx 2Q\left(\frac{D^{(\mathcal{S})}_{\min}\lambda_{\mathcal{H}}}{\sqrt{2N_0}}\right), \tag{3.24}$$

$$P^{(\mathrm{MA})}_{\mathcal{H},\Phi_{\mathrm{SP}}}(\mathcal{Z}_2) \approx Q\left(\frac{D^{(\mathcal{S})}_{\min}|H_1|\left|1-\frac{\gamma e^{j\theta}}{\mathcal{F}^{\gamma,\theta}_{\min}}\right|}{\sqrt{2N_0}}\right), \tag{3.25}$$

and

$$P_{\mathcal{H},\Phi_{\mathrm{SP}}}^{(\mathrm{MA})} \approx \frac{1}{2} P_{\mathcal{H},\Phi_{\mathrm{SP}}}^{(\mathrm{MA})}\left(\mathcal{Z}_1\right) + \frac{1}{2} P_{\mathcal{H},\Phi_{\mathrm{SP}}}^{(\mathrm{MA})}\left(\mathcal{Z}_2\right). \tag{3.26}$$

3.4 Adaptive PNC in OFDM

Over one frame duration, different subcarriers of an OFDM system experience different channel conditions, i.e., different fade states $\gamma \mathrm{e}^{j\theta}$. This means that there are different optimal clusterings for different subcarriers, although some close subcarriers (e.g., within the coherence bandwidth) might share the same clustering. The problem is that providing the information about all the optimal clusterings to the terminal nodes in the BC phase requires a large amount of overhead bits. On the other hand, if only one clustering is applied in all the subcarriers, there can be performance loss since the selected clustering might not be optimal for some subcarriers. To minimize the performance loss, it is desired to have a clustering method that takes into account the performance of all subcarriers.

Suppose there are K subcarriers and the channels corresponding to the kth subcarrier in the MA phase are denoted as $H_1^{(k)}$ and $H_2^{(k)}$. Also define $\mathcal{H}_k = \left(H_1^{(k)}, H_2^{(k)}\right)$ and $H_2^{(k)}/H_1^{(k)} = \gamma_k \mathrm{e}^{j\theta_k}$. For the kth subcarrier, an arbitrary fade state $\gamma_k \mathrm{e}^{j\theta_k}$ may belong to different regions: Φ_{F}, Φ_{X} and Φ_{SP}. In the following, we present three criteria to select a common clustering in OFDM to minimize the performance loss.

- *Method 1: Min-SER*

For a given constellation $\mathcal{S}$ used by the terminal nodes, there is a finite number of optimal clusterings, each corresponding to one quantization region of the complex plane (representing $\gamma \mathrm{e}^{j\theta}$). Let $\mathcal{C}_n$, $n = 1, 2, \ldots, N$, denote these optimal clusterings. Based on the analysis in Section 3.3, the overall error probability when using the nth clustering can be approximated

as:

$$P_{\{\mathcal{H}_k\}_{k=1}^K}(E_{\mathrm{MA}}|\mathcal{C}_n) = \frac{1}{K}\Big[\sum_{\gamma_k e^{j\theta_k}\in\Phi_{\mathrm{F}}} P^{(\mathrm{MA})}_{\mathcal{H}_k,\Phi_{\mathrm{F}}} + \sum_{\substack{\gamma_k e^{j\theta_k}\in\Phi_{\mathrm{S}}\\ \mathcal{C}_n=\mathcal{C}^{\gamma_k,\theta_k}}} P^{(\mathrm{MA})}_{\mathcal{H}_k,\Phi_{\mathrm{F}}} + \sum_{\substack{\gamma_k e^{j\theta_k}\in\Phi_{\mathrm{X}}\\ \mathcal{C}_n\neq\mathcal{C}^{\gamma_k,\theta_k}}} P^{(\mathrm{MA})}_{\mathcal{H}_k,\Phi_{\mathrm{X}}} + \sum_{\substack{\gamma_k e^{j\theta_k}\in\Phi_{\mathrm{SP}}\\ \mathcal{C}_n\neq\mathcal{C}^{\gamma_k,\theta_k}}} P^{(\mathrm{MA})}_{\mathcal{H}_k,\Phi_{\mathrm{SP}}}\Big]. \tag{3.27}$$

The selection criterion is to find the clustering which minimizes the overall error probability. That is,

$$\hat{n} = \arg\min_{n=1,2,\ldots,N} P_{\{\mathcal{H}_k\}_{k=1}^K}(E_{\mathrm{MA}}|\mathcal{C}_n) \tag{3.28}$$

By directly minimizing the approximated error probability, it is expected that this method is almost globally optimal. However, its computation complexity is very high.

- *Method 2: Max-fade-SER*

For a given constellation $\mathcal{S}$, there is a finite number of singular fade states in the complex plane.[1] The singularity region, Φ_{S}, is quantized to multiple sub-regions, each centered by one singular fade state. For each sub-region of the fade states there is a clustering that removes the distance shortening effect caused the fade states in that region. From (3.16), one can see that the minimum distance is related to the distance between $\gamma e^{j\theta}$ and its closest singular fade state. Thus, instead of using the overall error probability, one can consider the error probability caused by critical fade states that are close to the singular fade states.

Suppose that there are I singular fade states and the ith state is $\mathcal{F}_i$ (a complex number). Based on the above discussion, the following metric is adopted for the kth subcarrier with respect to $\mathcal{F}_i$:

$$P_{\mathcal{H}_k\to\mathcal{F}_i}(E_{\mathrm{MA}}) = Q\left(\frac{D^{(\mathcal{S})}_{\min}|H_1^{(k)}|}{\sqrt{2N_0}}\left|1-\frac{\gamma_k e^{j\theta_k}}{\mathcal{F}_i}\right|\right). \tag{3.29}$$

Taking into account all the subcarriers, one has

$$P_{\{\mathcal{H}_k\}_{k=1}^K\to\mathcal{F}_i}(E_{\mathrm{MA}}) = \frac{1}{K}\sum_{k=1}^{K} P_{\mathcal{H}_k\to\mathcal{F}_i}(E_{\mathrm{MA}}). \tag{3.30}$$

[1]There are 12 and 104 singular fade states for QPSK and 8PSK, respectively [49].

Then the singular fade state which causes the largest error probability is identified, i.e.,

$$\hat{i} = \arg \max_{i=1,2,\ldots,I} P_{\{\mathcal{H}_k\}_{k=1}^{K} \to \mathcal{F}_i}(E_{\mathrm{MA}}) \tag{3.31}$$

The optimal clustering that corresponds to the identified singular fade state is then selected. Note that [49] provides the clusterings and mapping tables for singular fade states of QPSK and 8PSK.

- *Method 3: Min-fade-distance*

Although Method 2 is much simpler than Method 1, its computation is still subcarrier-by-subcarrier. Next, we suggest another clustering method that works directly with the time-domain channel responses. Let vectors $\mathbf{h}_1$ and $\mathbf{h}_2$ represent the time-domain channel responses and $\boldsymbol{G}$ be the DFT matrix. The summation of the minimum distances squared over all the subcarriers can be computed as:

$$\sum_{k=1}^{K} \left| D_{\min}^{(k)}(i) \right|^2 = |\boldsymbol{G}\mathbf{h}_1 - \boldsymbol{G}\mathbf{h}_2/\mathcal{F}_i|^2 = |\mathbf{h}_1|^2 + |\mathbf{h}_2/\mathcal{F}_i|^2 - 2\Re\left\{\mathbf{h}_1^H \mathbf{h}_2/\mathcal{F}_i\right\}. \tag{3.32}$$

Then the singular fade state that yields the minimum sum is identified:

$$\hat{i} = \arg \min_{i=1,2,\ldots,I} \sum_{k=1}^{K} \left| D_{\min}^{(k)}(i) \right|^2 \tag{3.33}$$

Finally, the corresponding clustering is selected.

3.5 Simulation Results

This section evaluates performance of the proposed clustering selection criteria in terms of the terminal-to-terminal frame error rate (FER). The size of the fast Fourier transform (FFT) is $K = 256$ and the length of cyclic prefix is $N_c = 32$ samples. The channels of all links are modeled as quasi-static frequency-selective with $L = 3$ paths. The coefficients of the channel impulse responses follow a Rician fading distribution with the Rician factor K_f and exponential power delay profile:

$$p(t) = \frac{1}{\tau} \sum_{l=0}^{L-1} \mathrm{e}^{-t/\tau} \delta\left(t - lT_s\right), \tag{3.34}$$

where τ denotes the delay spread and T_s is the symbol duration. In our simulation, $\tau = T_s/2$ is used. At the receiver, ideal synchronization and channel estimation are assumed.

Figs. 3.3 and 3.4 show the FER performance of the proposed methods when the terminal nodes use QPSK. In addition to the three proposed methods, other two methods are evaluated and used as references. The curve marked with "XOR" corresponds to the standard method that the relay uses pure XOR regardless of the channel condition. The "Per-sub" curve is for the case that each subcarrier uses its own optimal clustering. It can be observed that the "Max-fade-SER" method has almost the same performance as the "Min-SER" method, although the former requires less computation complexity than the latter. At the FER level of 10^{-1}, both of these two proposed methods have 3dB and 6dB gains over the pure XOR method when the Rician factor equals to 1 and 10, respectively. On the other hand, the performance loss of the "Min-fade-distance" method is quite significant, although it has small performance advantage over the pure XOR method and it has very low computational complexity.

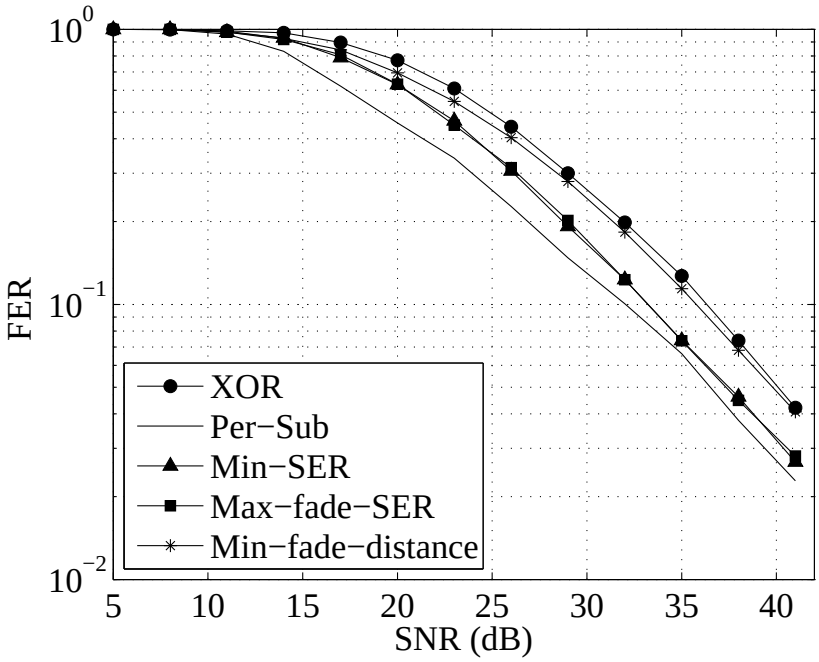

Figure 3.3 Terminal-to-terminal FER: QPSK, $K_f = 1$.

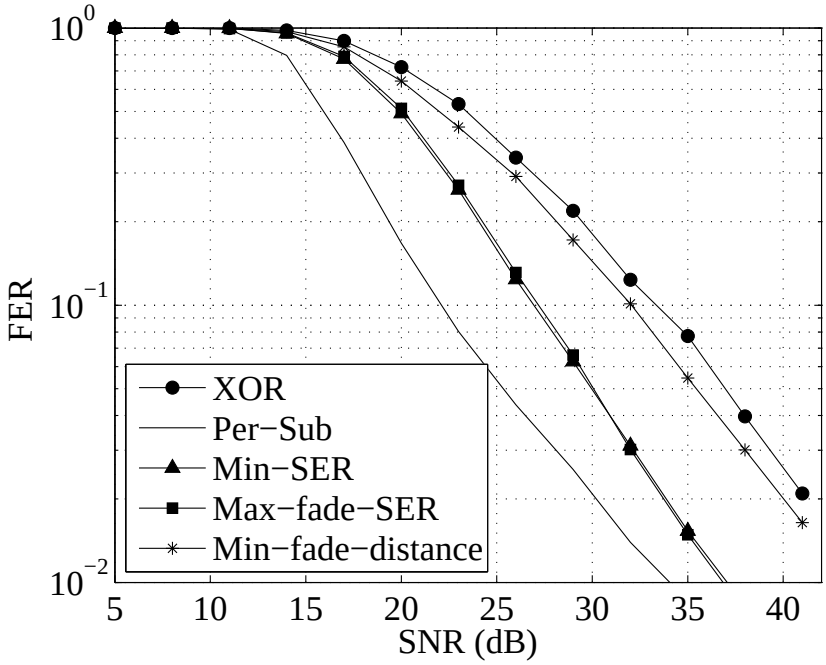

Figure 3.4 Terminal-to-terminal FER: QPSK, $K_f = 10$.

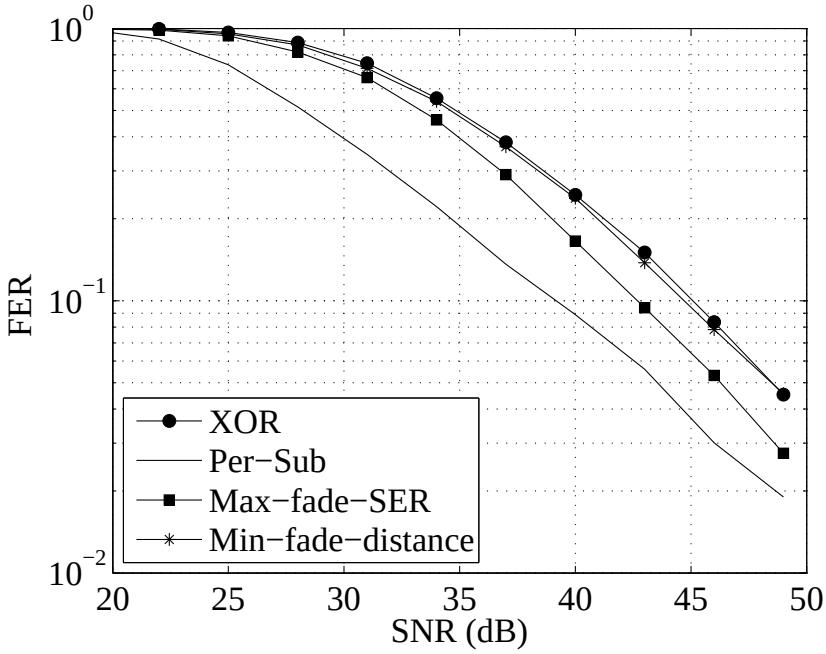

Figure 3.5 Terminal-to-terminal FER: 8PSK, $K_f = 1$.

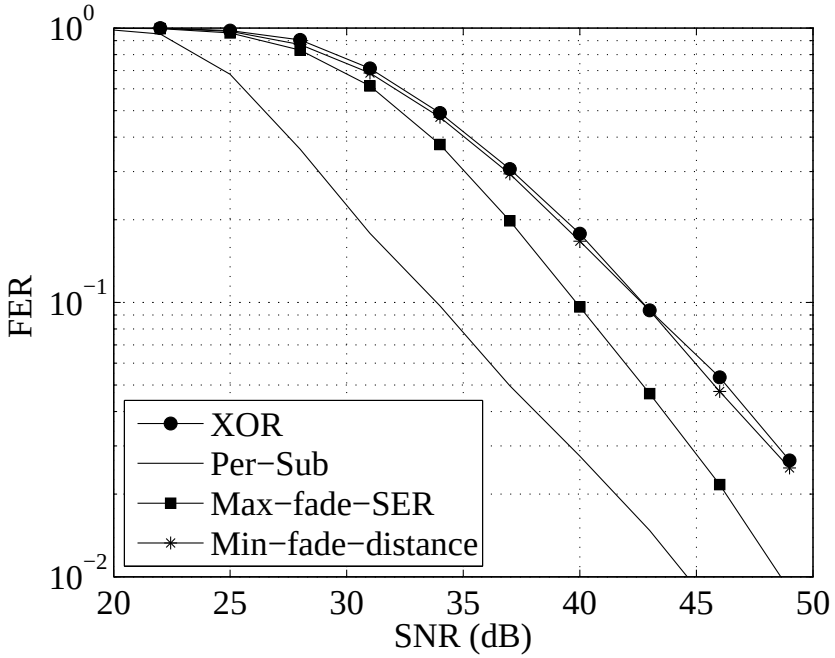

Figure 3.6 Terminal-to-terminal FER: 8PSK, $K_f = 10$.

Figs. 3.5 and 3.6 show the FER of the "Max-fade-SER" and "Min-fade-distance" methods, and the other methods when the terminal nodes use 8PSK. In QPSK, the "Max-fade-SER" method yields similar performance as the "Min-SER" method. However, the "Min-SER" method is very complicated when applied to for 8PSK and only the results obtained with the "Max-fade-SER" method are reported for 8PSK. It can be seen that, at the FER level of 10^{-1}, the "Max-fade-SER" method gives about 2dB and 3dB gains over the pure XOR method when the Rician factor equals to 1 and 10, respectively. On the other hand, for 8PSK, the "Min-fade-distance" method performs almost the same as the pure XOR method.

Considering the trade-off among performance, computation complexity and required overhead in the BC phase, the "Max-fade-SER" method is the most attractive method to obtain a common clustering for adaptive PNC in OFDM systems.

3.6 Conclusions

This paper is concerned with the application of adaptive PNC in OFDM systems. The error event in the multiple access (MA) phase is analyzed and an approximation of the error

probability for the MA phase is given. Three methods were proposed to find a common clustering for adaptive PNC in OFDM systems. Simulation results illustrate the performance of the proposed methods under different scenarios. From the analysis of error events in the MA phase and simulation results, it is concluded that the "Max-fade-SER" method is the most attractive clustering method for adaptive PNC in OFDM systems when considering the trade-off among performance, computational complexity and required overhead.

4. Distributed Precoding for OFDM in Two-Way Relaying Communications

The previous chapter investigated adaptive PNC to handle MAI in the MA phase of two-way relaying communications with OFDM. Adaptive PNC is effective to solve the distance shortening problem caused by MAI. However, adaptive PNC has the disadvantage that it needs to send the clustering information to the terminal nodes in the BC phase. As discussed in the previous chapter, the overhead in the BC phase is significant for an OFDM system with a large number of subcarriers. Using one clustering for all subcarriers minimizes the overhead but it also causes quite severe performance deterioration. Distributed space-time coding (DSTC) proposed in [39] is another approach to combat MAI. In fact DSTC is shown to achieve better performance in a high SNR region than adaptive PNC. In addition, DSTC requires no extra overhead in the BC phase.

The manuscript in this chapter studies the design of distributed precoding in the MA phase for TWRC system using OFDM. The distributed precoding has the similar form of DSTC and also does not require any extra overhead. Different from the conventional DSTC which only focuses on alleviating MAI in the MA phase, the distributed precoding proposed in this manuscript also aims to exploit the multipath diversity gains with OFDM. Specifically, the objective in this manuscript is to design a distributed precoding scheme which is able to handle MAI while achieving the maximum multipath diversity gain with OFDM. By analyzing the PEP in the MA system and introducing the three types of errors, the corresponding diversity and coding gains under different types of errors are derived. The conventional frequency-grouped linear constellation precoding (F-GLCP) is first examined and proved not able to achieve the maximum diversity gain under type-3 errors. Then,

frequency-time grouped linear constellation precoing (FT-GLCP) is proposed and theoretically proved to be able to achieve the maximum diversity gains under all three types of errors. Simulation results of different schemes in various fading channels are provided to verify the theoretic analysis and show the advantage of proposed FT-GLCP over other schemes.

The results of our studies on distributed precoding for OFDM in TWRC are reported in two manuscripts listed below. The journal paper [Ch4-2] is included in this chapter.

[Ch4-1] H. Yan, Ha H. Nguyen and J. Su, "Distributed Precoding for Two-Way Relaying with OFDM", *IEEE Int. Conf. Commun.*, Sydney, Australia, pp. 5432–5437, Jun. 2014.

[Ch4-2] H. Yan, Ha H. Nguyen and J. Su, "Distributed Precoding for OFDM in Two-Way Relaying Communications", *IEEE Trans. Veh. Technol.*, vol. 64, pp. 1930–1941, May 2015.

Distributed Precoding for OFDM in Two-Way Relaying Communications

Hongzhong Yan and Ha H. Nguyen and Jian Su

Abstract

This paper is concerned with the design of distributed precoding in the multiple access (MA) phase for two-way relaying communication (TWRC) systems using OFDM. The error probability analysis is conducted to establish the diversity and coding gains for three error types in the MA phase. Then the design criteria of distributed precoding to achieve the maximum diversity and coding gains are given. The frequency-grouped linear constellation precoding (F-GLCP) is first investigated and shown not to be able to achieve the maximum diversity gain under type-3 errors. A novel frequency-time GLCP (FT-GLCP) which performs precoding in both frequency and time domains is then proposed. It is proved that the proposed FT-GLCP is able to achieve the maximum diversity gain under type-3 errors, while maintaining the maximum diversity and coding gains under type-1 and type-2 errors. To corroborate the theoretical analysis, simulation results are provided to show the advantage of the proposed FT-GLCP over other schemes in both Rayleigh and Rician fading channels.

Index terms

Two-way relaying, OFDM, distributed precoding, diversity gain, coding gain.

4.1 Introduction

With the bi-directional transmission capability, two-way relaying communication (TWRC) systems have recently gained a strong interest in research community. Different protocols are proposed and analyzed in [46, 53, 54]. In these papers, the two-slot protocol is shown to provide capacity advantage over the conventional four-slot protocol as well as the three-slot protocol which is based on exclusive-OR (XOR) network coding [55]. In the first slot of

the two-slot protocol, the terminal nodes send their information to the relay node. This is also known as the multiple access (MA) phase. In the second slot, which is also called the broadcast (BC) phase, the relay node transmits the processed information back to the terminal nodes.

In designing the two-slot protocol, there are two problems that need to be addressed. One problem is how to combine the detected signals at the relay node. While XOR-based network coding is a simple approach to solve this problem at the bit level, other signal processing strategies have also been proposed in references [35, 36, 47]. In particular, the authors in [36] extend the *decode-and-forward* (DF) in one-way relay communications to TWRC in such a way that the relay broadcasts a linear combination of the detected signals. The authors in [35] study two versions of partial decode-and-forward (PDF) relaying. One PDF strategy combines the detected signals using weights that are determined by the channel responses. The other PDF performs a modular sum on the constellation indices of the detected signals and the obtained index is used to determine the broadcast signal. In addition, physical-layer network coding (PNC) is investigated in [47], which directly maps the received signal to a constellation symbol without first detecting signals from two terminal nodes. Since the focus of this paper is not on the design of a combining scheme, XOR-based network coding is adopted for its simplicity. The analysis performed and schemes designed in this paper are also applicable when other combining schemes mentioned above are employed.

The second problem is how to guarantee good detection quality in the MA phase. Two factors that influence the detection quality are multiple-access interference and channel fading. To handle multiple-access interference, *denoise-and-forward* (DNF) is proposed in [19, 20] which maps the close constellation pair in the MA phase to the same constellation point in the BC phase and thus avoids the influence of multiple-access interference. However, DNF has two main disadvantages: (i) high overhead in the BC phase in order to inform the denoising maps to the terminal nodes; and (ii) irregular constellation may need to be used in the BC phase which would cause performance degradation. It is recently demonstrated in [56] that DNF requires even larger overhead when combined with orthogonal frequency-division multiplexing (OFDM). This is because different channel responses in

different subcarriers require different denoising maps. Reference [56] also proposes a scheme to choose the best denoising map for all subcarriers which achieves a good trade-off between performance and complexity. More recently, the authors in [39] propose a scheme which uses distributed space-time coding (DSTC) at the terminal nodes to alleviate the influence of multiple-access interference instead of avoiding it. This scheme does not require any overhead in the BC phase and achieves better performance than DNF in high signal-to-noise ratio (SNR) region.

However, all of the schemes discussed above are mainly designed to handle multiple-access interference and they do not work well when one or more channels from the terminal nodes to the relay node are in deep fade. Exploiting diversity is an efficient way to reduce the influence of deep fading. In frequency-selective fading channels, multi-path diversity is an important source of diversity gain. On the other hand, OFDM is widely used in systems with frequency-selective fading channels because it is effective to combat inter-symbol interference (ISI) caused by the frequency-selective fading. In point-to-point communication systems using OFDM, schemes exploiting multi-path diversity gain have been well investigated [10, 15, 57]. Among these schemes, precoding-based schemes are easy to implement and able to achieve higher spectral efficiency compared to other schemes. The objective of this paper is to design a precoding-based scheme to efficiently exploit the multi-path diversity in TWRC systems using the two-slot protocol and OFDM. The design can also obtain cooperative diversity gain which is effective to alleviate the impact of the multiple-access interference on the detection performance.

This paper is organized as follows. The TWRC system using the two-slot protocol and OFDM is described in Section 4.2. Section 4.3 investigates the detection error probability in the MA phase under three error types. Then the design criteria regarding the diversity gains as well as the coding gains are given. The frequency-grouped linear constellation precoding (F-GLCP) [10, 58] is first analyzed and shown not to achieve the maximum diversity gain under type-3 errors. Then a novel frequency-time GLCP (FT-GLCP) is proposed in Section 4.4 and proved to achieve the maximum diversity gain under type-3 errors while maintaining the maximum diversity and coding gains under type-1 and type-2 errors. Section 4.5 provides

simulation results and conclusions are drawn in Section 4.6.

Notations: The complex number $\sqrt{-1}$ is denoted by j. The inverse, transpose, Hermitian transpose, rank, determinant, and trace of matrix $\boldsymbol{A}$ are denoted by $\boldsymbol{A}^{-1}$, $\boldsymbol{A}^T$, $\boldsymbol{A}^H$, $\mathrm{rank}\,(\boldsymbol{A})$, $\det(\boldsymbol{A})$ and $\mathrm{tr}\,(\boldsymbol{A})$, respectively. $\mathbf{0}_M$ is the length-M zero vector, $\mathbf{0}_{M\times N}$ is the $M \times N$ zero matrix and $\mathbf{I}_N$ is the $N \times N$ identity matrix. $\mathrm{diag}\,(\boldsymbol{a})$ denotes a diagonal matrix whose diagonal elements are from vector $\boldsymbol{a}$ and $\|\boldsymbol{a}\|_2$ denotes the Euclidean norm of vector $\boldsymbol{a}$.

4.2 System Model

The TWRC system under consideration has two terminal nodes, denoted as nodes $\mathbb{T}_1$ and $\mathbb{T}_2$, which exchange their information by the help of relay node $\mathbb{R}$. This information exchange happens in two phases. In the MA phase, both terminal nodes send their signal frames to the relay node. After processing the received signals, the relay node broadcasts a new signal frame in the BC phase.

In the MA phase, the multi-path channel from terminal node $\mathbb{T}_i$ to relay node $\mathbb{R}$ is represented by vector $\boldsymbol{h}_i = [h_i(1), \ldots, h_i(L_i)]^T$, where L_i is the number of channel taps, $i = 1, 2$. The components of a channel vector follow a joint complex Gaussian distribution with mean $\boldsymbol{\mu}_{\boldsymbol{h}_i}$ and covariance matrix $\boldsymbol{R}_{\boldsymbol{h}_i}$. The square root of matrix $\boldsymbol{R}_{\boldsymbol{h}_i}$, denoted by $\boldsymbol{B}_{\boldsymbol{h}_i}$, is assumed to be full rank.

Suppose that there are N subcarriers and M OFDM symbols in each signal frame. Let the mth OFDM symbol from terminal node $\mathbb{T}_i$ before precoding be $\boldsymbol{s}_{i,m} = [s_{i,m}(1), \ldots, s_{i,m}(N)]^T$, where each element belongs to a constellation set $\mathcal{S}$. The whole information frame is expressed as $\boldsymbol{S}_i = [\boldsymbol{s}_{i,1}, \ldots, \boldsymbol{s}_{i,M}]$ which contains $N \times M$ complex symbols. After precoding is performed on the whole information frame, the mth OFDM symbol is expressed as $\boldsymbol{x}_{i,m} = [x_{i,m}(1), \ldots, x_{i,m}(N)]^T$. At the relay node, the mth received OFDM symbol in the frequency domain is represented as $\boldsymbol{y}_m = [y_m(1), \ldots, y_m(N)]^T$. By letting $\boldsymbol{X}_{i,m} = \mathrm{diag}\,(\boldsymbol{x}_{i,m})$, $\boldsymbol{X}_i = [\boldsymbol{X}_{i,1}, \ldots, \boldsymbol{X}_{i,M}]^T$ and $\boldsymbol{y} = \left[\boldsymbol{y}_1^T, \ldots, \boldsymbol{y}_M^T\right]^T$, one has:

$$\boldsymbol{y} = \boldsymbol{X}_1\boldsymbol{W}_1\boldsymbol{h}_1 + \boldsymbol{X}_2\boldsymbol{W}_2\boldsymbol{h}_2 + \boldsymbol{\omega}_{\mathbb{R}}, \tag{4.1}$$

where $\boldsymbol{\omega}_{\mathbb{R}} \sim \mathcal{CN}\left(\mathbf{0}_{MN}, N_0\mathbf{I}_{MN}\right)$ is additive white Gaussian noise vector at the relay node, and $\boldsymbol{W}_i$ is the $N \times L_i$ truncated discrete Fourier transform (DFT) matrix with elements $\boldsymbol{W}_i\left(n,l\right) = \exp\left(\frac{-j2\pi(n-1)(l-1)}{N}\right)$. As usually, N_0 is the one-sided power spectral density of thermal noise at the terminal and relay nodes. By defining $\boldsymbol{X} = [\boldsymbol{X}_1 \quad \boldsymbol{X}_2]$, $\boldsymbol{h} = \begin{bmatrix}\boldsymbol{h}_1^T & \boldsymbol{h}_2^T\end{bmatrix}^T$ and $\boldsymbol{W} = \begin{pmatrix}\boldsymbol{W}_1 & \mathbf{0}_{N\times L_2} \\ \mathbf{0}_{N\times L_1} & \boldsymbol{W}_2\end{pmatrix}$, then (4.1) can be rewritten as:

$$\boldsymbol{y} = \boldsymbol{X}\boldsymbol{W}\boldsymbol{h} + \boldsymbol{\omega}_{\mathbb{R}}. \tag{4.2}$$

Let $\mathcal{X}\left(\boldsymbol{S}_1, \boldsymbol{S}_2\right) = \boldsymbol{X}$ denote the mapping from the information frames $(\boldsymbol{S}_1, \boldsymbol{S}_2)$ to $\boldsymbol{X}$, which includes precoding, diagonalization and combination of both terminal nodes' signals as described above. Then, based on the signal in (4.2), the relay node performs the maximum-likelihood (ML) detection to obtain the estimates of the information frames as:

$$\left(\boldsymbol{S}_1', \boldsymbol{S}_2'\right) = \arg \min_{(\boldsymbol{S}_1,\boldsymbol{S}_2)\in\mathcal{S}^{N\times M}\times\mathcal{S}^{N\times M}} \left\|\tilde{\boldsymbol{y}} - \mathcal{X}\left(\boldsymbol{S}_1, \boldsymbol{S}_2\right)\boldsymbol{W}\boldsymbol{h}\right\|_2^{\,2}, \tag{4.3}$$

The ML estimates are then demapped into information bits as $\boldsymbol{b}_{i,m}'(n) = \mathcal{M}^{-1}\left(s_{i,m}'(n)\right)$, where $\mathcal{M}^{-1}$ indicates the symbol-to-bits demapping function. The bit-wise XOR operation is then performed on the demapped bits and the resulting bits are mapped into a constellation point. That is, $u_m(n) = \mathcal{M}\left(\boldsymbol{b}_{1,m}'(n) \oplus \boldsymbol{b}_{2,m}'(n)\right)$, where $\mathcal{M}$ is the bits-to-symbol mapping function. The frame of the network-coded signal is represented as $\boldsymbol{U} = [\boldsymbol{u}_1, \ldots, \boldsymbol{u}_M]$, where $\boldsymbol{u}_m = \left[u_m\left(1\right), \ldots, u_m\left(N\right)\right]^T$.

In the BC phase, the channel from relay node $\mathbb{R}$ to terminal node $\mathbb{T}_i$ is represented by vector $\boldsymbol{g}_i = [g_i(1), \ldots, g_i(P_i)]^T$, where P_i is the number of channel taps and the corresponding mean vector, covariance matrix and its square root matrix are $\boldsymbol{\mu}_{\boldsymbol{g}_i}$, $\boldsymbol{R}_{\boldsymbol{g}_i}$ and $\boldsymbol{B}_{\boldsymbol{g}_i}$, respectively. Before being broadcast back to the terminal nodes, the network-coded signal is precoded and the mth OFDM symbol after precoding is $\boldsymbol{d}_m = \left[d_m\left(1\right), \ldots, d_m\left(N\right)\right]^T$. The corresponding mth received OFDM symbol in the frequency domain is represented by $\boldsymbol{z}_{i,m} = \left[z_{i,m}\left(1\right), \ldots, z_{i,m}\left(N\right)\right]^T$. By letting $\boldsymbol{D}_m = \mathrm{diag}\left(\boldsymbol{d}_m\right)$, $\boldsymbol{D} = \left[\boldsymbol{D}_1, \ldots, \boldsymbol{D}_M\right]^T$ and

$\boldsymbol{z}_i = \left[\boldsymbol{z}_{i,1}^T, \ldots, \boldsymbol{z}_{i,M}^T\right]^T$, one has

$$\boldsymbol{z}_i = \boldsymbol{D}\boldsymbol{F}_i\boldsymbol{g}_i + \boldsymbol{\omega}_i, \quad i \in \{1,2\}, \tag{4.4}$$

where $\boldsymbol{\omega}_i \sim \mathcal{CN}\left(\mathbf{0}_{MN}, N_0\mathbf{I}_{MN}\right)$ is additive white Gaussian noise vector, $\boldsymbol{F}_i$ is the $N \times P_i$ truncated DFT matrix with elements $\boldsymbol{F}_i\left(n,p\right) = \exp\left(\frac{-j2\pi(n-1)(p-1)}{N}\right)$.

Finally, the ML detection is performed at each terminal node to obtain:

$$\boldsymbol{u}_i' = \arg\min_{\boldsymbol{U}\in\mathcal{S}^{N\times M}} \left\|\boldsymbol{z}_i - \mathcal{D}\left(\boldsymbol{U}\right)\boldsymbol{F}_i\boldsymbol{g}_i\right\|_2^2, \quad i \in \{1,2\}, \tag{4.5}$$

where $\mathcal{D}$ is used to describe the function performed on the network-coded signal $\boldsymbol{U}$ at the relay node, which includes precoding and diagonalization operations. Terminal node $\mathbb{T}_i$ then demaps the ML detected symbol into bits and performs XOR operation with its own information bits to extract the information bits of the other terminal node.

Before closing this section, it is pointed out that the complexity of the ML detection in (4.3) appears to be high in general, but it is not the case when practical precoding of OFDM signals is implemented. This is because with OFDM transmission, precoding can be done jointly with subcarrier grouping. Specifically, the total N subcarriers are divided in $V = N/K$ disjoint groups such that each group has only K subcarriers, where K can be as small as the maximum number of multi-path channel components, i.e., is much smaller than N. Precoding is then performed independently across subcarriers in each group. For our proposed FT-GLCP scheme, the search space of the ML detection in (4.3) reduces to $\mathcal{S}^{K\times 2} \times \mathcal{S}^{K\times 2}$.

4.3 Performance Analysis in the MA Phase

As described in the previous section, precoding is performed in both the MA and BC phases. This section focuses on performance analysis of precoding in the MA phase. There are two reasons for this.

First, in the MA phase, the detection quality is influenced not only by fading but also by multiple-access interference due to simultaneous signal transmissions from two terminal

nodes. Multiple-access interference causes the phenomenon of *distance shortening* and deteriorates the detection performance [20,51]. Therefore, the error probability in the MA phase is typically much higher than that in the BC phase since the later is only affected by fading. Second, as far as transmitting and detecting the network-coded signals are concerned, signal processing in the BC phase is almost the same as that in point-to-point communication systems. As such, precoding design for the BC phase can directly follow existing designs for point-to-point communication systems.

Referring to (4.2) and (4.3), let $\boldsymbol{e} = \{(\boldsymbol{S}_1, \boldsymbol{S}_2) \to (\boldsymbol{S}_1', \boldsymbol{S}_2')\}$, where $(\boldsymbol{S}_1, \boldsymbol{S}_2) \neq (\boldsymbol{S}_1', \boldsymbol{S}_2')$, denote the error event that the relay node decodes $(\boldsymbol{S}_1, \boldsymbol{S}_2)$ erroneously to $(\boldsymbol{S}_1', \boldsymbol{S}_2')$. Focusing on the case of Rayleigh fading, i.e., $\boldsymbol{\mu}_{\boldsymbol{h}_i} = \boldsymbol{0}_{L_i}$, the channel response vector can be expressed as $\boldsymbol{h} = \boldsymbol{B}_{\boldsymbol{h}}\bar{\boldsymbol{h}}$ where elements in $\bar{\boldsymbol{h}}$ are i.i.d. zero-mean complex Gaussian variables with unit variance. By letting $\mathcal{X}(\boldsymbol{S}_1, \boldsymbol{S}_2) = \boldsymbol{X}$, $\mathcal{X}(\boldsymbol{S}_1', \boldsymbol{S}_2') = \boldsymbol{X}'$ and $\boldsymbol{\Lambda}_{\boldsymbol{e}} = \boldsymbol{X} - \boldsymbol{X}'$, the following upper bound on the conditional pairwise-error probability (PEP) can be obtained [42]:

$$P\left(\boldsymbol{e}|\bar{\boldsymbol{h}}\right) \leq \exp\left[-\frac{\bar{\boldsymbol{h}}^H \boldsymbol{B}_{\boldsymbol{h}}^H \boldsymbol{W}^H \boldsymbol{\Lambda}_{\boldsymbol{e}}^H \boldsymbol{\Lambda}_{\boldsymbol{e}} \boldsymbol{W} \boldsymbol{B}_{\boldsymbol{h}} \bar{\boldsymbol{h}}}{4N_0}\right] = \exp\left[-\frac{\bar{\boldsymbol{h}}^H \boldsymbol{\Psi}_{\boldsymbol{e}} \bar{\boldsymbol{h}}}{4N_0}\right], \tag{4.6}$$

where the $(L_1 + L_2) \times (L_1 + L_2)$ matrix $\boldsymbol{\Psi}_{\boldsymbol{e}}$ is $\boldsymbol{\Psi}_{\boldsymbol{e}} = \boldsymbol{B}_{\boldsymbol{h}}^H \boldsymbol{W}^H \boldsymbol{\Lambda}_{\boldsymbol{e}}^H \boldsymbol{\Lambda}_{\boldsymbol{e}} \boldsymbol{W} \boldsymbol{B}_{\boldsymbol{h}}$ with

$$\boldsymbol{B}_{\boldsymbol{h}} = \begin{pmatrix} \boldsymbol{B}_{\boldsymbol{h}_1} & \boldsymbol{0}_{L_1 \times L_2} \\ \boldsymbol{0}_{L_2 \times L_1} & \boldsymbol{B}_{\boldsymbol{h}_2} \end{pmatrix}.$$

Averaging the conditional PEP with respect to $\bar{\boldsymbol{h}}$, one obtains the following upper bound on the average PEP:

$$P(\boldsymbol{e}) \leq \left(\delta_{\boldsymbol{e},c} \frac{1}{4N_0}\right)^{-\delta_{\boldsymbol{e},d}}, \tag{4.7}$$

where $\delta_{\boldsymbol{e},d} = \operatorname{rank}(\boldsymbol{\Psi}_{\boldsymbol{e}})$ and $\delta_{\boldsymbol{e},c} = \left(\prod_{l=0}^{\operatorname{rank}(\boldsymbol{\Psi}_{\boldsymbol{e}})-1} \lambda_l\right)^{\frac{1}{\operatorname{rank}(\boldsymbol{\Psi}_{\boldsymbol{e}})}}$ with λ_l, $l = 0, \ldots, \operatorname{rank}(\boldsymbol{\Psi}_{\boldsymbol{e}}) - 1$, are the nonzero eigenvalues of $\boldsymbol{\Psi}_{\boldsymbol{e}}$.

Under the MAC of two terminal nodes, all the error events can be partitioned into 3 types of errors [59, 60]:

- Type-1 errors: $\mathcal{E}_1 = \{\boldsymbol{e} : \boldsymbol{S}_1 \neq \boldsymbol{S}_1', \boldsymbol{S}_2 = \boldsymbol{S}_2'\}$. For this error type, the signals from

terminal node $\mathbb{T}_1$ are erroneously detected at the relay node, while the signals from terminal node $\mathbb{T}_2$ are correctly detected.

- Type-2 errors: $\mathcal{E}_2 = \{\boldsymbol{e} : \boldsymbol{S}_1 = \boldsymbol{S}_1', \boldsymbol{S}_2 \neq \boldsymbol{S}_2'\}$. For this error type, the signals from terminal node $\mathbb{T}_2$ are erroneously detected at the relay node, while the signals from terminal node $\mathbb{T}_1$ are correctly detected.

- Type-3 errors: $\mathcal{E}_3 = \{\boldsymbol{e} : \boldsymbol{S}_1 \neq \boldsymbol{S}_1', \boldsymbol{S}_2 \neq \boldsymbol{S}_2'\}$. For this error type, signals from both terminal nodes are erroneously detected at the relay node.

It is noted that type-1 and type-2 errors are likely caused by channel fading while type-3 errors are likely caused by both channel fading and multiple access interference.

The total error probability can be expressed as:

$$P_{\boldsymbol{e}} = \sum_{\boldsymbol{e}\in\mathcal{E}_1} P\left(\boldsymbol{e}|\boldsymbol{e}\in\mathcal{E}_1\right) + \sum_{\boldsymbol{e}\in\mathcal{E}_2} P\left(\boldsymbol{e}|\boldsymbol{e}\in\mathcal{E}_2\right) + \sum_{\boldsymbol{e}\in\mathcal{E}_3} P\left(\boldsymbol{e}|\boldsymbol{e}\in\mathcal{E}_3\right) \tag{4.8}$$

Applying (4.7) for type-1 and type-2 errors, one has

$$P\left(\boldsymbol{e}|\boldsymbol{e}\in\mathcal{E}_i\right) \leq \left(\delta_{\boldsymbol{e},c,i}\frac{1}{4N_0}\right)^{-\delta_{\boldsymbol{e},d,i}}, \quad i\in\{1,2\}, \tag{4.9}$$

where $\delta_{\boldsymbol{e},d,i} = \text{rank}\left(\boldsymbol{\Psi}_{\boldsymbol{e},i}\right)$ and $\boldsymbol{\Psi}_{\boldsymbol{e},i} = \boldsymbol{B}_{\boldsymbol{h}_i}^H {\boldsymbol{W}_i}^H \boldsymbol{\Lambda}_{\boldsymbol{e},i}^H \boldsymbol{\Lambda}_{\boldsymbol{e},i} \boldsymbol{W}_i \boldsymbol{B}_{\boldsymbol{h}_i}$ with $\boldsymbol{\Lambda}_{\boldsymbol{e},i} = \boldsymbol{X}_i - \boldsymbol{X}_i'$. Likewise, for type-3 errors, one has

$$P\left(\boldsymbol{e}|\boldsymbol{e}\in\mathcal{E}_3\right) \leq \left(\delta_{\boldsymbol{e},c,3}\frac{1}{4N_0}\right)^{-\delta_{\boldsymbol{e},d,3}}, \tag{4.10}$$

where $\delta_{\boldsymbol{e},d,3} = \text{rank}\left(\boldsymbol{\Psi}_{\boldsymbol{e}}\right)$ and $\boldsymbol{\Psi}_{\boldsymbol{e}} = \boldsymbol{B}_{\boldsymbol{h}}^H \boldsymbol{W}^H \boldsymbol{\Lambda}_{\boldsymbol{e}}^H \boldsymbol{\Lambda}_{\boldsymbol{e}} \boldsymbol{W} \boldsymbol{B}_{\boldsymbol{h}}$.

If $\boldsymbol{\Psi}_{\boldsymbol{e},i}$ and $\boldsymbol{\Psi}_{\boldsymbol{e}}$ are of full rank, one has:

$$\begin{aligned}
\delta_{\boldsymbol{e},c,i} &= \left[\det\left(\boldsymbol{\Psi}_{\boldsymbol{e},i}\right)\right]^{\frac{1}{L_i}} = \left[\det\left(\boldsymbol{R}_{\boldsymbol{h}_i}\right)\right]^{\frac{1}{L_i}} \left[\det\left({\boldsymbol{W}_i}^H \boldsymbol{\Lambda}_{\boldsymbol{e},i}^H \boldsymbol{\Lambda}_{\boldsymbol{e},i} \boldsymbol{W}_i\right)\right]^{\frac{1}{L_i}}, \quad i\in\{1,2\} \\
\delta_{\boldsymbol{e},c,3} &= \left[\det\left(\boldsymbol{\Psi}_{\boldsymbol{e}}\right)\right]^{\frac{1}{L_1+L_2}} = \left[\det\left(\boldsymbol{R}_{\boldsymbol{h}}\right)\right]^{\frac{1}{L_1+L_2}} \left[\det\left(\boldsymbol{W}^H \boldsymbol{\Lambda}_{\boldsymbol{e}}^H \boldsymbol{\Lambda}_{\boldsymbol{e}} \boldsymbol{W}\right)\right]^{\frac{1}{L_1+L_2}},
\end{aligned} \tag{4.11}$$

Finally, the diversity and coding gains under each error type are defined as:

$$\delta_{d,i} := \min_{\forall \boldsymbol{e}\in\mathcal{E}_i, \boldsymbol{e}\neq\boldsymbol{0}} \delta_{\boldsymbol{e},d,i} \quad \text{and} \quad \delta_{c,i} := \min_{\forall \boldsymbol{e}\in\mathcal{E}_i, \boldsymbol{e}\neq\boldsymbol{0}} \delta_{\boldsymbol{e},c,i}, \quad i\in\{1,2,3\}. \tag{4.12}$$

It is pointed out that, for the case of Rician fading, the diversity gain has the same form as that of the Rayleigh fading case, whereas the coding gain is slightly different as it depends on the non-zero mean $\boldsymbol{\mu}_{\boldsymbol{h}_i}$ [42].

Obviously, larger diversity and coding gains lead to smaller error probabilities for all three types of errors. Therefore, to enhance the detection quality, the diversity and coding gains need to be maximized. On one hand, from the definition of the diversity gains and the size of $\boldsymbol{\Psi}_{\boldsymbol{e},1}$, $\boldsymbol{\Psi}_{\boldsymbol{e},2}$ and $\boldsymbol{\Psi}_{\boldsymbol{e}}$, the maximum diversity gains under three types of errors are $\max \delta_{d,1} = L_1$, $\max \delta_{d,2} = L_2$ and $\max \delta_{d,3} = L_1 + L_2$, respectively. On the other hand, the maximum coding gains that can be achieved depend on the specific precoding scheme employed and this will be investigated in detail in the following section. As mentioned, the objective of this paper is to design the precoding scheme which can achieve the maximum diversity and coding gains for all three types of errors. As can be seen from (4.9) and (4.10), the diversity gain is a more influential factor since it determines the slope of the error probability curve. As such, the diversity gain is considered first in the design and then the coding gain is optimized once the maximum diversity gain is achieved.

4.4 Precoding Design in Two-Way Relaying Communication Systems

4.4.1 Frequency-Grouped Linear Constellation Precoding

In point-to-point communication systems with OFDM, frequency GLCP (F-GLCP) was proposed [10] to achieve the maximum diversity and coding gains while maintaining acceptable complexity of the receiver. In F-GLCP, all N subcarriers are equally divided into V disjoint groups with K subcarriers in each group. LCP is performed separately in each group by using the following $Q \times Q$ rotation matrix as the precoding matrix:

$$\boldsymbol{\Theta} = \frac{1}{\beta} \begin{pmatrix} 1 & \alpha_1 & \dots & \alpha_1^{Q-1} \\ \vdots & \vdots & \ddots & \vdots \\ 1 & \alpha_Q & \dots & \alpha_Q^{Q-1} \end{pmatrix}, \tag{4.13}$$

where β is the normalization factor such that $\mathrm{tr}\left(\boldsymbol{\Theta}\boldsymbol{\Theta}^H\right) = Q$. The parameters $\{\alpha_q\}$, $1 \leq q \leq Q$, are chosen according to the following rules for different values of Q [10]:

- If Q is an Euler number, i.e., $Q \in \mathcal{Q}_1 := \{\eta(Z) : Z \neq 0 \mod 4\}$, where $\eta(Z)$ is the number of positive integers less than Z and relatively prime to Z, then $\{\alpha_q\}$ are the roots of $\eta(x) = \prod_{z\in\mathcal{Z}} (x - \exp(j2\pi z/Z))$, and $\mathcal{Z} := \{1 \leq z \leq Z : \gcd(z, Z) = 1\}$.

- If Q is a power of 2, i.e., $Q \in \mathcal{Q}_2 := \{2^z : z \text{ is an integer}\}$, then $\{\alpha_q\}$ are the roots of $x^Q - \sqrt{-1} = 0$.

- If $Q \notin \mathcal{Q} = \mathcal{Q}_1 \cup \mathcal{Q}_2$, then $\{\alpha_q\}$ are the roots of $x^Q - \left(1 + \sqrt{-1}\right) = 0$.

It is proved in [10] that if Q is larger than the number of channel taps, the maximum diversity gain is achieved. Furthermore, if $Q \in \mathcal{Q}$, the maximum coding gain is achieved. Otherwise, if $Q \notin \mathcal{Q}$, at least 70% of the maximum coding gain is achieved.

In addition, as proved in [10, 58], to guarantee the maximum diversity and coding gains in a point-to-point communication system, the indices of the K subcarriers belonging to the vth group are $\mathcal{I}_v = \{v, V + v, \ldots, (K - 1)V + v\}$, i.e., *interleaved* subcarrier grouping.

Next, the diversity and coding gains achieved by F-GLCP are analyzed for TWRC systems. Since subcarrier grouping is used, the system model for F-GLCP in TWRC systems can be examined by focusing on the vth group (all other groups experience the same signal processing). In the MA phase, the information symbols in the subcarriers of the vth group from terminal $\mathbb{T}_i$ are $\boldsymbol{S}_i^{(v)} = \left[\boldsymbol{s}_{i,1}^{(v)}, \ldots, \boldsymbol{s}_{i,M}^{(v)}\right]$, where

$$\boldsymbol{s}_{i,m}^{(v)} = \left[s_{i,m}(v), s_{i,m}(V + v), \ldots, s_{i,m}((K - 1)V + v)\right]^T, \quad i \in \{1, 2\}.$$

The LCP is then applied as follows:

$$\boldsymbol{x}_{i,m}^{(v)} = \boldsymbol{\Theta}_i \boldsymbol{s}_{i,m}^{(v)}, \quad i \in \{1, 2\}, \tag{4.14}$$

where both $\boldsymbol{\Theta}_1$ and $\boldsymbol{\Theta}_2$ are the rotation matrix in (4.13) with $Q = K$.

By defining $\boldsymbol{X}_{i,m}^{(v)} = \mathrm{diag}\left(\boldsymbol{x}_{i,m}^{(v)}\right)$, $\boldsymbol{X}_i^{(v)} = \left[\boldsymbol{X}_{i,1}^{(v)}, \ldots, \boldsymbol{X}_{i,M}^{(v)}\right]^T$, $\boldsymbol{X}^{(v)} = \left[\boldsymbol{X}_1^{(v)} \quad \boldsymbol{X}_2^{(v)}\right]$ and the $K \times L_i$ truncated DFT matrix $\boldsymbol{W}_i^{(v)}$ with $\boldsymbol{W}_i^{(v)}(k, l) = \exp\left(\frac{-j2\pi((k-1)V+v)(l-1)}{N}\right)$, the

following input-output equation, in a similar form as (4.2), is obtained:

$$\boldsymbol{y}^{(v)} = \boldsymbol{X}^{(v)}\boldsymbol{W}^{(v)}\boldsymbol{h} + \boldsymbol{z}_{\mathbb{R}}^{(v)}, \tag{4.15}$$

where $\boldsymbol{y}^{(v)}$ and $\boldsymbol{z}_{\mathbb{R}}^{(v)}$ are obtained from $\boldsymbol{y}$ and $\boldsymbol{z}_{\mathbb{R}}$ by extracting the symbols in the subcarriers of the vth group and

$$\boldsymbol{W}^{(v)} = \begin{pmatrix} \boldsymbol{W}_1^{(v)} & \boldsymbol{0}_{K\times L_2} \\ \boldsymbol{0}_{K\times L_1} & \boldsymbol{W}_2^{(v)} \end{pmatrix}$$

To analyze the diversity and coding gains of F-GLCP under three types of errors, define the error event $\boldsymbol{e}^{(v)} = \left\{ \left(\boldsymbol{S}_1^{(v)}, \boldsymbol{S}_2^{(v)} \right) \to \left(\boldsymbol{S'}_1^{(v)}, \boldsymbol{S'}_2^{(v)} \right) \right\}$. Then one has

$$\boldsymbol{\Lambda}_{\boldsymbol{e}^{(v)},i,m} = \boldsymbol{X}_{i,m}^{(v)} - \boldsymbol{X'}_{i,m}^{(v)} = \mathrm{diag}\left(\boldsymbol{\Theta}_i \left(\boldsymbol{s}_{i,m}^{(v)} - \boldsymbol{s'}_{i,m}^{(v)} \right) \right) \tag{4.16}$$

and

$$\boldsymbol{\Lambda}_{\boldsymbol{e}^{(v)},i} = \boldsymbol{X}_{i}^{(v)} - \boldsymbol{X'}_{i}^{(v)} = \left[\boldsymbol{\Lambda}_{\boldsymbol{e}^{(v)},i,1}, \ldots, \boldsymbol{\Lambda}_{\boldsymbol{e}^{(v)},i,M} \right]^T. \tag{4.17}$$

As far as type-1 and type-2 errors are concerned, the error performance behaves the same as in point-to-point communication systems. It follows that F-GLCP can achieve the maximum diversity and coding gains of $\delta_{d,i} = L_i$ and $\delta_{c,i} = \left[\det\left(\boldsymbol{R}_{\boldsymbol{h}_i}\right)\right]^{\frac{1}{L_i}} \Delta_{\min}^2$ [10], respectively, where $\Delta_{\min}$ is the minimum Euclidean distance among constellation points in $\mathcal{S}$.

For type-3 errors, as mentioned in Section 4.3, the (inherent) maximum diversity gain is $L_1 + L_2$. However, as stated in the following theorem, using F-GLCP can only achieve a diversity gain of $\max(L_1, L_2)$.

Theorem 1 *The maximum diversity gain that F-GLCP can achieve under type-3 errors in the MA phase is* $\delta_{d,3} = \max(L_1, L_2)$, *as long as* $K \geq \max(L_1, L_2)$.

Proof: Let m_1 and m_2 be the symbol indices of signals transmitted from $\mathbb{T}_1$ and $\mathbb{T}_2$, respectively. According to the definition of type-3 errors, $\boldsymbol{S}_1^{(v)} - \boldsymbol{S'}_1^{(v)}$ and $\boldsymbol{S}_2^{(v)} - \boldsymbol{S'}_2^{(v)}$ are both non-zero. Since $\boldsymbol{S}_1^{(v)}$ and $\boldsymbol{S}_2^{(v)}$ consist of $\boldsymbol{s}_{1,m_1}^{(v)}$ and $\boldsymbol{s}_{2,m_2}^{(v)}$, respectively, there must exist non-zero vectors $\boldsymbol{s}_{1,m_1}^{(v)} - \boldsymbol{s'}_{1,m_1}^{(v)}$ and $\boldsymbol{s}_{2,m_2}^{(v)} - \boldsymbol{s'}_{2,m_2}^{(v)}$. According to (4.16) and the properties

of LCP rotation matrix, for all type-3 errors, there must exist $K \times K$ diagonal matrices $\mathbf{\Lambda}_{\boldsymbol{e}^{(v)},1,m_1}$ and $\mathbf{\Lambda}_{\boldsymbol{e}^{(v)},2,m_2}$ whose diagonal elements are all non-zero.

Without loss of generality, assume that $L_2 \geq L_1$. Then $\boldsymbol{W}_2^{(v)}$ is a truncated DFT matrix with size $K \times L_2$ and $K \geq L_2$. Therefore rank $\left(\boldsymbol{W}_2^{(v)}\right) = L_2$. In addition, since $\mathbf{\Lambda}_{\boldsymbol{e}^{(v)},2,m_2}$ is a $K \times K$ diagonal matrix whose diagonal elements are all non-zero, one has rank $\left(\mathbf{\Lambda}_{\boldsymbol{e}^{(v)},2,m_2}\boldsymbol{W}_2^{(v)}\right) = L_2$.

Since $\mathbf{\Lambda}_{\boldsymbol{e}^{(v)},2,m_2}\boldsymbol{W}_2^{(v)}$ is a submatrix of $\mathbf{\Lambda}_{\boldsymbol{e}^{(v)}}\boldsymbol{W}^{(v)}$, it follows that rank $\left(\mathbf{\Lambda}_{\boldsymbol{e}^{(v)}}\boldsymbol{W}^{(v)}\right) \geq L_2$. Furthermore, because $\boldsymbol{B_h}$ is a full-rank square matrix, one has

$$\text{rank}\left(\mathbf{\Psi}_{\boldsymbol{e}^{(v)}}\right) = \text{rank}\left(\mathbf{\Lambda}_{\boldsymbol{e}^{(v)}}\boldsymbol{W}^{(v)}\boldsymbol{B_h}\right) = \text{rank}\left(\mathbf{\Lambda}_{\boldsymbol{e}^{(v)}}\boldsymbol{W}^{(v)}\right) \geq L_2. \tag{4.18}$$

Next consider the special case of type-3 errors where $m_1 = m_2 = m$. In addition, except for the non-zero submatrix $\mathbf{\Lambda}_{\boldsymbol{e}^{(v)},m} = \begin{bmatrix}\mathbf{\Lambda}_{\boldsymbol{e}^{(v)},1,m} & \mathbf{\Lambda}_{\boldsymbol{e}^{(v)},2,m}\end{bmatrix}$, other parts of $\mathbf{\Lambda}_{\boldsymbol{e}^{(v)}}$ are all zeros. Accordingly, with $\mathbf{\Psi}_{\boldsymbol{e}^{(v)},m} = \boldsymbol{B}_{\boldsymbol{h}}^H(\boldsymbol{W}^{(v)})^H\mathbf{\Lambda}_{\boldsymbol{e}^{(v)},m}^H\mathbf{\Lambda}_{\boldsymbol{e}^{(v)},m}\boldsymbol{W}^{(v)}\boldsymbol{B_h}$, one has

$$\text{rank}\left(\mathbf{\Psi}_{\boldsymbol{e}^{(v)}}\right) = \text{rank}\left(\mathbf{\Psi}_{\boldsymbol{e}^{(v)},m}\right) = \text{rank}\left(\boldsymbol{A}_{\boldsymbol{e}^{(v)},m}\right), \tag{4.19}$$

where $\boldsymbol{A}_{\boldsymbol{e}^{(v)},m} = \mathbf{\Lambda}_{\boldsymbol{e}^{(v)},m}\boldsymbol{W}^{(v)} = \begin{bmatrix}\mathbf{\Lambda}_{\boldsymbol{e}^{(v)},1,m}\boldsymbol{W}_1^{(v)} & \mathbf{\Lambda}_{\boldsymbol{e}^{(v)},2,m}\boldsymbol{W}_2^{(v)}\end{bmatrix}$.

It is known from the system model that $\boldsymbol{W}_1^{(v)}$ and $\boldsymbol{W}_2^{(v)}$ have L_1 identical columns. Furthermore, for the specific error event that causes $\mathbf{\Lambda}_{\boldsymbol{e}^{(v)},1,m} = \mathbf{\Lambda}_{\boldsymbol{e}^{(v)},2,m}$, it follows that matrix $\mathbf{\Lambda}_{\boldsymbol{e}^{(v)},1,m}\boldsymbol{W}_1^{(v)}$ and $\mathbf{\Lambda}_{\boldsymbol{e}^{(v)},2,m}\boldsymbol{W}_2^{(v)}$ have L_1 identical columns. Therefore, rank $\left(\boldsymbol{A}_{\boldsymbol{e}^{(v)},m}\right) = L_2$. Combing this result with (4.18), and according to the definition of the diversity gain, one has $\delta_{d,3} = L_2$. Similarly, in the case that $L_1 \geq L_2$, it can be shown that $\delta_{d,3} = L_1$. Therefore, $\delta_{d,3} = \max(L_1, L_2)$. ■

4.4.2 Frequency-Time Grouped Linear Constellation Precoding

It is recognized from the proof of Theorem 1 that the rank deficiency of $\boldsymbol{A}_{\boldsymbol{e}^{(v)},m}$ is the main reason that F-GLCP cannot achieve the maximum diversity gain under type-3 errors. Observing that $\boldsymbol{A}_{\boldsymbol{e}^{(v)},m}$ depends on $\mathbf{\Lambda}_{\boldsymbol{e}^{(v)},m}$ and $\boldsymbol{W}^{(v)}$, two strategies can be considered to solve this rank deficiency problem. One strategy is to change the form of $\boldsymbol{W}^{(v)}$. For example,

by adding a proper cyclic delay [11] at one of the terminal nodes, all columns of $\boldsymbol{W}_1^{(v)}$ and $\boldsymbol{W}_2^{(v)}$ can be guaranteed to be independent. Then if $\boldsymbol{\Lambda}_{\boldsymbol{e}^{(v)},1,m} = \boldsymbol{\Lambda}_{\boldsymbol{e}^{(v)},2,m}$, $\boldsymbol{A}_{\boldsymbol{e}^{(v)},m}$ will be column independent and the maximum diversity gain can be achieved. However, in a TWRC system, it is possible that $\boldsymbol{\Lambda}_{\boldsymbol{e}^{(v)},1,m} \neq \boldsymbol{\Lambda}_{\boldsymbol{e}^{(v)},2,m}$. Therefore adding a cyclic delay is not good enough and joint optimization on both rotation matrices and $\boldsymbol{W}^{(v)}$ is required. Such joint optimization appears to be difficult and will not be pursued in this paper. Another strategy is to manipulate $\boldsymbol{\Lambda}_{\boldsymbol{e}^{(v)},m}$. Since it is determined by $\boldsymbol{\Theta}_1$ and $\boldsymbol{\Theta}_2$, intuitively, one would consider using different rotation matrices at the two terminal nodes. However, in optimizing $\boldsymbol{\Theta}_1$ and $\boldsymbol{\Theta}_2$ based on the F-GLCP framework, the influence of $\boldsymbol{W}^{(v)}$ needs to be considered, which leads to complicated joint optimization similar to what just discussed above.

Our approach is to consider adjacent OFDM symbols and perform precoding in both frequency and time domains. In this way $\boldsymbol{\Theta}_1$ and $\boldsymbol{\Theta}_2$ can be easily designed without considering $\boldsymbol{W}^{(v)}$ (Theorem 3 gives the mathematical explanation for this). In designing $\boldsymbol{\Theta}_1$ and $\boldsymbol{\Theta}_2$, only one parameter γ needed to be adjusted to achieve the maximum diversity gain under all types of errors. This scheme shall be called *frequency-time* GLCP (FT-GLCP) to distinguish it with the F-GLCP discussed before.

Specifically, the proposed FT-GLCP is performed on the information data in one subcarrier group and over two adjacent OFDM symbols. It is mathematically described as,

$$\begin{array}{l} \begin{pmatrix} \boldsymbol{x}_{1,2m'-1}^{(v)} \\ \boldsymbol{x}_{1,2m'}^{(v)} \end{pmatrix} = \boldsymbol{\Theta}_1 \begin{pmatrix} \boldsymbol{s}_{1,2m'-1}^{(v)} \\ \boldsymbol{s}_{1,2m'}^{(v)} \end{pmatrix}, \ m' = 1, \ldots, M/2, \\ \\ \begin{pmatrix} \boldsymbol{x}_{2,2m'-1}^{(v)} \\ \boldsymbol{x}_{2,2m'}^{(v)} \end{pmatrix} = \boldsymbol{\Theta}_2 \begin{pmatrix} \boldsymbol{s}_{2,2m'-1}^{(v)} \\ \boldsymbol{s}_{2,2m'}^{(v)} \end{pmatrix}, \ m' = 1, \ldots, M/2, \end{array} , \tag{4.20}$$

where $\boldsymbol{\Theta}_1$ is a rotation matrix as defined in (4.13) with $Q = 2K$, and m' is the pair index for two adjacent OFDM symbols taken in the joint precoding operation. The rotation matrix $\boldsymbol{\Theta}_2$ is defined as

$$\boldsymbol{\Theta}_2 = \boldsymbol{\Theta}_1 \begin{pmatrix} \mathbf{I}_K & \mathbf{0}_{K\times K} \\ \mathbf{0}_{K\times K} & \gamma \mathbf{I}_K \end{pmatrix} \tag{4.21}$$

where γ is a parameter that can be adjusted. How to set the value of γ is discussed in the

following.

For convenience of further analysis, define $\phi_{i,2m'-1}^{(v)}(k) = x_{i,2m'-1}^{(v)}(k) - x'^{(v)}_{i,2m'-1}(k)$ and $\phi_{i,2m'}^{(v)}(k) = x_{i,2m'}^{(v)}(k) - x'^{(v)}_{i,2m'}(k)$. According to equation (4.20), one has

$$\begin{aligned}
\phi_{i,2m'-1}^{(v)}(k) &= \boldsymbol{\theta}_i^{(k)} \begin{pmatrix} \boldsymbol{s}_{i,2m'-1}^{(v)} - \boldsymbol{s}'^{(v)}_{i,2m'-1} \\ \boldsymbol{s}_{i,2m'}^{(v)} - \boldsymbol{s}'^{(v)}_{i,2m'} \end{pmatrix}, \\
\phi_{i,2m'}^{(v)}(k) &= \boldsymbol{\theta}_i^{(k+K)} \begin{pmatrix} \boldsymbol{s}_{i,2m'-1}^{(v)} - \boldsymbol{s}'^{(v)}_{i,2m'-1} \\ \boldsymbol{s}_{i,2m'}^{(v)} - \boldsymbol{s}'^{(v)}_{i,2m'} \end{pmatrix},
\end{aligned} \tag{4.22}$$

where $\boldsymbol{\theta}_i^{(k)}$ denotes the kth row of $\boldsymbol{\Theta}_i$.

In addition, since $\boldsymbol{\Lambda}_{\boldsymbol{e}^{(v)},i,2m'-1} = \boldsymbol{X}_{\boldsymbol{e}^{(v)},i,2m'-1} - \boldsymbol{X'}_{\boldsymbol{e}^{(v)},i,2m'-1}$ and $\boldsymbol{\Lambda}_{\boldsymbol{e}^{(v)},i,2m'} = \boldsymbol{X}_{\boldsymbol{e}^{(v)},i,2m'} - \boldsymbol{X'}_{\boldsymbol{e}^{(v)},i,2m'}$, one has:

$$\begin{aligned}
\boldsymbol{\Lambda}_{\boldsymbol{e}^{(v)},i,2m'-1} &= \mathrm{diag}\left(\left[\phi_{i,2m'-1}^{(v)}(1), \phi_{i,2m'-1}^{(v)}(2), \cdots, \phi_{i,2m'-1}^{(v)}(K)\right]\right), \\
\boldsymbol{\Lambda}_{\boldsymbol{e}^{(v)},i,2m'} &= \mathrm{diag}\left(\left[\phi_{i,2m'}^{(v)}(1), \phi_{i,2m'}^{(v)}(2), \cdots, \phi_{i,2m'}^{(v)}(K)\right]\right).
\end{aligned} \tag{4.23}$$

Under type-1 and type-2 errors, with some restrictions on K and λ, the proposed FT-GLCP achieves the maximum diversity gain and coding gain. This is proved in the following theorem. **Theorem 2** *If $K \geq \max(L_1, L_2)$ and $2K \in \mathcal{Q}$, the proposed FT-GLCP achieves $\delta_{d,1} = L_1$ and $\delta_{c,1} \geq [\det(\boldsymbol{R}_{\boldsymbol{h}_1})]^{\frac{1}{L_1}} \Delta_{\min}^2$. Furthermore, if $|\gamma| = 1$, FT-GLCP achieves $\delta_{d,2} = L_2$ and $\delta_{c,2} \geq [\det(\boldsymbol{R}_{\boldsymbol{h}_2})]^{\frac{1}{L_2}} \Delta_{\min}^2$.*

Proof: First, the following lemma is needed, whose proof is given in Appendix 4.A.

Lemma 1 *$\boldsymbol{A}$ is a $K \times L$ truncated DFT matrix and its row indices followsthe rule for subcarrier grouping described in Section 4.4. $\boldsymbol{\Xi}$ is a $K \times K$ diagonal matrix with positive elements $\xi_1, \xi_2, \ldots, \xi_K$. Then if $K \geq L$, the following inequality holds true:*

$$\det\left(\boldsymbol{A}^H \boldsymbol{\Xi} \boldsymbol{A}\right) \geq K^L \left(\prod_{k=1}^{K} \xi_k\right)^{\frac{L}{K}}. \tag{4.24}$$

Next, consider type-1 errors. One has:

$$\boldsymbol{\Lambda}_{\boldsymbol{e}^{(v)},1}^{H}\boldsymbol{\Lambda}_{\boldsymbol{e}^{(v)},1} = \begin{pmatrix} \Phi_1 & 0 & \dots & 0 \\ 0 & \Phi_2 & \dots & 0 \\ \vdots & \vdots & \ddots & \vdots \\ 0 & 0 & \dots & \Phi_K \end{pmatrix}, \tag{4.25}$$

where, according to equation (4.17) and (4.23), $\Phi_k = \sum_{m'=1}^{M/2}\left(|\phi_{1,2m'-1}^{(v)}(k)|^2 + |\phi_{1,2m'}^{(v)}(k)|^2\right)$.

With $K \geq \max(L_1, L_2)$, it follows from Lemma 1 that

$$\det\left((\boldsymbol{W}_1^{(v)})^H\boldsymbol{\Lambda}_{\boldsymbol{e}^{(v)},1}^{H}\boldsymbol{\Lambda}_{\boldsymbol{e}^{(v)},1}\boldsymbol{W}_1^{(v)}\right) \geq K^{L_1}\left(\prod_{k=1}^{K}\Phi_k\right)^{\frac{L_1}{K}}. \tag{4.26}$$

From the definition of type-1 errors, there must exist non-zero vector $\boldsymbol{s}_{1,2m'-1}^{(v)} - \boldsymbol{s}'^{(v)}_{1,2m'-1}$ or $\boldsymbol{s}_{1,2m'}^{(v)} - \boldsymbol{s}'^{(v)}_{1,2m'}$. Then according to the property of LCP rotation matrix and equations (4.22)-(4.23), there must exist two diagonal matrices $\boldsymbol{\Lambda}_{\boldsymbol{e}^{(v)},1,2m'-1}$ and $\boldsymbol{\Lambda}_{\boldsymbol{e}^{(v)},1,2m'}$ whose diagonal elements are all non-zero.

Applying Jensen's inequality, one obtains

$$\prod_{k=1}^{K}(\Phi_k) \geq \prod_{k=1}^{K}\left(|\phi_{1,2m'-1}^{(v)}(k)|^2 + |\phi_{1,2m'}^{(v)}(k)|^2\right) \geq 2^K\prod_{k=1}^{K}\left(|\phi_{1,2m'-1}^{(v)}(k)||\phi_{1,2m'}^{(v)}(k)|\right). \tag{4.27}$$

Since $\phi_{1,2m'-1}^{(v)}(k)$ and $\phi_{1,2m'}^{(v)}(k)$, $k = 1, \dots, K$, are generated from the same finite algebraic extension by using one $2K \times 2K$ rotation matrix $\boldsymbol{\Theta}_1$ (4.20), with $2K \in \mathcal{Q}$, it is known from [10] that

$$\prod_{k=1}^{K}\left(|\phi_{1,2m'-1}^{(v)}(k)||\phi_{1,2m'}^{(v)}(k)|\right) \geq \left(\frac{\Delta_{\min}}{\sqrt{2K}}\right)^{2K} = \left(\frac{\Delta_{\min}^2}{2K}\right)^{K}. \tag{4.28}$$

Combining (4.26), (4.27) and (4.28) gives

$$\det\left((\boldsymbol{W}_1^{(v)})^H\boldsymbol{\Lambda}_{\boldsymbol{e}^{(v)},1}^{H}\boldsymbol{\Lambda}_{\boldsymbol{e}^{(v)},1}\boldsymbol{W}_1^{(v)}\right) \geq (\Delta_{\min})^{2L_1}. \tag{4.29}$$

Therefore, for all type-1 errors, one has $\delta_{c,1} \geq [\det(\boldsymbol{R}_{\boldsymbol{h}_1})]^{\frac{1}{L_1}}\Delta_{\min}^2$, which shows the maximum coding gain is achieved. Furthermore, since $\boldsymbol{R}_{\boldsymbol{h}_1}$ is of full rank and the determinant in (4.29) is non-zero, $\boldsymbol{\Psi}_{\boldsymbol{e},1}$ is guaranteed to be of full rank, which means that $\delta_{d,1} = L_1$.

Under type-2 errors, the derivations of the diversity and coding gains are similar to that under type-1 errors. However, due to the existence of γ, $\boldsymbol{\Theta}_2$ is not a standard form of LCP rotation matrix and the following inequality may not hold.

$$\prod_{k=1}^{K}\left(|\phi_{2,2m'-1}^{(v)}(k)||\phi_{2,2m'}^{(v)}(k)|\right) \geq \left(\frac{\Delta_{\min}^2}{2K}\right)^K. \tag{4.30}$$

According to the structure of $\boldsymbol{\Theta}_2$, one can express $\phi_{2,2m'-1}^{(v)}(k)$ and $\phi_{2,2m'}^{(v)}(k)$ as

$$\begin{aligned}
\phi_{2,2m'-1}^{(v)}(k) &= \boldsymbol{\theta}_1^{(k)}\begin{pmatrix}\boldsymbol{s}_{2,2m'-1}^{(v)} - \boldsymbol{s'}_{2,2m'-1}^{(v)} \\ \boldsymbol{s}_{2,2m'}^{(v)} - \boldsymbol{s'}_{2,2m'}^{(v)}\end{pmatrix}, \\
\phi_{2,2m'}^{(v)}(k) &= \gamma\boldsymbol{\theta}_1^{(k+K)}\begin{pmatrix}\boldsymbol{s}_{2,2m'-1}^{(v)} - \boldsymbol{s'}_{2,2m'-1}^{(v)} \\ \boldsymbol{s}_{2,2m'}^{(v)} - \boldsymbol{s'}_{2,2m'}^{(v)}\end{pmatrix},
\end{aligned} \tag{4.31}$$

It is observed that the absolute values of $\phi_{2,2m'-1}^{(v)}(k)$ and $\phi_{2,2m'}^{(v)}(k)$ are involved in (4.30). Thus, if γ is chosen to have unit magnitude, the influence of γ disappears. Then by using (4.31), $\phi_{2,2m'-1}^{(v)}(k)$ and $\phi_{2,2m'}^{(v)}(k)$ also can be considered as being generated by $\boldsymbol{\Theta}_1$. Therefore, according to the properties of LCP rotation matrix [10], the inequality in (4.30) holds and one can show that $\delta_{c,2} \geq [\det(\boldsymbol{R}_{\boldsymbol{h}_2})]^{\frac{1}{L_1}}\Delta_{\min}^2$ and $\delta_{d,2} = L_2$, i.e., the maximum diversity and coding gains are also achieved under type-2 errors. ■

Finally, the diversity performance of the proposed FT-GLCP under type-3 errors is stated in the following theorem.

Theorem 3 *Under type-3 errors, if γ is a transcendental number and $2K \geq L_1 + L_2$, the proposed FT-GLCP achieves $\delta_{d,3} = L_1 + L_2$.*

Proof: Let m_i' denotes the pair index of the adjacent OFDM symbols transmitted from $\mathbb{T}_i$. According to the definition of type-3 errors there must exist two non-zero vectors: $\boldsymbol{s}_{1,2m_1'-1}^{(v)} - \boldsymbol{s'}_{1,2m_1'-1}^{(v)}$ or $\boldsymbol{s}_{1,2m_1'}^{(v)} - \boldsymbol{s'}_{1,2m_1'}^{(v)}$, and $\boldsymbol{s}_{2,2m_2'-1}^{(v)} - \boldsymbol{s'}_{2,2m_2'-1}^{(v)}$ or $\boldsymbol{s}_{2,2m_2'}^{(v)} - \boldsymbol{s'}_{2,2m_2'}^{(v)}$. Then according to the property of LCP rotation matrix and equations (4.22)-(4.23), there must exists diagonal matrices $\boldsymbol{\Lambda}_{\boldsymbol{e}^{(v)},1,2m_1'-1}$, $\boldsymbol{\Lambda}_{\boldsymbol{e}^{(v)},1,2m_1'}$, $\boldsymbol{\Lambda}_{\boldsymbol{e}^{(v)},2,2m_2'-1}$ and $\boldsymbol{\Lambda}_{\boldsymbol{e}^{(v)},2,2m_2'}$ whose diagonal elements are non-zero.

If $m_1' \neq m_2'$, there exists a submatrix in $\mathbf{\Lambda}_{\boldsymbol{e}^{(v)}}$ such that

$$\bar{\mathbf{\Lambda}}_{\boldsymbol{e}^{(v)}} = \begin{pmatrix} \mathbf{\Lambda}_{\boldsymbol{e}^{(v)},1,2m_1'-1} & \mathbf{0}_{K\times K} \\ \mathbf{0}_{K\times K} & \mathbf{\Lambda}_{\boldsymbol{e}^{(v)},2,2m_2'-1} \end{pmatrix}.$$

Since $\bar{\mathbf{\Lambda}}_{\boldsymbol{e}^{(v)}}$ is a diagonal matrix, one can easily conclude that $\operatorname{rank}\left(\bar{\mathbf{\Lambda}}_{\boldsymbol{e}^{(v)}}\right) = 2K$. On the other hand, if $m_1' = m_2' = m'$, there exists a submatrix in $\mathbf{\Lambda}_{\boldsymbol{e}^{(v)}}$ such that

$$\bar{\mathbf{\Lambda}}_{\boldsymbol{e}^{(v)}} = \begin{pmatrix} \mathbf{\Lambda}_{\boldsymbol{e}^{(v)},1,2m'-1} & \mathbf{\Lambda}_{\boldsymbol{e}^{(v)},2,2m'-1} \\ \mathbf{\Lambda}_{\boldsymbol{e}^{(v)},1,2m'} & \mathbf{\Lambda}_{\boldsymbol{e}^{(v)},2,2m'} \end{pmatrix}.$$

Using the determinant equality [61],

$$\det\begin{pmatrix} \boldsymbol{A} & \boldsymbol{B} \\ \boldsymbol{C} & \boldsymbol{D} \end{pmatrix} = \det(\boldsymbol{A}) \det\left(\boldsymbol{D} - \boldsymbol{C}\boldsymbol{A}^{-1}\boldsymbol{B}\right), \tag{4.32}$$

one has

$$\det\left(\bar{\mathbf{\Lambda}}_{\boldsymbol{e}^{(v)}}\right) = \det\left(\mathbf{\Lambda}_{\boldsymbol{e}^{(v)},1,2m'-1}\right) \det\left(\mathbf{\Lambda}_{\boldsymbol{e}^{(v)},2,2m'} - \mathbf{\Lambda}_{\boldsymbol{e}^{(v)},1,2m'}\mathbf{\Lambda}^{-1}_{\boldsymbol{e}^{(v)},1,2m'-1}\mathbf{\Lambda}_{\boldsymbol{e}^{(v)},2,2m'-1}\right), \tag{4.33}$$

Furthermore, using (4.23), it can be shown that

$$\det\left(\bar{\mathbf{\Lambda}}_{\boldsymbol{e}^{(v)}}\right) = \prod_{k=1}^{K}\left(\gamma\phi^{(v)}_{1,2m'-1}(k)\bar{\phi}^{(v)}_{2,2m'}(k) - \phi^{(v)}_{1,2m'}(k)\phi^{(v)}_{2,2m'-1}(k)\right), \tag{4.34}$$

where $\bar{\phi}^{(v)}_{2,2m'}(k) = \phi^{(v)}_{2,2m'}(k)/\gamma$.

It is known from (4.22) and (4.31) that all components in

$$\left(\gamma\phi^{(v)}_{1,2m'-1}(k)\bar{\phi}^{(v)}_{2,2m'}(k) - \phi^{(v)}_{1,2m'}(k)\phi^{(v)}_{2,2m'-1}(k)\right),$$

except γ, belong to the same finite algebraic extension formed by $\mathbf{\Theta}_1$. Since γ is a transcendental number which does not belong to any finite algebraic extension, it is guaranteed that $\left(\gamma\phi^{(v)}_{1,2m'-1}(k)\bar{\phi}^{(v)}_{2,2m'}(k) - \phi^{(v)}_{1,2m'}(k)\phi^{(v)}_{2,2m'-1}(k)\right) \neq 0$.

Therefore, $\det\left(\bar{\mathbf{\Lambda}}_{\boldsymbol{e}^{(v)}}\right) \neq 0$ and hence $\operatorname{rank}\left(\bar{\mathbf{\Lambda}}_{\boldsymbol{e}^{(v)}}\right) = 2K$.

Because $\boldsymbol{W}_i^{(v)}$ is a truncated DFT matrix with size $K \times L_i$, where $2K \geq L_1 + L_2$, then one has $\text{rank}\left(\boldsymbol{W}^{(v)}\right) = L_1 + L_2$. In addition, $\bar{\boldsymbol{\Lambda}}_{\boldsymbol{e}^{(v)}}$ is a $2K \times 2K$ full-rank matrix, it is true that $\text{rank}\left(\bar{\boldsymbol{\Lambda}}_{\boldsymbol{e}^{(v)}}\boldsymbol{W}^{(v)}\right) = L_1 + L_2$. Since $\bar{\boldsymbol{\Lambda}}_{\boldsymbol{e}^{(v)}}\boldsymbol{W}^{(v)}$ is a submatrix of $\boldsymbol{\Lambda}_{\boldsymbol{e}^{(v)}}\boldsymbol{W}^{(v)}$, it follows that $\text{rank}\left(\boldsymbol{\Lambda}_{\boldsymbol{e}^{(v)}}\boldsymbol{W}^{(v)}\right) \geq L_1 + L_2$. Finally, because $\boldsymbol{B_h}$ is a full-rank square matrix, one has

$$\text{rank}\left(\boldsymbol{\Psi}_{\boldsymbol{e}^{(v)}}\right) = \text{rank}\left(\boldsymbol{\Lambda}_{\boldsymbol{e}^{(v)}}\boldsymbol{W}^{(v)}\boldsymbol{B_h}\right) = \text{rank}\left(\boldsymbol{\Lambda}_{\boldsymbol{e}^{(v)}}\boldsymbol{W}^{(v)}\right) \geq L_1 + L_2. \tag{4.35}$$

Now, consider the worst case that $m_1' = m_2'$ and all parts of $\boldsymbol{\Lambda}_{\boldsymbol{e}^{(v)}}$, except for $\bar{\boldsymbol{\Lambda}}_{\boldsymbol{e}^{(v)}}$, are zeros. It can be seen that

$$\text{rank}\left(\boldsymbol{\Psi}_{\boldsymbol{e}^{(v)}}\right) = \text{rank}\left(\boldsymbol{\Lambda}_{\boldsymbol{e}^{(v)}}\boldsymbol{W}^{(v)}\boldsymbol{B_h}\right) = \text{rank}\left(\bar{\boldsymbol{\Lambda}}_{\boldsymbol{e}^{(v)}}\boldsymbol{W}^{(v)}\boldsymbol{B_h}\right) = L_1 + L_2. \tag{4.36}$$

According to the definition of the diversity gain, which is the minimum rank of $\boldsymbol{\Psi}_{\boldsymbol{e}^{(v)}}$, one concludes that $\delta_{d,3} = L_1 + L_2$. ■

From the proof of Throrem 3, it can be seen that a proper choice of parameter γ is very important to achieve the maximum diversity gain under type-3 errors. To illustrate this point further, the following theorem states that if $\gamma = 1$, the proposed FT-GLCP cannot achieve the maximum diversity gain of $L_1 + L_2$, but only $\max(L_1, L_2)$ under type-3 errors. The proof is give in Appendix 4.B.

Theorem 4 *Under type-3 errors, if $\gamma = 1$, FT-GLCP achieves $\delta_{d,3} = \max(L_1, L_2)$.*

In summary, to achieve the maximum diversity and coding gains under type-1 and type-2 errors, γ should have unit magnitude. To achieve the maximum diversity gain under type-3 errors, γ should be a transcendental number. The number γ satisfying these two requirements can be expressed as $\gamma = \exp(j\varphi)$, where φ is a rational number [62] chosen to make γ a transcendental number. Unfortunately, analytically finding the value of φ to maximize the coding gain under type-3 errors appears difficult, if not impossible. Nevertheless, the optimal value of φ can be easily found by computer search and this is explained further in Section 4.5. In addition to the choice of γ, according to Theorems 2 and 3, the subcarrier grouping size K should satisfy $K \geq \max(L_1, L_2)$ and $2K \in \mathcal{Q}$.

4.5 Simulation Results

This section provides various simulation results to validate the analysis in previous sections. In all simulations, the size of FFT is $N = 128$, the length of cyclic prefix is $N_c = 16$ and the number of OFDM symbols is $M = 2$. In addition, QPSK is adopted as the modulation scheme for all nodes. All channels are assumed to be quasi-static fading and have the same number of channel taps. Both cases of flat fading ($L_i = P_i = 1$) and frequency-selective fading with $L_i = P_i = 2$ are tested and the average norms of the channel vectors for all links are assumed to be unity. The size of subcarrier group is set to be $K = 2$ for the case of frequency-selective fading channels. Let the transmitted powers of both terminals and the relay be the same as P_t. Given that the average power gains of all channels are set to unity (i.e., no large-scale pass loss is taken into account), the received SNR is the same as the transmitted SNR and it is defined as P_t/N_0, where N_0 is the one-sided power spectral density of thermal noise at the terminal and relay nodes. In addition, the performances are evaluated in terms of both the terminal-to-terminal frame error rate (FER) and bit error rate (BER) , which means that both the MA and BC phases are included in the simulation.

For the MA phase, four schemes, F-GLCP, FT-GLCP, no-precoding, and DSTC are compared. As explained before, for the BC phase, the system model and signal processing is basically the same as that in the point-to-point communication system. As such, the F-GLCP scheme is applied in the BC phase of TWRC. It is pointed out that, with subcarrier grouping, only K instead of total N subcarriers are jointly precoded. Thus, the search space is $\mathcal{S}^{K\times 2} \times \mathcal{S}^{K\times 2}$ for the ML detection of (4.3), whereas it is $\mathcal{S}^{K\times 1}$ for the ML detection of (4.5).

In fact, the F-GLCP scheme reduces to no-precoding in the case of flat fading. In frequency-selective channels with two channel taps, the rotation matrices adopted for F-GLCP are:

$$\mathbf{\Theta}_1^{(\mathrm{F})} = \mathbf{\Theta}_2^{(\mathrm{F})} = \frac{1}{\sqrt{2}} \begin{pmatrix} 1 & \mathrm{e}^{-j\frac{\pi}{4}} \\ 1 & \mathrm{e}^{-j\frac{5\pi}{4}} \end{pmatrix}. \tag{4.37}$$

For FT-GLCP, the rotation matrices used in flat fading case are:

$$\mathbf{\Theta}_1^{(\mathrm{FT})} = \frac{1}{\sqrt{2}} \begin{pmatrix} 1 & \mathrm{e}^{-j\frac{\pi}{4}} \\ 1 & \mathrm{e}^{-j\frac{5\pi}{4}} \end{pmatrix}, \ \mathbf{\Theta}_2^{(\mathrm{FT})} = \frac{1}{\sqrt{2}} \begin{pmatrix} 1 & \mathrm{e}^{-j\frac{\pi}{4}} \\ \gamma & \gamma\mathrm{e}^{-j\frac{5\pi}{4}} \end{pmatrix}. \tag{4.38}$$

For frequency-selective channels with two channel taps, the rotation matrices used in FT-GLCP are:

$$\mathbf{\Theta}_1^{(\mathrm{FT})} = \frac{1}{2} \begin{pmatrix} 1 & \mathrm{e}^{-j\frac{\pi}{8}} & \mathrm{e}^{-j\frac{\pi}{4}} & \mathrm{e}^{-j\frac{3\pi}{8}} \\ 1 & \mathrm{e}^{-j\frac{5\pi}{8}} & \mathrm{e}^{-j\frac{5\pi}{4}} & \mathrm{e}^{-j\frac{15\pi}{8}} \\ 1 & \mathrm{e}^{-j\frac{9\pi}{8}} & \mathrm{e}^{-j\frac{\pi}{4}} & \mathrm{e}^{-j\frac{11\pi}{8}} \\ 1 & \mathrm{e}^{-j\frac{13\pi}{8}} & \mathrm{e}^{-j\frac{5\pi}{4}} & \mathrm{e}^{-j\frac{7\pi}{8}} \end{pmatrix}, \ \mathbf{\Theta}_2^{(\mathrm{FT})} = \frac{1}{2} \begin{pmatrix} 1 & \mathrm{e}^{-j\frac{\pi}{8}} & \mathrm{e}^{-j\frac{\pi}{4}} & \mathrm{e}^{-j\frac{3\pi}{8}} \\ 1 & \mathrm{e}^{-j\frac{5\pi}{8}} & \mathrm{e}^{-j\frac{5\pi}{4}} & \mathrm{e}^{-j\frac{15\pi}{8}} \\ \gamma & \gamma\mathrm{e}^{-j\frac{9\pi}{8}} & \gamma\mathrm{e}^{-j\frac{\pi}{4}} & \gamma\mathrm{e}^{-j\frac{11\pi}{8}} \\ \gamma & \gamma\mathrm{e}^{-j\frac{13\pi}{8}} & \gamma\mathrm{e}^{-j\frac{5\pi}{4}} & \gamma\mathrm{e}^{-j\frac{7\pi}{8}} \end{pmatrix}. \tag{4.39}$$

For each case of fading channels (i.e., flat or frequency-selective), the optimum value of $\gamma = \mathrm{e}^{j\varphi}$ that maximizes the coding gain under type-3 errors can be found by computer search. Due to the symmetry of QPSK constellation, it is sufficient to search over the range of $[0, \pi/2)$ for the rotation angle φ. As an example, Fig. 4.1 plots the coding gain (under type-3 errors) as a function of $\varphi \in [0, \pi/2)$. The figure shows that the optimal value of γ corresponds to $\varphi = 0.881 \approx 0.28\pi$. A similar plot of coding gain can be obtained for the case of frequency-selective fading channels, which reveals that the optimum rotation angle is $\varphi = 0.786 \approx 0.25\pi$. Since these two optimal angles are very close, for simplicity $\gamma = \mathrm{e}^{j0.881}$ shall be used in all simulations.

For DSTC [39], precoding is performed over two adjacent OFDM symbols and it is mathematically expressed as:

$$\begin{aligned} \begin{pmatrix} x_{1,2m'-1}(n) \\ x_{1,2m'}(n) \end{pmatrix} &= \mathbf{\Theta}_1 \begin{pmatrix} s_{1,2m'-1}(n) \\ s_{1,2m'}(n) \end{pmatrix}, \ m' = 1, \ldots, M/2, \ n = 1, \ldots, N, \\ &\qquad\qquad , \\ \begin{pmatrix} x_{2,2m'-1}(n) \\ x_{2,2m'}(n) \end{pmatrix} &= \mathbf{\Theta}_2 \begin{pmatrix} s_{2,2m'-1}(n) \\ s_{2,2m'}(n) \end{pmatrix}, \ m' = 1, \ldots, M/2, \ n = 1, \ldots, N. \end{aligned} \tag{4.40}$$

where

$$\mathbf{\Theta}_1 = \frac{1}{\sqrt{5}} \begin{pmatrix} a & a\theta \\ \bar{a} & \bar{a}\bar{\theta} \end{pmatrix}, \quad \mathbf{\Theta}_2 = \frac{1}{\sqrt{5}} \begin{pmatrix} ja & ja\theta \\ \bar{a} & \bar{a}\bar{\theta} \end{pmatrix},$$

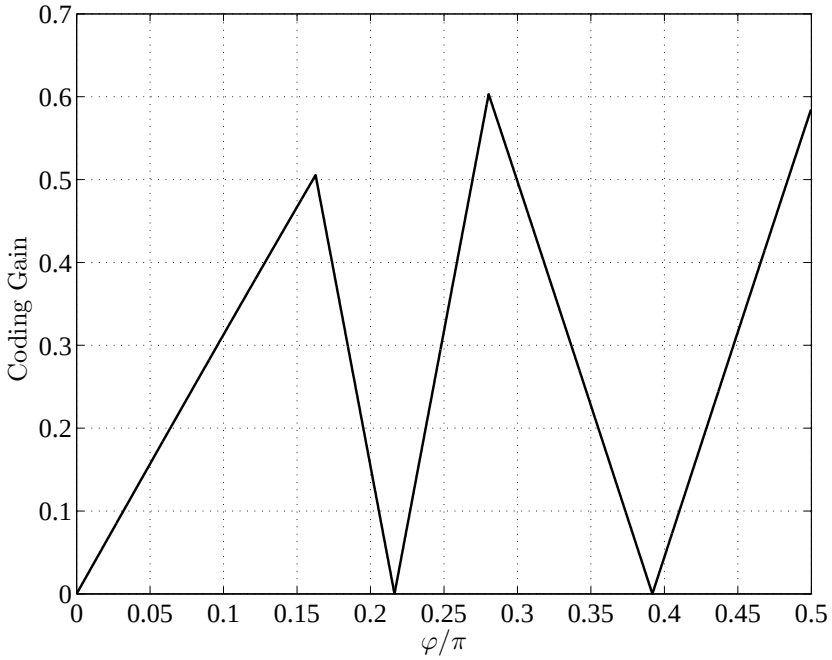

Figure 4.1 Coding gain under type-3 errors as a function of φ for the case of flat Rayleigh fading channels.

with $\theta = \frac{1+\sqrt{5}}{2}$, $\bar{\theta} = \frac{1-\sqrt{5}}{2}$, $a = 1 + j - j\theta$ and $\bar{a} = 1 + j - j\bar{\theta}$.

It is useful to summarize in Table 4.1 the diversity gains achieved by all schemes in the MA phase under comparison.

Table 4.1 Diversity gains of different precoding schemes in the MA phase.

	no-precoding	DSTC	F-GLCP	FT-GLCP ($\gamma = 1$)	FT-GLCP ($\gamma = \mathrm{e}^{j\varphi}$)
$\delta_{d,1}$	1	1	L_1	L_1	L_1
$\delta_{d,2}$	1	1	L_2	L_2	L_2
$\delta_{d,3}$	1	2	$\max(L_1, L_2)$	$\max(L_1, L_2)$	$L_1 + L_2$

Figs. 4.2 to 4.5 show the FER and BER performances in the flat fading case ($L_i = P_i = 1$). According to Table 4.1, in this case, all schemes have the same diversity gain of 1 under type-1 and type-2 errors. Under type-3 errors, DSTC and FT-GLCP ($\gamma = \mathrm{e}^{j\varphi}$) can achieve a higher diversity gain of 2 while no-precoding and F-GLCP still have a diversity gain of 1.

This is because in flat fading channels, no multi-path diversity gain is available. However, DSTC and FT-GLCP ($\gamma = e^{j\varphi}$) can obtain extra diversity gain by combating multiple-access interference using precoding in the time domain.

The system model in the MA phase can be viewed as a system with two antennas at the transmitter. By using DSTC or FT-GLCP ($\gamma = e^{j\varphi}$), the maximum spatial diversity gain of 2 is achieved. Since this spatial diversity gain is actually obtained via the cooperation of the two terminal nodes (i.e., joint precoder design), it can be considered as cooperative diversity gain. It is important to point out that, the ability of FT-GLCP to provide cooperative diversity gain is only possible by using proper values for γ. For example, with $\gamma = 1$, FT-GLCP has the same diversity gain as that of using no-precoding.

Figs. 4.2 and 4.4 show that under Rayleigh fading channels, the advantage on diversity gain achieved by DSTC and FT-GLCP ($\gamma = e^{j\varphi}$) over other schemes is not obvious. In contrast, as shown in Fig. 4.3, under Rician fading channels, the diversity advantage achieved by DSTC and FT-GLCP ($\gamma = e^{j\varphi}$) is very clear. This phenomenon can be explained as follows. From (4.8), it can be found that the total error probability is the sum of the probabilities of three types of errors. Among these three types of errors, type-1 and type-2 errors are mainly caused by deep fades of the channels from the terminal nodes to the relay node. Compared to a Rayleigh fading channel, the probability of being in a deep fade is lower for a Rician fading channel and thus the probabilities of type-1 and type-2 errors are lower. However, the main cause of type-3 errors is multiple-access interference which is determined by the ratio of the channel responses from two terminal nodes to the relay node [20, 51]. The probability of experiencing severe multiple-access interference in a Rician fading channel is not lower than that in a Rayleigh fading channel. Therefore, the probability of type-3 errors in a Rician fading channel is nearly the same as that in a Rayleigh fading channel. As a result, when considering the diversity gain of the total error probability in Rician fading channels, the diversity gain advantage of the DSTC and FT-GLCP schemes under type-3 errors becomes evident.

The performance curves in Figs. 4.2 to 4.5 show that DSTC achieves the same diversity

gain as FT-GLCP ($\gamma = e^{j\varphi}$). This is because in flat fading channels, DSTC is equivalent to FT-GLCP ($\gamma = e^{j\varphi}$). Note that there exists a gap of 1 to 2 dB between the coding gain achieved by DSTC and FT-GLCP ($\gamma = e^{j\varphi}$). This is because in FT-GLCP ($\gamma = e^{j\varphi}$), an optimized γ is used while in DSTC, the value of γ is not optimized.

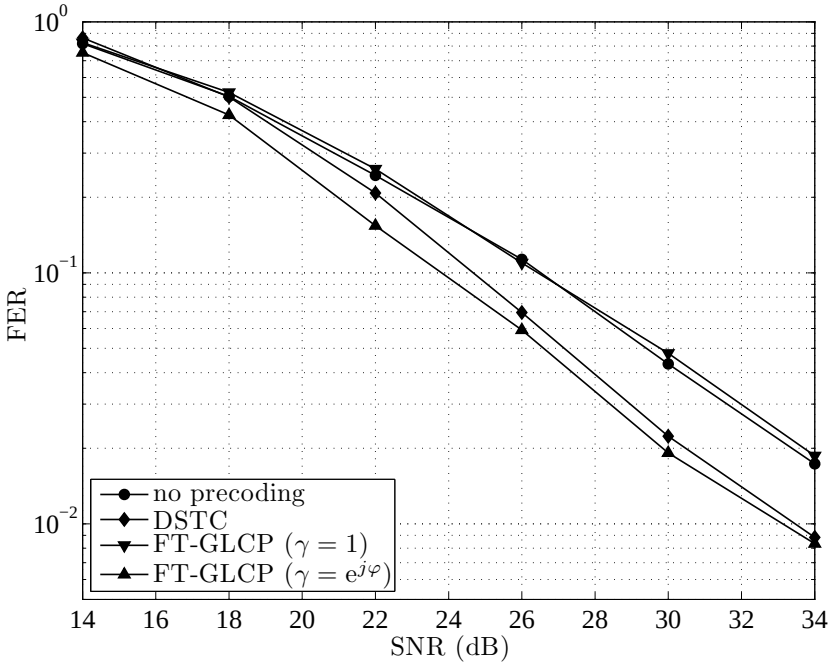

Figure 4.2 FER performance for flat Rayleigh fading channels.

Figs. 4.6 to 4.9 show the FER and BER performance in frequency-selective channels with two independent and identically distributed (i.i.d.) channel taps. It can be seen that larger diversity gains are achieved by F-GLCP and FT-GLCP (for both cases of $\gamma = 1$ and $\gamma = e^{j\varphi}$) as compared to no-precoding and DSTC. This is because only F-GLCP and FT-GLCP can exploit multi-path diversity gain in frequency-selective fading channels. In addition, FT-GLCP ($\gamma = e^{j\varphi}$) can further exploit cooperative diversity gain under type-3 errors. As a result, FT-GLCP ($\gamma = e^{j\varphi}$) has advantage on diversity gain over all other schemes. Although simulation results in both Rayleigh and Rician fading channels show performance advantage of the proposed FT-GLCP ($\gamma = e^{j\varphi}$), the performance advantage is more significant in Rician fading channels. Again, this is also because in Rician fading channels, type-3 errors contribute more to the total error probability and FT-GLCP ($\gamma = e^{j\varphi}$) behaves much better than other schemes under type-3 errors.

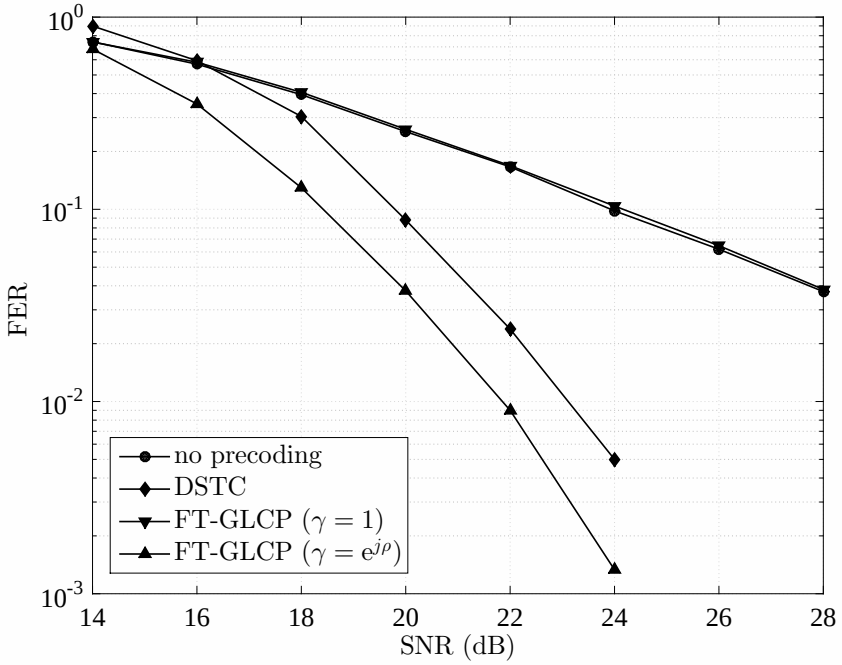

Figure 4.3 FER performance for flat Rician fading channels ($K_f = 10$).

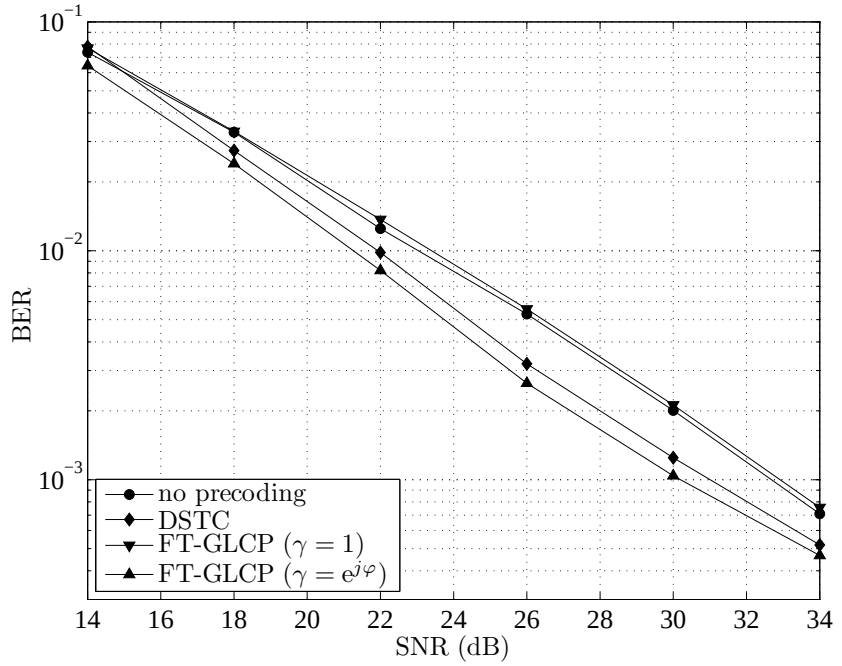

Figure 4.4 BER performance for flat Rayleigh fading channels.

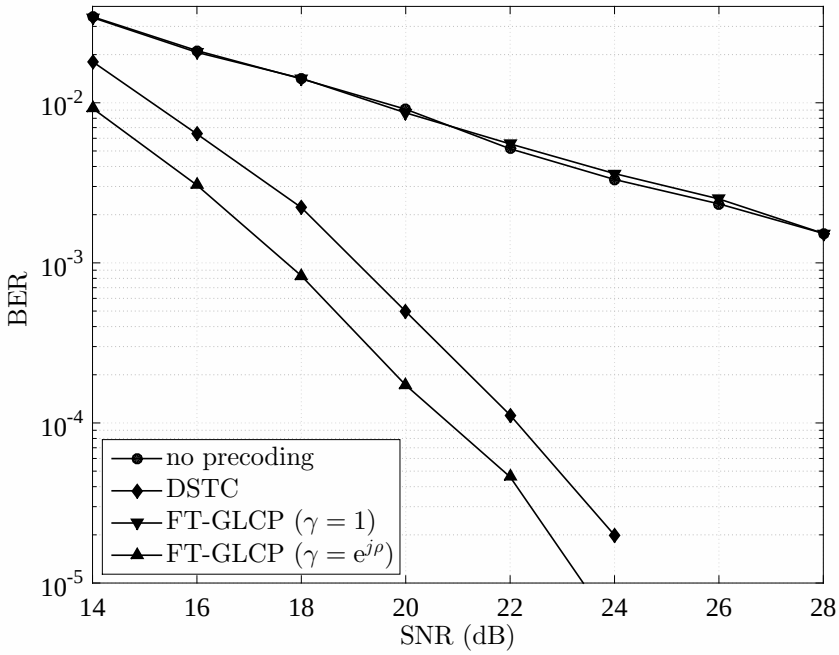

Figure 4.5 BER performance for flat Rician fading channels ($K_f = 10$).

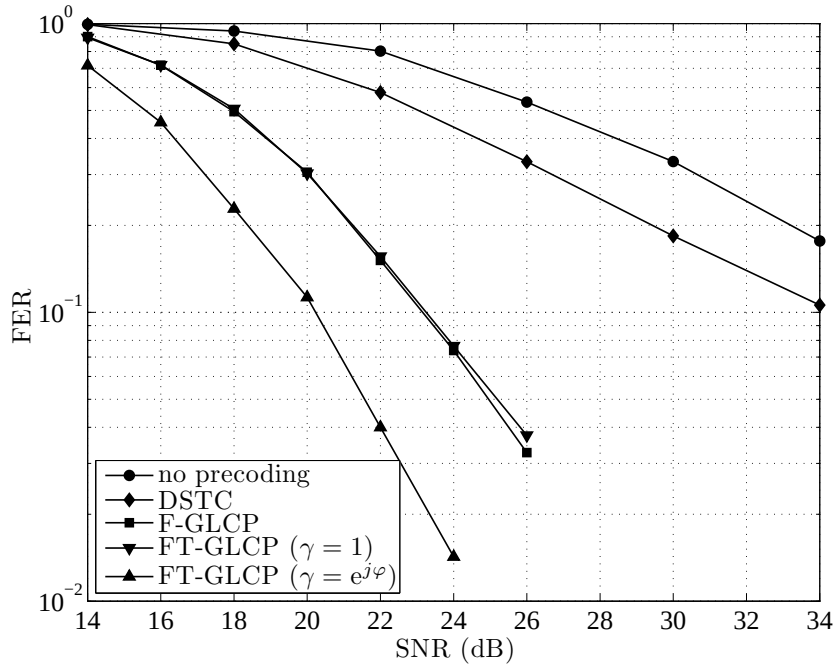

Figure 4.6 FER performance for i.i.d. frequency-selective Rayleigh fading channels ($L = 2$).

Finally, simulation results are also provided for correlated channels. Specifically, the fol-

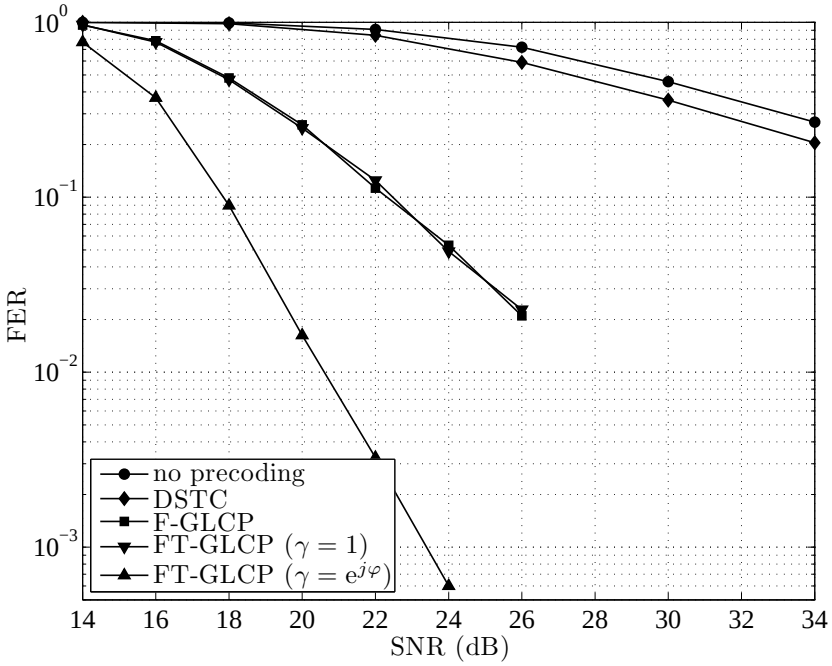

Figure 4.7 FER performance for i.i.d. frequency-selective Rician ($K_f = 10$) fading channels ($L = 2$).

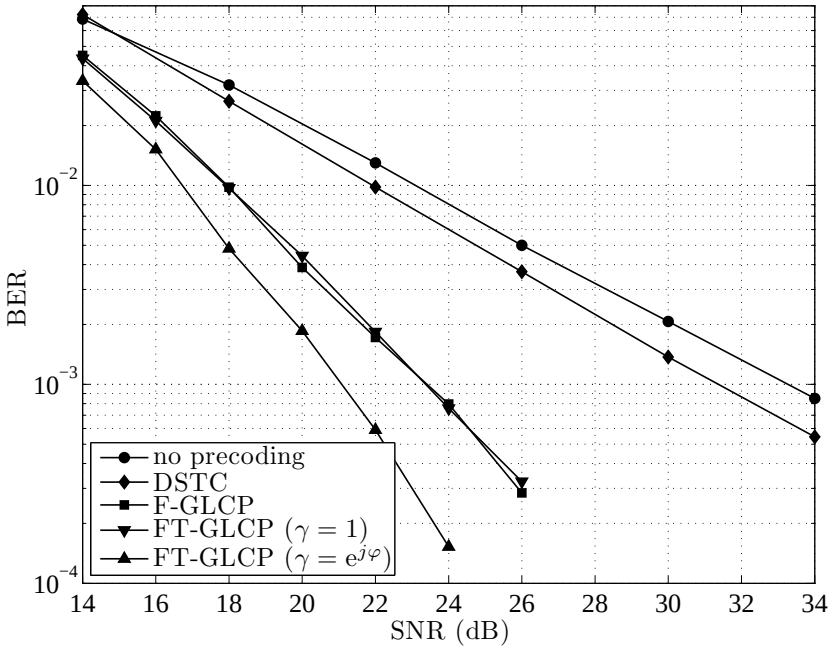

Figure 4.8 BER performance for i.i.d. frequency-selective Rayleigh fading channels ($L = 2$).

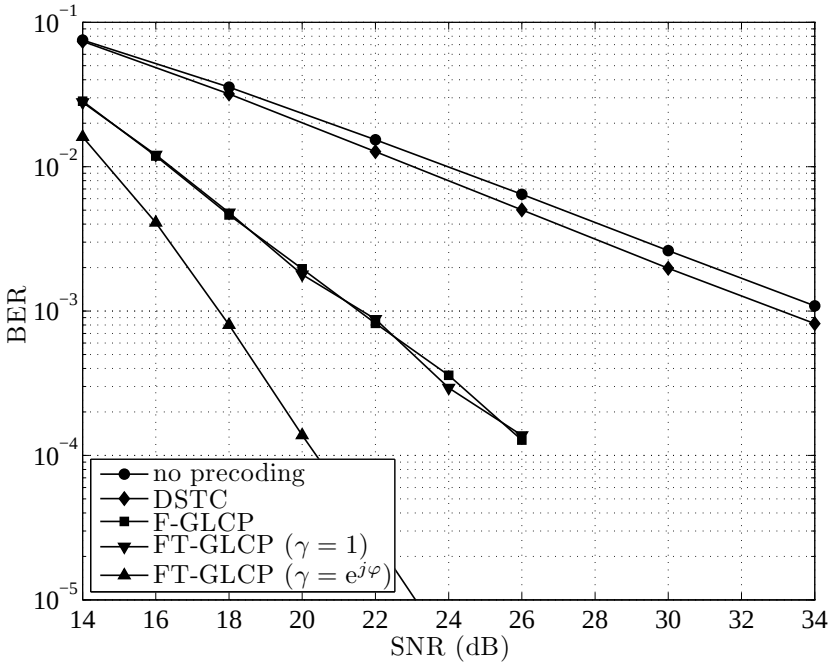

Figure 4.9 BER performance for i.i.d. frequency-selective Rician ($K_f = 10$) fading channels ($L = 2$).

lowing correlation matrix is assumed for 2-tap frequency-selective Rayleigh fading channels:

$$\boldsymbol{R}_{\boldsymbol{h}_i} = \boldsymbol{R}_{\boldsymbol{g}_i} = \begin{pmatrix} 1 & 0.6 \\ 0.6 & 1 \end{pmatrix}. \tag{4.41}$$

As expected, the FER and BER plotted in Figs. 4.10 and 4.11 show that channel correlation will cause performance degradation. In addition, the performance superiority of the proposed FT-GLCP ($\gamma = e^{j\varphi}$) method over all other methods is also clearly observed for correlated frequency-selective Rayleigh fading channels.

4.6 Conclusions

The design of distributed precoding in TWRC systems using OFDM was studied in this paper. A novel frequency-time grouped linear constellation precoding (FT-GLCP) was proposed by minimizing the error probability in the MA communications phase. Compared to the no-precoding scheme and the precoding scheme based on distributed space time coding, the proposed scheme successfully utilizes the multi-path diversity gain to alleviate the

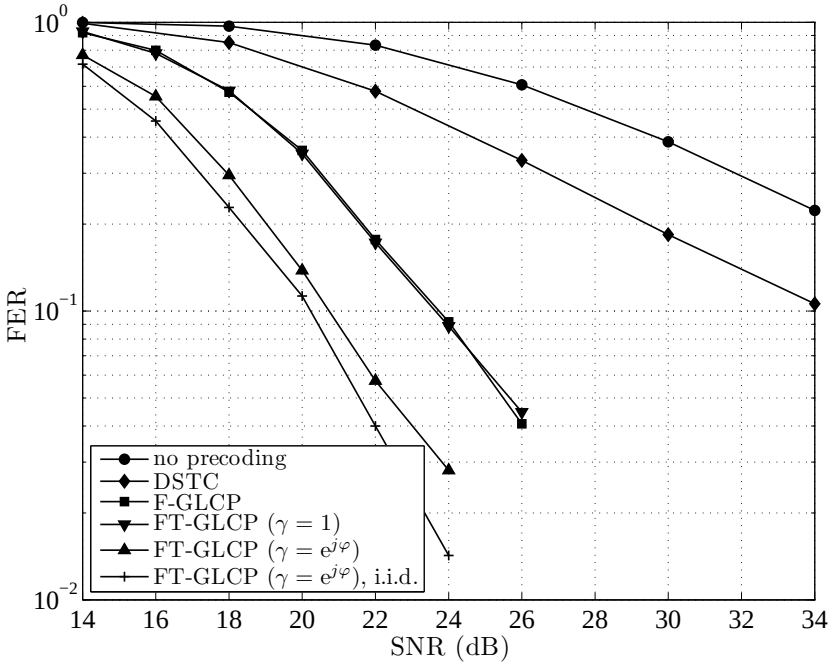

Figure 4.10 FER performance for correlated frequency-selective Rayleigh channels ($L = 2$).

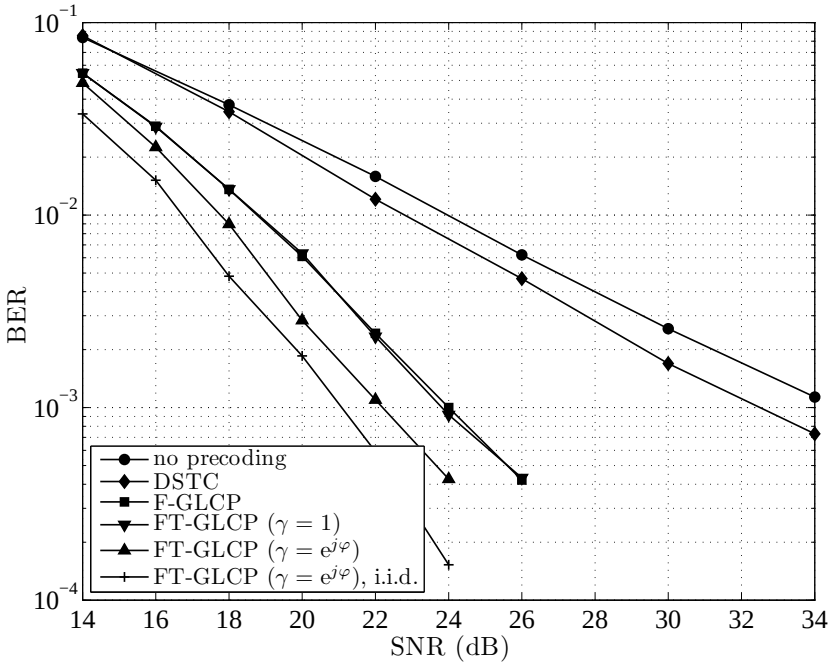

Figure 4.11 BER performance for correlated frequency-selective Rayleigh channels ($L = 2$).

influence of deep fading. Also compared to the scheme that employs the conventional frequency GLCP, the proposed scheme was shown to achieve the cooperative diversity gain under type-3 errors, while the frequency GLCP cannot. Simulation results validated the theoretical analysis and showed the performance advantage of the proposed scheme over other schemes.

4.A Proof of Lemma 1

Recall that $\boldsymbol{A}$ is a $K \times L$ truncated DFT matrix and its row indices follow the rule for subcarrier grouping described in Section 4.4. Without loss of generality, assume that the row indices are of the vth group. Thus the (k,l)th element of $\boldsymbol{A}$ can be expressed as: $\boldsymbol{A}(k,l) = \exp\left(\frac{-j2\pi((k-1)V+v)(l-1)}{N}\right)$. By constructing the matrix $\bar{\boldsymbol{A}}$ with (k,l)th element being $\bar{\boldsymbol{A}}(k,l) = \sqrt{\xi_k}\exp\left(\frac{-j2\pi((k-1)V+v)(l-1)}{N}\right)$, the determinant can be expressed as:

$$\det\left(\boldsymbol{A}^H \boldsymbol{\Xi} \boldsymbol{A}\right) = \det\left(\bar{\boldsymbol{A}}^H \bar{\boldsymbol{A}}\right). \tag{4.42}$$

Applying the Binet-Cauchy theorem [63], one has

$$\det\left(\bar{\boldsymbol{A}}^H \bar{\boldsymbol{A}}\right) = \sum_I \left|\det\left(\bar{\boldsymbol{A}}_I\right)\right|^2, \tag{4.43}$$

where $I = (i_1, i_2, \cdots, i_L), 1 \le i_1 < i_2 < \cdots < i_L \le K$, runs through all such indices, $\bar{\boldsymbol{A}}_I$ denotes the matrix formed from $\bar{\boldsymbol{A}}$ using columns in the set I. By expressing the (t,l)th element in $\bar{\boldsymbol{A}}_I$ as: $\bar{\boldsymbol{A}}_I(t,l) = \sqrt{\xi_{i_t}}\exp\left(\frac{-j2\pi((i_t-1)V+v)(l-1)}{N}\right)$, it can be observed that $\bar{\boldsymbol{A}}_I$ is closely related to a Vandermonde matrix. Therefore one has:

$$\left|\det\left(\bar{\boldsymbol{A}}_I\right)\right|^2 = \kappa(I)\prod_{t=1}^{L}\xi_{i_t}, \tag{4.44}$$

where $\kappa(I) = \prod_{1\le t<l\le L} 4\sin^2\left(\frac{\pi}{K}(i_t - i_l)\right)$. Following the derivation in [58], divide the $\binom{K}{L}$ combinations I into M groups in which any combination I in the same group $G_m, 1 \le m \le M$, results in the same value $\kappa(I) = b_m$ and the group G_m contains a_m combinations. Then the following conclusions are proved in [58]: (i) $\sum_{m=1}^{M} a_m b_m = K^L$; (ii) For any group G_m, $a_m L = s_m K$, where s_m is an integer; (iii) each element in $\{1, 2, \cdots, K\}$ appears s_m times in

group G_m. Therefore, applying the Cauchy inequality for each group G_m gives:

$$\sum_{I\in G_m} b_m \prod_{t=1}^{L} \xi_{i_t} \geq b_m a_m \left(\prod_{k=1}^{K} \xi_k\right)^{\frac{L}{K}} = K^L \left(\prod_{k=1}^{K} \xi_k\right)^{\frac{L}{K}}.$$

Then using (4.42)-(4.44), the Lemma is proved:

$$\det\left(\boldsymbol{A}^H \boldsymbol{\Xi} \boldsymbol{A}\right) \geq K^L \left(\prod_{k=1}^{K} \xi_k\right)^{\frac{L}{K}}.$$

■

4.B Proof of Theorem 4

Following the same reasoning as in the proof of Theorem 4, for all type-3 errors, there must exist $K \times K$ diagonal matrices $\boldsymbol{\Lambda}_{\boldsymbol{e}^{(v)},1,2m'_1-1}$, $\boldsymbol{\Lambda}_{\boldsymbol{e}^{(v)},1,2m'_1}$, $\boldsymbol{\Lambda}_{\boldsymbol{e}^{(v)},2,2m'_2-1}$ and $\boldsymbol{\Lambda}_{\boldsymbol{e}^{(v)},2,2m'_2}$ whose diagonal elements are non-zero. Assume that $L_2 \geq L_1$. Since $\boldsymbol{W}_2^{(v)}$ is a truncated DFT matrix with size $K \times L_2$ and $K \geq L_2$, one has $\operatorname{rank}\left(\boldsymbol{W}_2^{(v)}\right) = L_2$. Since $\boldsymbol{\Lambda}_{\boldsymbol{e}^{(v)},2,2m'_2-1}\boldsymbol{W}_2^{(v)}$ is a submatrix of $\boldsymbol{\Lambda}_{\boldsymbol{e}^{(v)}}\boldsymbol{W}^{(v)}$, it follows that $\operatorname{rank}\left(\boldsymbol{\Lambda}_{\boldsymbol{e}^{(v)}}\boldsymbol{W}^{(v)}\right) \geq L_2$. Furthermore, because $\boldsymbol{B_h}$ is a full-rank square matrix, one has

$$\operatorname{rank}\left(\boldsymbol{\Psi}_{\boldsymbol{e}^{(v)}}\right) = \operatorname{rank}\left(\boldsymbol{\Lambda}_{\boldsymbol{e}^{(v)}}\boldsymbol{W}^{(v)}\boldsymbol{B_h}\right) = \operatorname{rank}\left(\boldsymbol{\Lambda}_{\boldsymbol{e}^{(v)}}\boldsymbol{W}^{(v)}\right) \geq L_2.$$

If $m'_1 = m'_2 = m'$, there exists a submatrix in $\boldsymbol{\Lambda}_{\boldsymbol{e}^{(v)}}$ such that

$$\bar{\boldsymbol{\Lambda}}_{\boldsymbol{e}^{(v)}} = \begin{pmatrix} \boldsymbol{\Lambda}_{\boldsymbol{e}^{(v)},1,2m'-1} & \boldsymbol{\Lambda}_{\boldsymbol{e}^{(v)},2,2m'-1} \\ \boldsymbol{\Lambda}_{\boldsymbol{e}^{(v)},1,2m'} & \boldsymbol{\Lambda}_{\boldsymbol{e}^{(v)},2,2m'} \end{pmatrix}.$$

Define,

$$\bar{\boldsymbol{\Psi}}_{\boldsymbol{e}^{(v)}} = \boldsymbol{B}_{\boldsymbol{h}}^H (\boldsymbol{W}^{(v)})^H \bar{\boldsymbol{\Lambda}}_{\boldsymbol{e}^{(v)}}^H \bar{\boldsymbol{\Lambda}}_{\boldsymbol{e}^{(v)}} \boldsymbol{W}^{(v)} \boldsymbol{B_h}.$$

Consider the case that all parts of $\boldsymbol{\Lambda}_{\boldsymbol{e}^{(v)}}$, except $\bar{\boldsymbol{\Lambda}}_{\boldsymbol{e}^{(v)}}$, are zeros, since $\boldsymbol{B_h}$ is a full-rank square matrix, one has

$$\operatorname{rank}\left(\boldsymbol{\Psi}_{\boldsymbol{e}^{(v)}}\right) = \operatorname{rank}\left(\bar{\boldsymbol{\Psi}}_{\boldsymbol{e}^{(v)}}\right) = \operatorname{rank}\left(\bar{\boldsymbol{A}}_{\boldsymbol{e}^{(v)}}\right),$$

where

$$\bar{\boldsymbol{A}}_{\boldsymbol{e}^{(v)}} = \begin{pmatrix} \boldsymbol{\Lambda}_{\boldsymbol{e}^{(v)},1,2m'-1}\boldsymbol{W}_1^{(v)} & \boldsymbol{\Lambda}_{\boldsymbol{e}^{(v)},2,2m'-1}\boldsymbol{W}_2^{(v)} \\ \boldsymbol{\Lambda}_{\boldsymbol{e}^{(v)},1,2m'}\boldsymbol{W}_1^{(v)} & \boldsymbol{\Lambda}_{\boldsymbol{e}^{(v)},2,2m'}\boldsymbol{W}_2^{(v)} \end{pmatrix}$$

Under the scenario that the error events from two terminal nodes are the same, and using the fact that $\boldsymbol{W}_1^{(v)}$ has L_1 identical columns with $\boldsymbol{W}_2^{(v)}$, one can conclude that rank $\left(\bar{\boldsymbol{A}}_{\boldsymbol{e}^{(v)}}\right) = L_2$. According to the definition of the diversity gain, it follows that $\delta_{d,3} = L_2$. Similarly, under the case that $L_1 \geq L_2$, it can be shown that $\delta_{d,3} = L_1$. Therefore, $\delta_{d,3} = \max(L_1, L_2)$. ■

5. Distributed Linear Constellation Precoding with BICM/BICM-ID in Two-Way Relaying Communications

The previous chapter presented a novel design of distributed linear constellation precoding (DLCP) to achieve the multipath diversity gain with OFDM in TWRC. Besides LCP, bit-interleaved coded modulation (BICM) is another technique which is widely used to achieve diversity gains. By using channel coding and interleaving, BICM provides a low complexity method to achieve diversity gains in fading channels. To further enhance the performance of BICM, an iterative processing between the demodulator and the decoder is conducted. A BICM system with such iterative processing at the receiver is usually called BICM with iterative decoding (BICM-ID). In point-to-point communication systems, BICM-ID is demonstrated to achieve much better performance than BICM. To apply BICM and BICM-ID in TWRC systems, one also needs to consider how to handle the detection deterioration caused by MAI. As discussed and demonstrated in the previous chapter, DLCP is an efficient scheme to alleviate MAI. Therefore, DLCP shall be investigated in conjunction with BICM and BICM-ID for TWRC in this manuscript

Different from point-to-point communications, the relay node in TWRC needs to decode from the superimposed signal arriving from the two terminal nodes. Therefore, to achieve the best performance, decoding based on the quaternary code representation is first developed. Furthermore, the quaternary-digit error probability (QEP) and bit error probability (BEP) under network coding are evaluated. For BICM without iterative decoding, union bounds on QEP and BEP under network coding are derived and used to design DLCP. The analysis

based on three types of errors is performed to simplify the performance metric. The key performance parameter is identified and optimized in different fading channels. Simulation results obtained with BICM in various fading channels are provided to verify the effectiveness of the design metric and demonstrate performance advantage of the DLCP scheme with the optimal parameter over other schemes. For BICM-ID, by invoking the error-free (EF) feedback assumption, the upper bounds of QEP and BEP under network coding are derived. Based on the EF bound of QEP, the optimal parameter for DLCP is calculated. Through the analysis of the EF bound of the BEP under network coding, it is shown that MAI is successfully eliminated with iterative decoding and XOR-based network coding for BICM-ID systems. Simulation results obtained with BICM-ID in various fading channels are provided to verify the analysis and show the advantage of using iterative decoding based on quaternary code representation.

The results of our studies on DLCP for BICM/BICM-ID in TWRC systems are reported in three manuscripts listed below. The submitted journal paper [Ch5-3] is included in this chapter.

[Ch5-1] H. Yan and Ha H. Nguyen, "Distributed Space Time Coding for Bit-Interleaved Coded Modulation in Two-Way Relaying Communications", *IEEE Global Telecommun. Conf.*, San Diego, CA, USA, Dec. 2015.

[Ch5-2] H. Yan and Ha H. Nguyen, "BICM-ID in Two-Way Relaying Communications", to appear in *Proc. IEEE Int. Conf. Commun.*, Kuala Lumpur, Malaysia, May 2016.

[Ch5-3] H. Yan and Ha H. Nguyen, "Distributed Linear Constellation Precoding for BICM/BICM-ID in Two-Way Relaying Communications", revised version submitted to *IEEE Trans. Veh. Technol.*, Jan. 2016.

Distributed Linear Constellation Precoding with BICM/BICM-ID in Two-Way Relaying Communications

Hongzhong Yan and Ha H. Nguyen

Abstract

This paper investigates distributed linear constellation precoding (DLCP) for two-way relaying communication (TWRC) systems in conjunction with the techniques of bit-interleaved coded modulation (BICM) and BICM with iterative decoding (BICM-ID). First, a decoding strategy for the relay node that is based quaternary code representation is developed. Then the union bounds (for the case of BICM) and error-free feedback (EF) bounds (for the case of BICM-ID) on the quaternary digit error probability (QEP) and bit error probability (BEP) under network coding in the multiple access phase are obtained. Based on the obtained bounds, the impact of DLCP on the error performance is analyzed by considering three error types in the multiple-access (MA) phase. It is shown that type-3 errors need to be carefully taken into account in the design of a DLCP scheme. By developing a performance metric related to type-3 errors, the design parameter of DLCP is optimized when BICM is used, whereas it is shown that DLCP is not needed when BICM-ID is used. Extensive simulation results are provided to corroborate the analysis and demonstrate the performance superiority of the proposed decoding strategy over the one that directly decodes the XOR code. For the case of BICM, the performance advantage achieved by properly designing DLCP is also illustrated.

Index terms

Two-way relaying, BICM, BICM-ID, iterative decoding, distributed linear constellation precoding, quaternary decoding, network coding.

5.1 Introduction

Two-way relaying communication (TWRC) systems have recently gained a strong interest in research community because of its bi-directional transmission capability. In a TWRC system a relay node is used to support information exchange between two terminal nodes. The full information exchange process includes the multiple access (MA) and broadcast (BC) phases. In the MA phase, the terminal nodes send their information to the relay node, while in the BC phase the relay node transmits the processed information back to the two terminal nodes. In a simple, but low-efficiency protocol, each of the MA and BC phases needs two time slots. In [55], a protocol based on the exclusive-OR (XOR) network coding is proposed so that the BC phase requires only one time slot. To further improve the transmission efficiency, a two-slot protocol is proposed in [47, 54] so that each phase only needs one time slot.

Different from the four-slot and three-slot protocols which use two time slots for the two terminal nodes in the MA phase, the two-slot protocol faces the challenge of performance deterioration caused by multiple access interference (MAI). Denoise-and-forward (DNF) is proposed in [19, 20] to avoid the influence of MAI to the end performance of each terminal node. Specifically, the DNF gathers pairs of close constellation points into one group according to the channel response. Then in the BC phase, the pairs of those close constellation points are mapped to one new constellation point for broadcasting. However, to implement DNF, the *denosing maps* which are used to indicate how the pairs of constellation points are grouped and mapped also need to be transmitted to the terminal nodes in the BC phase and thus causes extra overhead. When the DNF is used with orthogonal frequency-division multiplexing (OFDM) over frequency-selective fading channels, the overhead is even larger since different channel responses in different subcarriers require different denoising maps [56]. Later on, distributed space-time coding (DSTC) is proposed in [39] as another approach to handle the MAI issue in TWRC. Instead of avoiding MAI, DSTC alleviates the impact of MAI by performing precoding at both the terminal nodes. The authors of [39] give two specific precoding matrices and show that DSTC does not require overhead for the BC phase and achieves better performance than DNF in the high signal-to-noise ratio (SNR) region.

More recently, [64] provides a more general form of DSTC by using distributed linear constellation precoding (DLCP) and proposes frequency-time DLCP to be used with OFDM, which can also achieve multipath diversity in addition to handling MAI.

While all the schemes discussed above are only designed for the uncoded two-slot protocol of a TWRC system, other researchers also consider channel coding in TWRC systems. Specifically, reference [65] proposes and evaluates different decoding strategies for a two-slot TWRC system in an additive white Gaussian noise (AWGN) channel, while [66] provides distance spectrum and performance analysis. Furthermore, decoding schemes for TWRC systems using low-density parity-check (LDPC) codes, convolutional codes and turbo codes under a fading channel are investigated in [67–69]. For coded systems using the two-slot protocol, the MAI problem still exists and needs to be handled properly. References [70, 71] present the modified DNF schemes when LDPC codes and convolutional codes are adopted in TWRC systems.

For communication systems employing channel coding, bit-interleaved coded modulation (BICM) [14] is an effective method to achieve the diversity gain over fading channels. Later on, the works in [18, 44, 72] apply iterative processing between the demodulator and decoder in a BICM receiver. Such iterative decoding (ID) is shown to significantly enhance the system's bit-error-rate performance. A BICM system that employs iterative decoding is usually referred to as BICM-ID. Due to the popularity and performance advantages of BICM and BICM-ID, this paper aims to study how to adopt BICM and BICM-ID in a TWRC system, especially when DLCP is performed at the two terminal nodes.

Relevant to the study in this paper, references [73, 74] discuss detection techniques when BICM and BICM-ID is used in a TWRC system. However, there has been no study on how to handle MAI when BICM or BICM-ID is adopted in TWRC systems. Since DLCP is shown to efficiently alleviate the influence of MAI [64], one objective of this paper is to develop DLCP to be used with BICM and BICM-ID in a TWRC system. The decoding developed in reference [74] is based on a reduced trellis to directly decode the codewords after network coding. It was pointed out in [67, 68, 75] that decoding based on a reduced trellis

may incur a performance loss. As such, in this paper decoding based on the quaternary code representation at the relay node is developed for both BICM and BICM-ID. The asymptotic error performance is analyzed by means of the union bound and EF bound for BICM and BICM-ID, respectively. Based on the union bound, DLCP is optimized to be used with BICM so that MAI can be efficiently suppressed. On the other hand, based on the EF bound analysis, the paper also demonstrates that BICM-ID is able to eliminate MAI in the MA phase when combining with XOR-based network coding, i.e., DLCP is not needed. Performance comparison with different precoding schemes and between BICM and BICM-ID is thoroughly conducted by computer simulation.

This paper is organized as follows. Section 5.2 describes the TWRC system employing the two-slot protocol and BICM/BICM-ID. Section 5.3 introduces decoding based on the quaternary code representation. Section 5.4 investigates the error probability in the MA phase and derives the union bounds and EF bounds for BICM and BICM-ID, respectively. The proposed DLCP design is presented in Section 5.5 by making use of the bounds derived in Section 5.4. Section 5.6 provides the simulation results and conclusions are drawn in Section 5.7.

Notations: The complex number $\sqrt{-1}$ is denoted by j. The conjugate of complex number a is denoted by a^*. The elements in the ith row, from the jth to the kth columns of $\boldsymbol{A}$ are denoted by $\boldsymbol{A}(i, j:k)$. The transpose, Hermitian transpose, determinant of matrix $\boldsymbol{A}$ are denoted by $\boldsymbol{A}^T$, $\boldsymbol{A}^H$ and $\det(\boldsymbol{A})$, respectively. $\mathrm{diag}(\boldsymbol{a})$ denotes a diagonal matrix whose diagonal elements are from vector $\boldsymbol{a}$ and $\|\boldsymbol{a}\|$ denotes the Euclidean norm of vector $\boldsymbol{a}$.

5.2 System Model

The TWRC system under consideration has two terminal nodes, denoted as nodes $\mathbb{T}_1$ and $\mathbb{T}_2$, which exchange information to each other by the help of relay node $\mathbb{R}$. This information exchange happens in two phases. In the MA phase, both terminal nodes send their signals to the relay node. After processing the received signal, the relay node broadcasts a new signal in the BC phase.

The MA phase of such a TWRC system using DLCP and BICM/BICM-ID is shown in Fig. 5.1. It is pointed out that BICM is a special case of BICM-ID when no iterations are performed between the demodulator and the decoder. The L-bit information vector $\boldsymbol{u}_i = [u_i(1), \cdots, u_i(L)]^T$ from node $\mathbb{T}_i$ is first encoded into an M-bit coded vector $\boldsymbol{c}_i = [c_i(1), \cdots, c_i(M)]^T$. This means that the code rate is $R = L/M$. The coded vector $\boldsymbol{c}_i$ is then interleaved by a bit-wise interleaver to become the interleaved vector $\boldsymbol{v}_i = [v_i(1), \cdots, v_i(M)]^T$. Then each group of K coded bits in $\boldsymbol{v}_i$ is mapped to a complex constellation symbol, where the set of constellation symbols is denoted as $\mathcal{S}$. This results in vector $\boldsymbol{s}_i = [s_i(1), \cdots, s_i(N)]^T$ consisting of N constellation symbols. To apply DLCP, two consecutive symbols in $\boldsymbol{s}_i$ are grouped, i.e., $\boldsymbol{s}_i$ is divided into $G = N/2$ groups and the gth group is defined as $\boldsymbol{s}_{i,g} = [s_i(2g-1),\ \ s_i(2g)]^T$. Then the corresponding gth precoded vector $\boldsymbol{x}_{i,g} = [x_i(2g-1),\ \ x_i(2g)]^T$ is obtained by

$$\boldsymbol{x}_{i,g} = \boldsymbol{\Theta}_i \boldsymbol{s}_{i,g}, \tag{5.1}$$

where $\boldsymbol{\Theta}_i$ is a *precoding matrix*. Finally, all precoded symbols are arranged as $\boldsymbol{x}_i = [x_i(1), \cdots, x_i(N)]^T$ and sent to relay node $\mathbb{R}$.

Let $\boldsymbol{r} = [r(1), \cdots, r(N)]^T$ denote the received symbol vector at the relay node. It can be expressed as:

$$\boldsymbol{r} = \boldsymbol{H}_1 \boldsymbol{x}_1 + \boldsymbol{H}_2 \boldsymbol{x}_2 + \boldsymbol{\omega}, \tag{5.2}$$

where $\boldsymbol{H}_i = \mathrm{diag}\left([h_i(1), \cdots, h_i(N)]\right)$ is the $N \times N$ diagonal matrix whose components are impulse responses of the channel from $\mathbb{T}_i$ to $\mathbb{R}$. In this paper, $h_i(n)$ is assumed to follow a Rician distribution with mean value ε_{h_i} and variance $\sigma_{h_i}^2$ and the corresponding Rician factor $K_f = |\varepsilon_{h_i}|^2 / \sigma_{h_i}^2$ Also, for convenience of analysis, $|\varepsilon_{h_1}| = |\varepsilon_{h_2}| = |\varepsilon_h|$ and $\sigma_{h_1}^2 = \sigma_{h_1}^2 = \sigma_h^2$ are assumed. The vector $\boldsymbol{\omega} = [\omega(1), \cdots, \omega(N)]^T$ contains additive white Gaussian noise (AWGN) samples, which are modelled as i.i.d. zero-mean complex Gaussian random variables with variance N_0. Furthermore, under the condition that the channel responses corresponding to each group of precoded symbols are approximately constant (i.e., slow fading) so that $h_i(2g-1) \approx h_i(2g) = h_{i,g}$, the gth group of received symbol vector in $\boldsymbol{r}$ can be expressed as:

$$\boldsymbol{r}_g = [r(2g-1),\ \ r(2g)]^T = h_{1,g}\boldsymbol{x}_{1,g} + h_{2,g}\boldsymbol{x}_{2,g} + \boldsymbol{\omega}_g \tag{5.3}$$

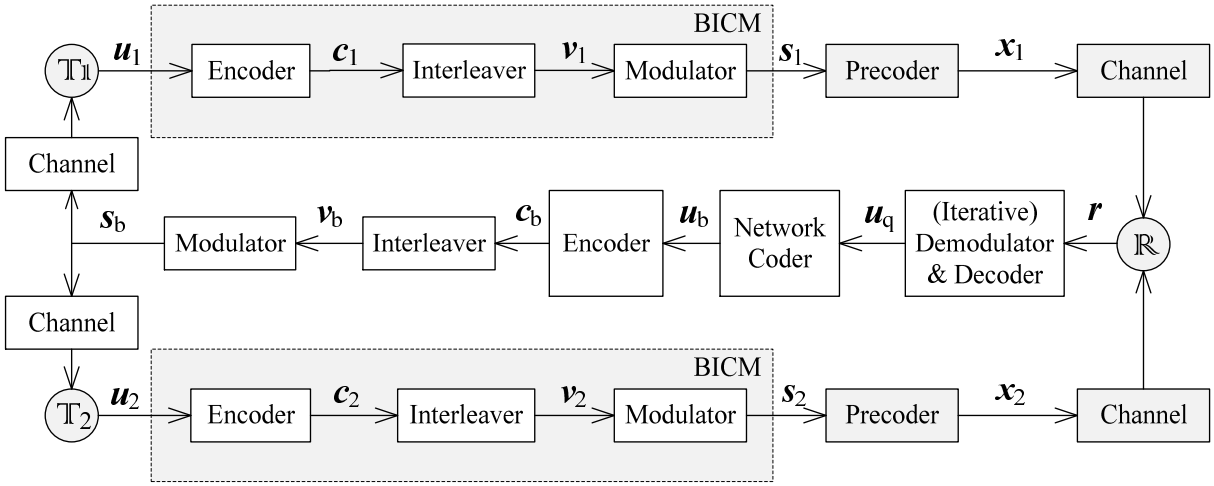

Figure 5.1 A TWRC system employing BICM-ID.

where $\boldsymbol{\omega}_g = [\omega(2g-1),\ \ \omega(2g)]^T$.

Let E_s denote the average energy of the transmitted (i.e., precoded) symbols in $\boldsymbol{x}_i$ and E_b is the average energy per *information* bit. Since one symbol in $\boldsymbol{x}_i$ corresponds to K coded bits and because the code rate is $R = L/M$, one has $E_b = \frac{E_s}{K \times R} = \frac{M \times E_s}{K \times L}$. To facilitate performance comparison among various precoding schemes and transmission techniques considered in this paper, the received signal-to-noise ratio (SNR) per node is defined as $\text{SNR} = \frac{E_s \times \sigma_h^2}{N_0}$.

Based on $\boldsymbol{r}$, the relay node performs (*iterative*)[1] demodulation and decoding to obtain $\boldsymbol{u}_q$ as illustrated in Fig. 5.1. In this paper, decoding at the relay is based on the quaternary code representation [75]. As such, $\boldsymbol{u}_q$ is a vector consisting of quaternary digits. The details of the (iterative) demodulation and decoding based on quaternary code representation are deferred to Section 5.3.

For transmission in the BC phase, $\boldsymbol{u}_q$ is first network coded to obtain $\boldsymbol{u}_b$. In this paper, the XOR-based network coding is adopted so that the *ideal* code is expressed as $\boldsymbol{u}_o = \boldsymbol{u}_1 \oplus \boldsymbol{u}_2$, whereas the mapping from $\boldsymbol{u}_q$ to $\boldsymbol{u}_b$ is given in (5.10) in the next section when decoding based on quaternary code representation is described. Due to possible decoding errors in $\boldsymbol{u}_q$, the network-coded codeword $\boldsymbol{u}_b$ obtained from $\boldsymbol{u}_q$ might be different from the true codeword $\boldsymbol{u}_o$. As such, one can define the bit error probability when comparing $\boldsymbol{u}_b$ and $\boldsymbol{u}_o$. Next,

[1]Iterations are performed only for the case of BICM-ID.

$\boldsymbol{u}_b$ is encoded, interleaved and modulated as $\boldsymbol{s}_b$ and broadcast to the two terminal nodes. After receiving the broadcast signal, terminal node $\mathbb{T}_i$ performs conventional point-to-point (iterative) demodulation and decoding to get $\hat{\boldsymbol{u}}_{b,i}$. Finally, by conducting XOR between $\hat{\boldsymbol{u}}_{b,i}$ and self information, the information of the other terminal node is extracted as:

$$\hat{\boldsymbol{u}}_1 = \hat{\boldsymbol{u}}_{b,1} \oplus \boldsymbol{u}_2; \quad \hat{\boldsymbol{u}}_2 = \hat{\boldsymbol{u}}_{b,2} \oplus \boldsymbol{u}_1. \tag{5.4}$$

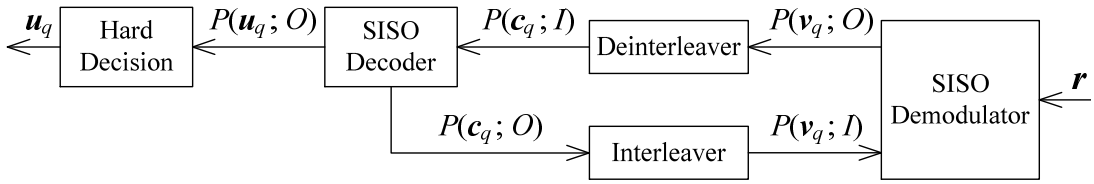

Figure 5.2 Iterative decoding based on quaternary code representation.

5.3 Iterative Decoding Based on Quaternary Code Representation

As illustrated in Fig. 5.2, iterative decoding involves two blocks: the soft-input soft-output (SISO) demodulator and the SISO decoder which uses the maximum *a posteriori* probability (MAP) algorithm [43]. Because the received signal is from a multiple-access channel, applying a conventional decoding approach designed for point-to-point communications does not achieve the best performance. Instead, iterative decoding based on the equivalent quaternary code representation [75] shall be used. To this end, the equivalent coded quaternary vector $\boldsymbol{c}_q = [c_q(1), \cdots, c_q(M)]^T$ is defined as $\boldsymbol{c}_q = 2\boldsymbol{c}_1 + \boldsymbol{c}_2$. For simplicity of analysis, the same length of information bits, code generator and interleaver are used in both terminal nodes. Based on this assumption, one can construct the interleaved quaternary vector $\boldsymbol{v}_q = [v_q(1), \cdots, v_q(M)]^T$ by $\boldsymbol{v}_q = 2\boldsymbol{v}_1 + \boldsymbol{v}_2$ and the equivalent information quaternary vector $\boldsymbol{u}_q = [u_q(1), \cdots, u_q(L)]^T$ by $\boldsymbol{u}_q = 2\boldsymbol{u}_1 + \boldsymbol{u}_2$. The components of $\boldsymbol{c}_q$, $\boldsymbol{v}_q$ and $\boldsymbol{u}_q$ are quaternary digits belonging to the set $\{0, 1, 2, 3\}$. As an example, the trellis diagram of the corresponding quaternary code when both nodes use a convolutional code with generator polynomials (in octal form) $\boldsymbol{g} = (5, 7)$ is shown in Fig. 5.3. The trellis shows the joint state transfers of the two convolutional codes. The states tabulated on the left side are called quaternary states. Specifically, suppose that the contents in the first and second registers of

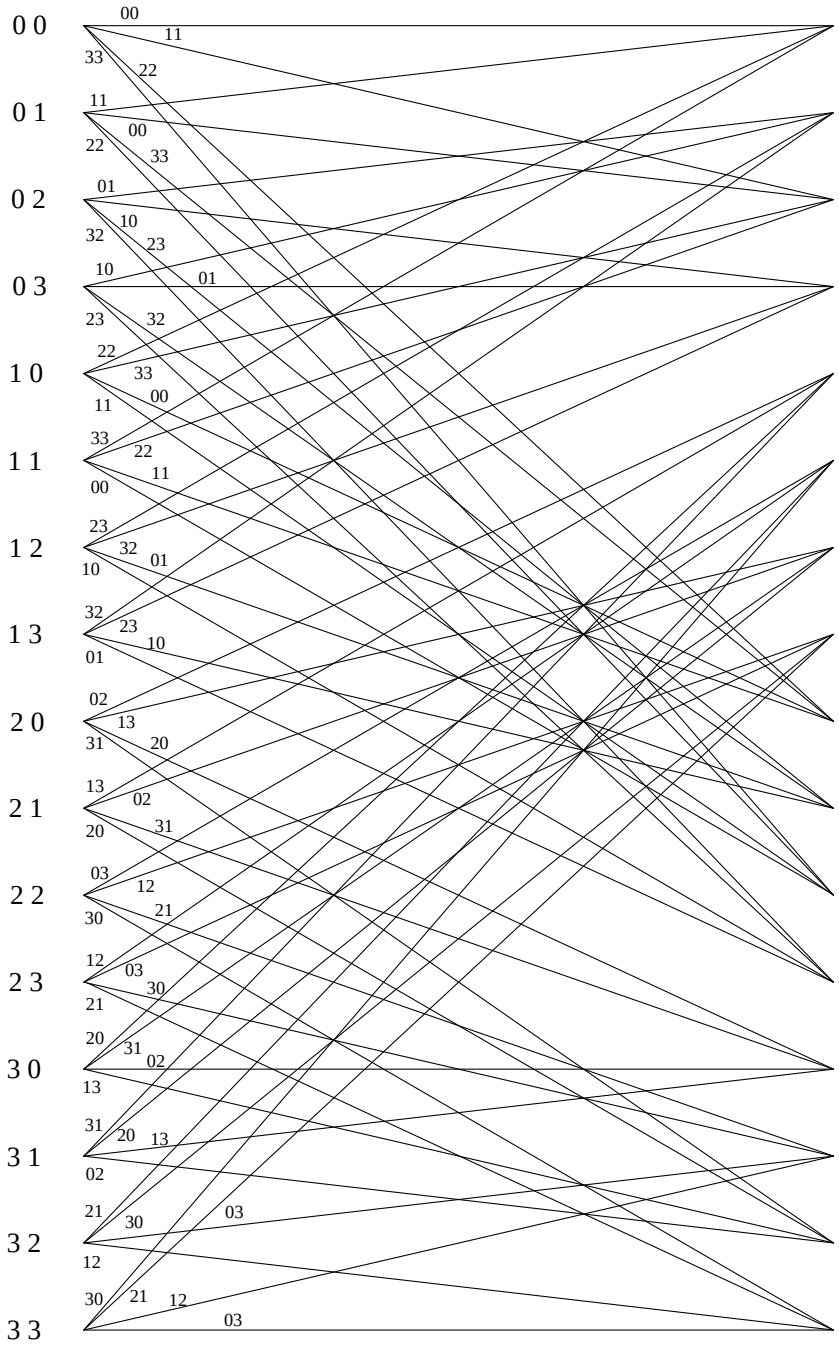

Figure 5.3 Trellis diagram of the equivalent quaternary code for a two-user MA channel when both terminal nodes use a convolutional code with generator polynomials $\boldsymbol{g} = (5, 7)$.

the encoder at terminal $\mathbb{T}_i$ are $\eta_i(1)$ and $\eta_i(2)$, respectively. Then the first and second digits defining a quaternary state are $\eta_q(1) = 2\eta_1(1) + \eta_2(1)$ and $\eta_q(2) = 2\eta_1(2) + \eta_2(2)$.

To elaborate the process of iterative decoding, (5.5) can be rewritten as:

$$\boldsymbol{r}_g = \boldsymbol{X}_g \boldsymbol{h}_g + \boldsymbol{\omega}_g \tag{5.5}$$

where $\boldsymbol{h}_g = [h_{1,g},\ \ h_{2,g}]^T$ and $\boldsymbol{X}_g = [\boldsymbol{x}_{1,g},\ \ \boldsymbol{x}_{2,g}]$. Let $\mathcal{M}$ be a function that maps K bits into a constellation symbol. That is $s_i(n) = \mathcal{M}\left(\boldsymbol{v}_i(n)\right)$ where $\boldsymbol{v}_i(n) = [v_i\left((n-1)K+1\right), \cdots, v_i\left(nK\right)]$. Similarly, taking into account the operation of DLCP and using the quaternary code representation, $\mathcal{M}_q$ is defined as the mapping from $2K$ quaternary digits to a 2×2 matrix $\boldsymbol{X}_g$. That is $\boldsymbol{X}_g = \mathcal{M}_q\left(\boldsymbol{v}_{q,g}\right)$ with $\boldsymbol{v}_{q,g} = [v_q\left(2(g-1)K+1\right), \cdots, v_q\left(2gK\right)]$. Furthermore, the set of distinct matrices $\boldsymbol{X}_g$ is defined as a *super constellation*, expressed as $\boldsymbol{\Psi}$.

Using the same notations as in [43], the *a priori* information and the *extrinsic* information of a random variable z are denoted by $P(z;I)$ and $P(z;O)$, respectively. In the first iteration, the *a priori* information sent to the deinterleaver is the *a posteriori* probability computed by the SISO demodulator. Given the received signal $\boldsymbol{r}_g$, the *a posteriori* probability for $2K$ coded quaternary digits $\boldsymbol{v}_{q,g}(k)$, $1 \leq k \leq 2K$, is computed as follows:

$$P\left(\boldsymbol{v}_{q,g}(k) = a|\boldsymbol{r}_g\right) = \sum_{\boldsymbol{X}_g \in \boldsymbol{\Psi}_a^k} P\left(\boldsymbol{X}_g|\boldsymbol{r}_g\right). \tag{5.6}$$

In (5.6), $P\left(\boldsymbol{X}_g|\boldsymbol{r}_g\right)$ is the *a posteriori* probability of the transmitted signal $\boldsymbol{X}_g$ given the received signal $\boldsymbol{r}_g$. The set $\boldsymbol{\Psi}_a^k$, $a \in \{0,1,2,3\}$, denotes the subset of $\boldsymbol{\Psi}$ that contains all signals whose labels have the value a at the kth position, $1 \leq k \leq 2K$. Using Bayes' rule, $P\left(\boldsymbol{v}_{q,g}(k) = a|\boldsymbol{r}_g\right)$ can be determined as follows:

$$P\left(\boldsymbol{v}_{q,g}(k) = a|\boldsymbol{r}_g\right) = \sum_{\boldsymbol{X}_g \in \boldsymbol{\Psi}_a^k} \frac{p\left(\boldsymbol{r}_g|\boldsymbol{X}_g\right) P\left(\boldsymbol{X}_g\right)}{p\left(\boldsymbol{r}_g\right)} \propto \sum_{\boldsymbol{X}_g \in \boldsymbol{\Psi}_a^k} p\left(\boldsymbol{r}_g|\boldsymbol{X}_g\right) P\left(\boldsymbol{X}_g\right) \tag{5.7}$$

where $P\left(\boldsymbol{X}_g\right)$ is the *a priori* probability of the transmitted $\boldsymbol{X}_g$. For the first iteration, the transmitted signals are equally likely, hence $P\left(\boldsymbol{X}_g\right) = 1/4^{2K}$.

From the second iteration, the *extrinsic* information $P\left(\boldsymbol{c}_q;O\right)$ of coded quaternary digits produced by the SISO decoder is sent to the interleaver. After being interleaved, it becomes the *a priori* information $P\left(\boldsymbol{v}_q;I\right)$ to enter the SISO demodulator. Thanks to interleaving, $2K$ digits corresponding to each vector $\boldsymbol{X}_g$ are assumed to be independent. Hence the *a*

priori information $P(\boldsymbol{X}_g)$ of $\boldsymbol{X}_g \in \boldsymbol{\Psi}$ can be obtained as:

$$P(\boldsymbol{X}_g) = P(\boldsymbol{v}_{q,g}(1 \multimap \boldsymbol{X}_g), \cdots, \boldsymbol{v}_{q,g}(2K \multimap \boldsymbol{X}_g)) = \prod_{k=1}^{2K} P(\boldsymbol{v}_{q,n}(k) = \boldsymbol{v}_{q,n}(k \multimap \boldsymbol{s}_{q,n}); I), \tag{5.8}$$

where the notation $\boldsymbol{v}_{q,g}(k \multimap \boldsymbol{X}_g) \in \{0,1,2,3\}$ means the value of the kth quaternary digit in the label of $\boldsymbol{X}_g$. Using (5.7) and (5.8), the *extrinsic* information from the second iteration can be computed as:

$$\begin{aligned} P(\boldsymbol{v}_{q,g}(k) = a; O) &= \frac{P(\boldsymbol{v}_{q,g}(k) = a|\boldsymbol{r}_g)}{P(\boldsymbol{v}_{q,g}(k) = a; I)} \propto \frac{\sum_{\boldsymbol{X}_g \in \boldsymbol{\Psi}_a^k} p(\boldsymbol{r}_g|\boldsymbol{X}_g) P(\boldsymbol{X}_g)}{P(\boldsymbol{v}_{q,g}(k) = a; I)} \\ &= \sum_{\boldsymbol{X}_g \in \boldsymbol{\Psi}_a^k} \left[p(\boldsymbol{r}_g|\boldsymbol{X}_g) \prod_{j \neq k} P(\boldsymbol{v}_{q,g}(j) = \boldsymbol{v}_{q,g}(j \multimap \boldsymbol{X}_g); I) \right]. \end{aligned} \tag{5.9}$$

The *extrinsic* information is then deinterleaved to become *a priori* information and delivered to the SISO decoder. At any iteration, the hard-decisions of quaternary digits $\boldsymbol{u}_q$ can be obtained based on the corresponding *extrinsic* information $P(\boldsymbol{u}_q; O)$. Furthermore, the lth bit in $\boldsymbol{u}_b$ can be obtained from $\boldsymbol{u}_q$ as:

$$u_b(l) = \begin{cases} 0, & \text{if} \quad u_q(l) = 0 \quad \text{or} \quad u_q(l) = 3 \\ 1, & \text{if} \quad u_q(l) = 1 \quad \text{or} \quad u_q(l) = 2 \end{cases} \tag{5.10}$$

5.4 Performance Analysis

In a TWRC system, the terminal-to-terminal bit error probability (BEP) is commonly used for performance evaluation. In this paper, the terminal-to-terminal errors are the errors between $\boldsymbol{u}_i$ and $\hat{\boldsymbol{u}}_i$. Since there are two transmission phases in a TWRC system, the errors between $\boldsymbol{u}_i$ and $\hat{\boldsymbol{u}}_i$ may happen in two stages: (i) transmitting $\boldsymbol{u}_i$ and obtaining $\boldsymbol{u}_b$, and (ii) transmitting $\boldsymbol{u}_b$ and obtaining $\hat{\boldsymbol{u}}_i$. From Equation (5.4), it is known that the errors in stage two are equivalent to the errors between $\boldsymbol{u}_b$ and $\hat{\boldsymbol{u}}_{b,i}$. Since the signal processing in the BC phase is the same as in the conventional point-to-point systems, the probability of errors between $\boldsymbol{u}_b$ and $\hat{\boldsymbol{u}}_{b,i}$ is not analyzed in this paper. On the other hand, since $\boldsymbol{u}_b$ is the actual version of the ideal network-coded codeword $\boldsymbol{u}_o = \boldsymbol{u}_1 \oplus \boldsymbol{u}_2$, the errors in stage one are equivalent to the errors between $\boldsymbol{u}_b$ and $\boldsymbol{u}_o$. In the following sections, the errors between $\boldsymbol{u}_b$

and $\boldsymbol{u}_o$ are called the *errors under network coding* and the corresponding BEP is called the *BEP under network coding*.

As seen from (5.10), $\boldsymbol{u}_b$ is obtained from $\boldsymbol{u}_q$. Therefore, in the following discussion, the error probability of decoding $\boldsymbol{u}_q$, which is called quaternary-digit error probability (QEP), is first derived to aid the analysis of the BEP under network coding. Following the same method in [44, 45, 75], an upper bound on the QEP of BICM-ID in the MA phase of the TWRC system where both nodes employ the same rate-k_c/n_c convolutional code, an equivalent super constellation $\boldsymbol{\Psi}$ and a mapping rule $\mathcal{M}_q$ can be written as follows:

$$P_e \leq \frac{1}{k_c} \sum_{d=d_H}^{\infty} \rho_d f\left(d, \boldsymbol{\Psi}, \mathcal{M}_q\right), \tag{5.11}$$

where ρ_d is the total information weight of all error events at Hamming distance d and d_H is the free Hamming distance of the equivalent quaternary code. The function $f\left(d, \boldsymbol{\Psi}, \mathcal{M}_q\right)$ is the average pairwise error probability (PEP), which depends on the Hamming distance d, the constellation $\boldsymbol{\Psi}$ and the mapping rule $\mathcal{M}_q$. Let $\boldsymbol{c}_q$ and $\hat{\boldsymbol{c}}_q$ denote the transmitted and decoded quaternary vectors (each with a length of M quaternary digits), respectively, with Hamming distance d between them. These quaternary vectors correspond to $N \times 2$ matrices $\boldsymbol{X} = [\boldsymbol{X}_1, \ldots, \boldsymbol{X}_G]$ and $\hat{\boldsymbol{X}} = [\hat{\boldsymbol{X}}_1, \ldots, \hat{\boldsymbol{X}}_G]$, where $G = N/2$ and each of the 2×2 matrices $\boldsymbol{X}_g$ and $\hat{\boldsymbol{X}}_g$, $1 \leq g \leq G$, is an element in the super constellation $\boldsymbol{\Psi}$. The function $f\left(d, \boldsymbol{\Psi}, \mathcal{M}_q\right)$ is computed from the PEP $P\left(\boldsymbol{X} \to \hat{\boldsymbol{X}}\right)$ by averaging over all possible matrices $\boldsymbol{X}$ and $\hat{\boldsymbol{X}}$. The calculation of $P\left(\boldsymbol{X} \to \hat{\boldsymbol{X}}\right)$ is as follows.

Without loss of generality, assume that $\boldsymbol{c}_q$ and $\hat{\boldsymbol{c}}_q$ differ in the first d consecutive quaternary digits. Hence, $\boldsymbol{X}$ and $\hat{\boldsymbol{X}}$ can be redefined as $\boldsymbol{X} = [\boldsymbol{X}_1, \cdots, \boldsymbol{X}_d]$ and $\hat{\boldsymbol{X}} = \left[\hat{\boldsymbol{X}}_1, \cdots, \hat{\boldsymbol{X}}_d\right]$. Also let $\boldsymbol{H}_d = [\boldsymbol{h}_1, \cdots, \boldsymbol{h}_d]$ where $\boldsymbol{h}_g$ $(1 \leq g \leq d)$ denotes the channel responses that affect the transmitted $\boldsymbol{X}_g$. Then the PEP conditioned on $\boldsymbol{H}_d$ can be computed as follows:

$$P\left(\boldsymbol{X} \to \hat{\boldsymbol{X}} | \boldsymbol{H}_d\right) = Q\left(\sqrt{\frac{1}{2N_0} \sum_{g=1}^{d} d^2\left(\boldsymbol{X}_g, \hat{\boldsymbol{X}}_g | \boldsymbol{h}_g\right)}\right). \tag{5.12}$$

In (5.12), $d^2\left(\boldsymbol{X}_g, \hat{\boldsymbol{X}}_g | \boldsymbol{h}_g\right)$ is the squared Euclidean distance between the two received signals corresponding to $\boldsymbol{X}_g$ and $\hat{\boldsymbol{X}}_g$, conditioned on $\boldsymbol{h}_g$. This squared Euclidean distance can be

expressed as:

$$d^2\left(\boldsymbol{X}_g, \hat{\boldsymbol{X}}_g|\boldsymbol{h}_g\right) = \left\|\left(\boldsymbol{X}_g - \hat{\boldsymbol{X}}_g\right)\boldsymbol{h}_g\right\|^2 = \boldsymbol{h}_g^H \boldsymbol{D}_g \boldsymbol{h}_g \tag{5.13}$$

where $\boldsymbol{D}_g = \left(\boldsymbol{X}_g - \hat{\boldsymbol{X}}_g\right)^H \left(\boldsymbol{X}_g - \hat{\boldsymbol{X}}_g\right)$. Furthermore, by performing singular value decomposition on $\boldsymbol{D}_g$, one has

$$\boldsymbol{h}_g^H \boldsymbol{D}_g \boldsymbol{h}_g = \boldsymbol{h}_g^H \boldsymbol{U}_g^H \boldsymbol{\Lambda}_g \boldsymbol{U}_g \boldsymbol{h}_g = \tilde{\boldsymbol{h}}_g^H \boldsymbol{\Lambda}_g \tilde{\boldsymbol{h}}_g = \left|\tilde{h}_{1,g}\right|^2 \left|\lambda_1\left(\boldsymbol{D}_g\right)\right|^2 + \left|\tilde{h}_{2,g}\right|^2 \left|\lambda_2\left(\boldsymbol{D}_g\right)\right|^2 \tag{5.14}$$

where $\boldsymbol{U}_g$ is an unitary matrix, $\lambda_1\left(\boldsymbol{D}_g\right)$ and $\lambda_2\left(\boldsymbol{D}_g\right)$ are singular values of $\boldsymbol{D}_g$. Since $\boldsymbol{D}_g$ is unitary, the variance of $\tilde{h}_{1,g}$ and $\tilde{h}_{2,g}$ are the same as that of $h_{1,g}$ and $h_{2,g}$. However, their expectations depend on $\boldsymbol{D}_g$ and are expressed as $\varepsilon_{h_1}\left(\boldsymbol{D}_g\right)$ and $\varepsilon_{h_2}\left(\boldsymbol{D}_g\right)$.

Using the Gaussian probability integral and averaging (5.12) over $\boldsymbol{H}_d$, or equivalently over $\tilde{\boldsymbol{H}}_d = \left[\tilde{\boldsymbol{h}}_1, \cdots, \tilde{\boldsymbol{h}}_d\right]$ gives

$$P\left(\boldsymbol{X} \to \hat{\boldsymbol{X}}\right) = E_{\boldsymbol{H}_d}\left\{P\left(\boldsymbol{X} \to \hat{\boldsymbol{X}}|\boldsymbol{H}_d\right)\right\} = \frac{1}{\pi}\int_0^{\pi/2}\left(\prod_{g=1}^{d}\zeta\left(\boldsymbol{X}_g \to \hat{\boldsymbol{X}}_g\right)\right)\mathrm{d}\theta \tag{5.15}$$

where

$$\zeta\left(\boldsymbol{X}_g \to \hat{\boldsymbol{X}}_g\right) = \prod_{i=1}^{2}\frac{\sin^2\theta}{\sin^2\theta + \Omega_{g,i}}\exp\left(-\frac{\left|\varepsilon_{h_i}\left(\boldsymbol{D}_g\right)\right|^2}{2\sigma_{h_i}^2}\frac{\Omega_{g,i}}{\sin^2\theta + \Omega_{g,i}}\right) \tag{5.16}$$

with $\Omega_{g,i} = \sigma_{h_i}^2 \lambda_i\left(\boldsymbol{D}_g\right)/4N_0$.

Next, by averaging (5.15) over all possible matrices $\boldsymbol{X}$ and $\hat{\boldsymbol{X}}$, the function $f\left(d, \boldsymbol{\Psi}, \mathcal{M}_q\right)$ can be calculated as follows:

$$f\left(d, \boldsymbol{\Psi}, \mathcal{M}_q\right) \leq \frac{1}{\pi}\int_0^{\pi/2}\left[\gamma\left(\boldsymbol{\Psi}, \mathcal{M}_q\right)\right]^d \mathrm{d}\theta, \tag{5.17}$$

where

$$\gamma\left(\boldsymbol{\Psi}, \mathcal{M}_q\right) = E\left\{\zeta\left(\boldsymbol{X}_g \to \hat{\boldsymbol{X}}_g\right)\right\} = \frac{1}{\mathcal{N}_1}\sum_{\boldsymbol{X}_g \in \boldsymbol{\Psi}}\sum_{k=1}^{2K}\frac{1}{\mathcal{N}_2}\sum_{\hat{\boldsymbol{X}}_g \in \bar{\boldsymbol{\Psi}}_{\boldsymbol{X}_g}^k}\zeta\left(\boldsymbol{X}_g \to \hat{\boldsymbol{X}}_g\right). \tag{5.18}$$

In the above expression, $\mathcal{N}_1 = 2K4^{2K}$ is the size of the super constellation $\boldsymbol{\Psi}$, whereas $\mathcal{N}_2$ is the number of matrices in the set $\bar{\boldsymbol{\Psi}}_{\boldsymbol{X}_g}^k$. The set $\bar{\boldsymbol{\Psi}}_{\boldsymbol{X}_g}^k$ is a subset of the super constellation $\boldsymbol{\Psi}$ and how it is defined depends on whether BICM or BICM-ID is adopted in the system. This is explained further in the following.

When *BICM-ID* is adopted and with enough iterations performed at the receiver, the error-free feedback (EF) bound [44] can be used to characterize the asymptotic performance of the system. Under the error-free feedback assumption, $\bar{\boldsymbol{\Psi}}^k_{\boldsymbol{X}_g}$ is defined as the set of matrices in $\boldsymbol{\Psi}$ whose labels differ *only* at position k compared to the label of a given matrix $\boldsymbol{X}_g$, i.e., the other $2K-1$ label digits of any matrix in $\bar{\boldsymbol{\Psi}}^k_{\boldsymbol{X}_g}$ must be the same as the corresponding $2K-1$ label digits of $\boldsymbol{X}_g$. It is pointed out that in the conventional point-to-point BICM-ID system, the set $\bar{\boldsymbol{\Psi}}^k_{\boldsymbol{X}_g}$ contains only one matrix whose label can be obtained by switching the kth bit of the label of $\boldsymbol{X}_g$, from "1" to "0" or "0" to "1". However, in a TWRC system, since decoding at the relay is based on quaternary code representation, the set $\bar{\boldsymbol{\Psi}}^k_{\boldsymbol{X}_g}$ contains $\mathcal{N}_2 = 3$ matrices. For example, suppose that both terminals use QPSK modulation and the label of $\boldsymbol{X}_g$ is [0 0 0 0], then the matrices in $\bar{\boldsymbol{\Psi}}^1_{\boldsymbol{X}_g}$ are those with labels $\{[1\ 0\ 0\ 0], [2\ 0\ 0\ 0], [3\ 0\ 0\ 0]\}$, whereas the labels of matrices in $\bar{\boldsymbol{\Psi}}^2_{\boldsymbol{X}_g}$ are $\{[0\ 1\ 0\ 0], [0\ 2\ 0\ 0], [0\ 3\ 0\ 0]\}$.

On the other hand, for *BICM*, the standard union bound [14] is commonly used for performance analysis. In this case, the $\bar{\boldsymbol{\Psi}}^k_{\boldsymbol{X}_g}$ is defined as the set of matrices whose labels differ at position k compared to the label of $\boldsymbol{X}_g$, i.e., the other $2K-1$ label digits can be the same or different as compared to the corresponding $2K-1$ label digits of $\boldsymbol{X}_g$. In a point-to-point system with binary labels, $\bar{\boldsymbol{\Psi}}^k_{\boldsymbol{X}_g}$ would contain 4^{2K-1} matrices. However, the size of $\bar{\boldsymbol{\Psi}}^k_{\boldsymbol{X}_g}$ is $\mathcal{N}_2 = 3(4^{2K-1})$ in a TWRC system.

Now, considering the BEP under network coding. The union bound and EF bound of BEP under network coding for BICM and BICM-ID, respectively, can be obtained in the same way, starting with (5.11) and yield the same expressions as those of QEP. The only difference is how the set $\bar{\boldsymbol{\Psi}}^k_{\boldsymbol{X}_g}$ is defined (hence, also the value $\mathcal{N}_2$). For the EF bound of BEP under network coding with BICM-ID, $\bar{\boldsymbol{\Psi}}^k_{\boldsymbol{X}_g}$ contains $\mathcal{N}_2 = 2$ matrices for each given $\boldsymbol{X}_g$. This is because the errors from "0" to "3", "3" to "0", "1" to "2" and "2" to "1" should not be counted in the view of XOR network coding. Using the same example for the label of $\boldsymbol{X}_g$ being [0 0 0 0], the labels of the matrices in $\bar{\boldsymbol{\Psi}}^1_{\boldsymbol{X}_g}$ are $\{[1\ 0\ 0\ 0], [2\ 0\ 0\ 0]\}$, whereas the labels of matrices in $\bar{\boldsymbol{\Psi}}^2_{\boldsymbol{X}_g}$ are $\{[0\ 1\ 0\ 0], [0\ 2\ 0\ 0]\}$. On the other hand, the size of $\bar{\boldsymbol{\Psi}}^k_{\boldsymbol{X}_g}$ used in the calculation of the union bound of BEP under network coding with BICM

is $\mathcal{N}_2 = 2(4^{2K-1})$.

Finally, for convenience in designing DLCP to be used with BICM and BICM-ID in TWRC, an upper bound of $f(d, \mathbf{\Psi}, \xi)$ is obtained by setting $\theta = \pi/2$, which yields:

$$f_{\text{up}}(d, \mathbf{\Psi}, \mathcal{M}_q) = \left[\gamma_{\text{up}}(\mathbf{\Psi}, \mathcal{M}_q)\right]^d, \tag{5.19}$$

where

$$\gamma_{\text{up}}(\mathbf{\Psi}, \mathcal{M}_q) = \frac{1}{\mathcal{N}_\infty} \sum_{\boldsymbol{X}_g \in \mathbf{\Psi}} \sum_{k=1}^{2K} \frac{1}{\mathcal{N}_\in} \sum_{\hat{\boldsymbol{X}}_g \in \bar{\mathbf{\Psi}}^k_{\boldsymbol{X}_g}} \zeta_{\text{up}}\left(\boldsymbol{X}_g \to \hat{\boldsymbol{X}}_g\right) \tag{5.20}$$

with

$$\zeta_{\text{up}}\left(\boldsymbol{X}_g \to \hat{\boldsymbol{X}}_g\right) = \prod_{i=1}^{2} \frac{1}{1+\Omega_{g,i}} \exp\left(-\frac{\left|\varepsilon_{h_i}(\boldsymbol{D}_g)\right|^2}{\sigma^2_{h_i}} \frac{\Omega_{g,i}}{1+\Omega_{g,i}}\right). \tag{5.21}$$

5.5 DLCP Designs For TWRC

LCP is originally proposed in [10,76] to achieve spatial and multipath diversity in single-user point-to-point communications. In [64], DLCP is employed in conjunction with OFDM at the terminal nodes to achieve diversity and reduce MAI in the two-slot TWRC. According to the scheme given in [64], the DLCP is expressed as:

$$\mathbf{\Theta}_1 = \frac{1}{\sqrt{2}} \begin{pmatrix} 1 & \mathrm{e}^{-j\frac{\pi}{4}} \\ 1 & \mathrm{e}^{-j\frac{5\pi}{4}} \end{pmatrix}, \quad \mathbf{\Theta}_2 = \frac{1}{\sqrt{2}} \begin{pmatrix} 1 & \mathrm{e}^{-j\frac{\pi}{4}} \\ \beta & \beta\mathrm{e}^{-j\frac{5\pi}{4}}, \end{pmatrix} \tag{5.22}$$

where β is a design parameter. As mentioned in Section 5.1, the objective of designing DLCP is to achieve good detection performance in the MA phase. Therefore, upperbounds on QEP and BEP under network coding are suitable metrics for the design. From (5.19), it can be seen that the QEP and BEP under network coding performances are strongly related to $\gamma_{\text{up}}(\mathbf{\Psi}, \mathcal{M}_q)$ for a specific convolutional code. Since this paper focuses on the design of DLCP, in the following discussion, the mapping rule $\mathcal{M}_q$ is not treated as a design variable. In addition, for a specific modulation scheme, the super constellation $\mathbf{\Psi}$ is completely determined by the DLCP matrices $\mathbf{\Theta}_1$ and $\mathbf{\Theta}_2$. Thus $\gamma_{\text{up}}(\mathbf{\Psi}, \mathcal{M}_q)$ is more meaningfully indicated as $\gamma_{\text{up}}(\mathbf{\Theta}_1, \mathbf{\Theta}_2)$. The form of DLCP given in (5.22) indicates that the LCP code used by terminal node $\mathbb{T}_1$ is fixed, while the LCP code used by terminal node $\mathbb{T}_2$ needs to be optimized

by choosing parameter β. In other words, the only parameter that needs to be optimized in the design is β.

Before explaining the optimization of β, some concepts need to be introduced. First, from (5.21), it can be found that $\zeta_{\text{up}}\left(\boldsymbol{X}_g \to \hat{\boldsymbol{X}}_g\right)$ is actually the PEP upperbound between $\boldsymbol{X}_g$ and $\hat{\boldsymbol{X}}_g$ and $\gamma_{\text{up}}\left(\boldsymbol{\Theta}_1, \boldsymbol{\Theta}_2\right)$ is the average of a set of PEPs. Since $\boldsymbol{X}_g$ is consisted of $\boldsymbol{x}_{1,g}$ and $\boldsymbol{x}_{2,g}$ which are precoded versions of $\boldsymbol{s}_{1,g}$ and $\boldsymbol{s}_{2,g}$, the pairwise error events $\boldsymbol{X}_g \to \hat{\boldsymbol{X}}_g$ can be partitioned into the following three types of errors [59, 60, 64]:

- Type-1 errors: $\mathcal{E}_1 = \{\boldsymbol{e} : \boldsymbol{s}_{1,g} \neq \hat{\boldsymbol{s}}_{1,g}, \boldsymbol{s}_{2,g} = \hat{\boldsymbol{s}}_{2,g}\}$.
- Type-2 errors: $\mathcal{E}_2 = \{\boldsymbol{e} : \boldsymbol{s}_{1,g} = \hat{\boldsymbol{s}}_{1,g}, \boldsymbol{s}_{2,g} \neq \hat{\boldsymbol{s}}_{2,g}\}$.
- Type-3 errors: $\mathcal{E}_3 = \{\boldsymbol{e} : \boldsymbol{s}_{1,g} \neq \hat{\boldsymbol{s}}_{1,g}, \boldsymbol{s}_{2,g} \neq \hat{\boldsymbol{s}}_{2,g}\}$.

With the above definitions of three types of errors and by knowing that the DLCP matrices are unitary, one has the following theorem.

Theorem 1 *If DLCP matrices are unitary, they will not influence the PEP performance under type-1 and type-2 errors.*

Proof: First, suppose that the error event belongs to type-1 errors. Then one has $\boldsymbol{s}_{1,g} \neq \hat{\boldsymbol{s}}_{1,g}, \boldsymbol{s}_{2,g} = \hat{\boldsymbol{s}}_{2,g}$ and thus $\boldsymbol{x}_{1,g} \neq \hat{\boldsymbol{x}}_{1,g}, \boldsymbol{x}_{2,g} = \hat{\boldsymbol{x}}_{2,g}$. Therefore the matrix $\boldsymbol{D}_g = \left(\boldsymbol{X}_g - \hat{\boldsymbol{X}}_g\right)^H \left(\boldsymbol{X}_g - \hat{\boldsymbol{X}}_g\right)$ takes the following form:

$$\boldsymbol{D}_g = \begin{pmatrix} \boldsymbol{x}_{1,g}^H - \hat{\boldsymbol{x}}_{1,g}^H \\ \mathbf{0} \end{pmatrix} \begin{pmatrix} \boldsymbol{x}_{1,g} - \hat{\boldsymbol{x}}_{1,g} & \mathbf{0} \end{pmatrix} = \begin{pmatrix} \left\|\boldsymbol{x}_{1,g} - \hat{\boldsymbol{x}}_{1,g}\right\|^2 & 0 \\ 0 & 0 \end{pmatrix}. \tag{5.23}$$

Because of the special form of matrix $\boldsymbol{D}_g$, the expectation of $\tilde{h}_{i,g}$ does not depend on $\boldsymbol{D}_g$ and can simply expressed as ε_{h_i}. On the other hand, the singular values of $\boldsymbol{D}_g$ are $\lambda_1\left(\boldsymbol{D}_g\right) = \left\|\boldsymbol{x}_{1,g} - \hat{\boldsymbol{x}}_{1,g}\right\|^2$ and $\lambda_2\left(\boldsymbol{D}_g\right) = 0$. Furthermore, using the facts that $\boldsymbol{x}_{i,g} = \boldsymbol{\Theta}_i \boldsymbol{s}_{i,g}$ and $\boldsymbol{\Theta}_i$ is a unitary matrix, one has $\left\|\boldsymbol{x}_{1,g} - \hat{\boldsymbol{x}}_{1,g}\right\|^2 = \left\|\boldsymbol{s}_{1,g} - \hat{\boldsymbol{s}}_{1,g}\right\|^2$ It then follows that the PEP upper

bound of type-1 errors can be expressed as:

$$\zeta_{\text{up},1}\left(\boldsymbol{X}_g \to \hat{\boldsymbol{X}}_g\right) = \left(1 + \frac{\delta_{h_1}^2 \left\|\boldsymbol{s}_{1,g} - \hat{\boldsymbol{s}}_{1,g}\right\|^2}{4N_0}\right)^{-1} \exp\left(-\frac{\left|\varepsilon_{h_1}\right|^2 \left\|\boldsymbol{s}_{1,g} - \hat{\boldsymbol{s}}_{1,g}\right\|^2}{4N_0 + \delta_{h_1}^2 \left\|\boldsymbol{s}_{1,g} - \hat{\boldsymbol{s}}_{1,g}\right\|^2}\right), \quad \text{for } \left\{\boldsymbol{X}_g \to \hat{\boldsymbol{X}}_g\right\} \in \mathcal{E}_1. \tag{5.24}$$

Similarly, the PEP upper bound of type-2 errors is:

$$\zeta_{\text{up},2}\left(\boldsymbol{X}_g \to \hat{\boldsymbol{X}}_g\right) = \left(1 + \frac{\delta_{h_2}^2 \left\|\boldsymbol{s}_{2,g} - \hat{\boldsymbol{s}}_{2,g}\right\|^2}{4N_0}\right)^{-1} \exp\left(-\frac{\left|\varepsilon_{h_2}\right|^2 \left\|\boldsymbol{s}_{2,g} - \hat{\boldsymbol{s}}_{2,g}\right\|^2}{4N_0 + \delta_{h_2}^2 \left\|\boldsymbol{s}_{2,g} - \hat{\boldsymbol{s}}_{2,g}\right\|^2}\right), \quad \text{for } \left\{\boldsymbol{X}_g \to \hat{\boldsymbol{X}}_g\right\} \in \mathcal{E}_2. \tag{5.25}$$

From the above expressions, it can be seen that the PEP upper bounds for type-1 and type-2 errors are only related to the channel parameters, but independent of the DLCP matrix. This completes the proof. ■

Theorem 1 implies that there is no need to consider type-1 and type-2 errors when designing DLCP for TWRC. This is reasonable since DLCP is meant to reduce the influence of MAI, which is the main cause of type-3 errors (type-1 and type-2 errors are mainly caused by channel fading [64]). In the following subsections, DLCP designs are considered for BICM and BICM-ID separately by examining type-3 errors in more details.

5.5.1 DLCP Design for TWRC with BICM

The DLCP design proposed here is to optimize the parameter β so that the union bound on the BEP under network coding is minimized. This approach is reasonable and commonly adopted for complex communications systems, such as the one considered in this paper. From the analysis given in [39, 64], it is known that to achieve the full diversity gain under type-3 errors, β needs to be a transcendental number. Furthermore, β can be expressed as $\beta = \exp(j\varphi)$, where φ is a rational number [62] chosen to make β a transcendental number. Since $\boldsymbol{\Theta}_1$ and $\boldsymbol{\Theta}_2$ depend only on φ, considering only type-3 errors, the metric that effectively determine the performance of DLCP can be expressed as:

$$\gamma_{\text{up},3}(\varphi) = \frac{1}{\mathcal{N}_1} \sum_{\boldsymbol{X}_g \in \boldsymbol{\Psi}} \sum_{k=1}^{2K} \frac{1}{\mathcal{N}_2 - \mathcal{N}_3} \sum_{\hat{\boldsymbol{X}}_g \in \bar{\boldsymbol{\Psi}}_{\boldsymbol{X}_g,3}^k} \zeta_{\text{up},3}\left(\boldsymbol{X}_g \to \hat{\boldsymbol{X}}_g\right), \tag{5.26}$$

where $\bar{\boldsymbol{\Psi}}^{k}_{\boldsymbol{X}_g,3}$ denotes the set of matrices $\hat{\boldsymbol{X}}_g$ so that $\boldsymbol{X}_g \to \hat{\boldsymbol{X}}_g$ is a type-3 error, $\mathcal{N}_1 = 2K4^{2K}$ and $\mathcal{N}_2 = 3(4^{(2K-1)})$ as explained in Section 5.4, while $\mathcal{N}_3 = 4^K$ is the number of matrices $\hat{\boldsymbol{X}}_g$ such that $\boldsymbol{X}_g \to \hat{\boldsymbol{X}}_g$ is a type-1 or type-2 error.

The search for φ that minimizes $\gamma_{\text{up},3}$ can be conducted over the range $0 \leq \varphi \leq \pi$. This is because the function $\gamma_{\text{up},3}$ is symmetric around $\varphi = \pi$ (see the proof in Appendix 5.A). As an example, Fig. 5.4 plots $\gamma_{\text{up},3}$ as a function of φ in the case of Rayleigh fading channels that are related to both QEP and BEP under network coding. It can be seen that, for each SNR value considered, the $\gamma_{\text{up},3}$ curves have very similar patterns. Specifically, the figure shows that the optimal value of φ varies for different SNRs. With low to moderate SNR values, e.g. SNR = 3 dB or SNR = 7 dB, $\varphi = 0$ minimizes $\gamma_{\text{up},3}$. However, for high SNR values, e.g. SNR = 11 dB or SNR = 15 dB, the optimal value of φ is close to $\pi/4$.

From the derivation of $\gamma_{\text{up},3}$, it can be seen that beside SNR, the expectations ε_{h_i} of channels h_i, $i = 1, 2$, also influence the performance. For a specific Rician factor K_f, define $\exp(j\theta) = \varepsilon_{h_2}/\varepsilon_{h_1}$. Fig. 5.5 plots $\gamma_{\text{up},3}$ related to QEP and BEP under network coding as a function of φ in the case of Rician fading channels with different values of θ and $K_f = 10$. As can be seen, for each SNR and θ, the $\gamma_{\text{up},3}$ curves also have similar patterns. In addition, it is found that for low to moderate SNR values, θ has a strong influence on the optimal value of φ. Take SNR = 3 dB and SNR = 7 dB as examples, one sees that $\varphi = 0$ minimizes $\gamma_{\text{up},3}$ for $\theta = 0$ and $\theta = \pi/4$, while φ close to $\pi/2$ is optimal for $\theta = \pi/2$. For high SNR values, all curves with different values of θ have similar patterns with φ close to $\pi/4$ being optimal.

5.5.2 DLCP Design for TWRC with BICM-ID

First, consider optimizing β to minimize the EF bound of QEP when BICM-ID is used. Making use of Theorem 1 and considering only type-3 errors, equation (5.20) can be rewritten as:

$$\gamma_{\text{up}}(\boldsymbol{\Psi}, \mathcal{M}_q) = \frac{1}{2K4^{2K}} \sum_{\boldsymbol{X}_g \in \boldsymbol{\Psi}} \sum_{k=1}^{2K} \sum_{\hat{\boldsymbol{X}}_g \in \bar{\boldsymbol{\Psi}}^{k}_{\boldsymbol{X}_g,3}} \zeta_{\text{up}}\left(\boldsymbol{X}_g \to \hat{\boldsymbol{X}}_g\right) \tag{5.27}$$

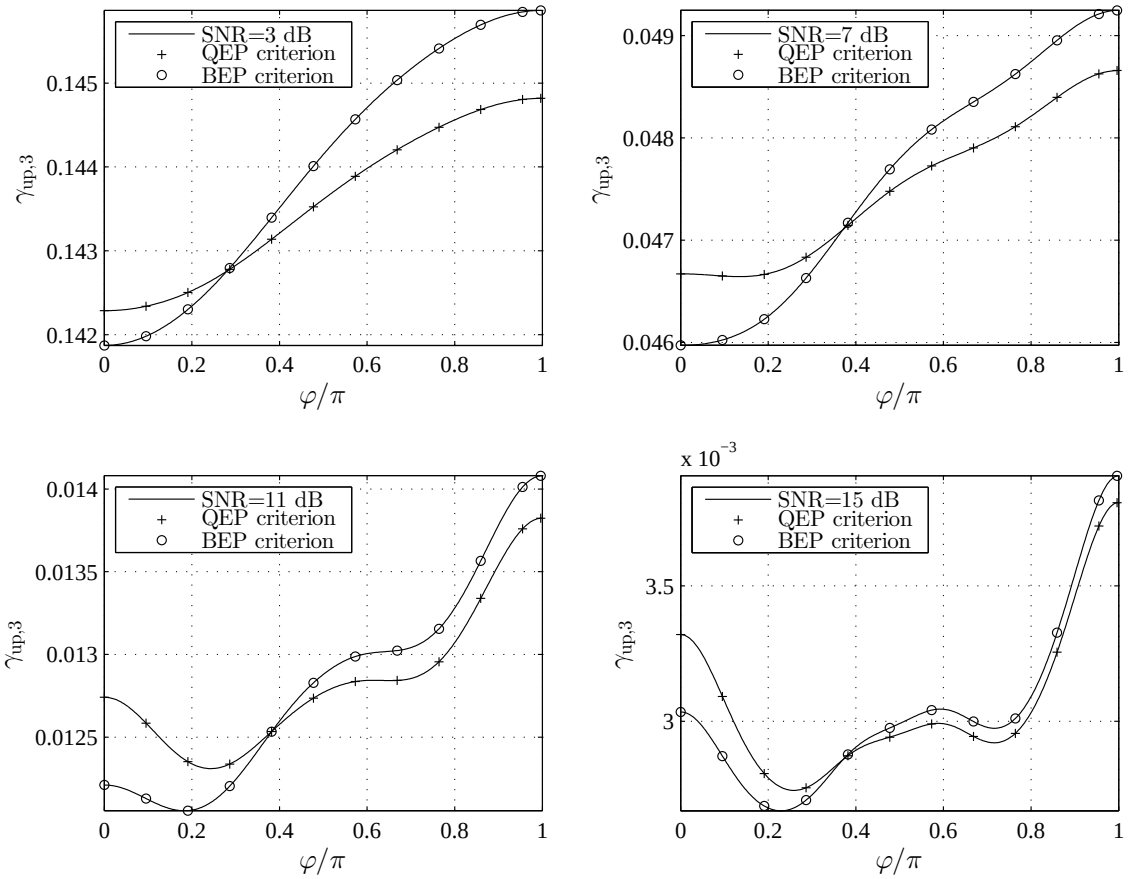

Figure 5.4 $\gamma_{\mathrm{up},3}$ versus φ for QPSK and at different SNR values over Rayleigh fading channels.

where $\bar{\boldsymbol{\Psi}}^{k}_{\boldsymbol{X}_{g,3}}$ contains only one matrix. Furthermore, in the high SNR region, one can approximate

$$\zeta_{\mathrm{up}}\left(\boldsymbol{X}_g \to \hat{\boldsymbol{X}}_g\right) \approx \left(\lambda_1^2\left(\boldsymbol{D}_g\right)\lambda_2^2\left(\boldsymbol{D}_g\right)\right)^{-1}\left(\frac{\sigma_h^2}{4N_0}\right)^{-2}\exp\left(\frac{\left|\varepsilon_{h_1}\left(\boldsymbol{D}_g\right)\right|^2+\left|\varepsilon_{h_2}\left(\boldsymbol{D}_g\right)\right|^2}{2\sigma_h^2}\right). \quad (5.28)$$

From (5.28), it can be seen that minimizing ζ_{up} is equivalent to maximizing $\lambda_1^2\left(\boldsymbol{D}_g\right)\lambda_2^2\left(\boldsymbol{D}_g\right)$, and thus equivalent to maximizing $\left|\det\left(\boldsymbol{D}_g\right)\right|$.

For the calculation of the EF bound, the matrices $\boldsymbol{X}_g$ and $\hat{\boldsymbol{X}}_g$ are such that their labels differ just in one digit. If the different label digit happens in any of the first to the Kth positions, then the constellation symbols corresponding to $\boldsymbol{X}_g$ and $\hat{\boldsymbol{X}}_g$ satisfy $s_1(2g) = \hat{s}_1(2g)$ and $s_2(2g) = \hat{s}_2(2g)$. Likewise, if the different label digit happens in any of the $(K+1)$th to the $(2K)$th positions, one has $s_1(2g-1) = \hat{s}_1(2g-1)$ and $s_2(2g-1) = \hat{s}_2(2g-1)$.

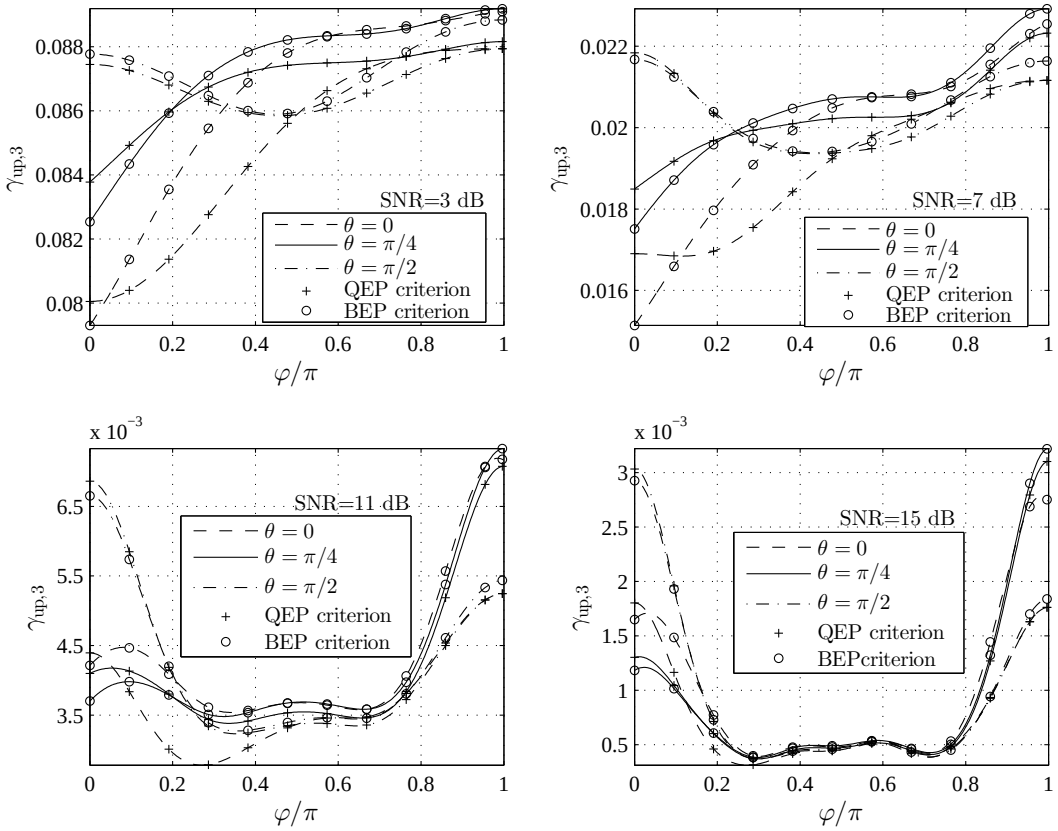

Figure 5.5 $\gamma_{\mathrm{up},3}$ versus φ for QPSK and at different SNR and θ values over Rician fading channels ($K_f = 10$).

Without loss of generality, the different label digit is assumed to be anywhere between the $(K+1)$th to the $(2K)$th positions. Then using $\boldsymbol{\Theta}_1$ and $\boldsymbol{\Theta}_2$ in (5.22) and defining $\alpha_1 = \mathrm{e}^{-j\frac{\pi}{4}}$ and $\alpha_2 = \mathrm{e}^{-j\frac{5\pi}{4}}$, one has

$$\begin{aligned} \boldsymbol{X}_g - \hat{\boldsymbol{X}}_g &= \frac{1}{\sqrt{2}} \begin{pmatrix} \alpha_1 \Delta s_1(2g) & \alpha_2 \Delta s_1(2g) \\ \alpha_1 \Delta s_2(2g) & \beta\alpha_2 \Delta s_2(2g) \end{pmatrix} \\ &= \frac{1}{\sqrt{2}} \begin{pmatrix} \Delta s_1(2g) & 0 \\ 0 & \Delta s_2(2g) \end{pmatrix} \begin{pmatrix} 1 & 1 \\ 1 & \beta \end{pmatrix} \begin{pmatrix} \alpha_1 & 0 \\ 0 & \alpha_2 \end{pmatrix} \end{aligned} \tag{5.29}$$

where $\Delta s_i(2g) = s_i(2g) - \hat{s}_i(2g)$. Lastly, from the definition of $\boldsymbol{D}_g$, $|\det(\boldsymbol{D}_g)|$ is computed as

$$|\det(\boldsymbol{D}_g)| = |\Delta s_1(2g)\Delta s_2(2g)|^2 \, |\beta - 1|^2 . \tag{5.30}$$

Because β is defined to have unity magnitude [64, 75], one concludes that $\beta = -1$ achieves the maximum $|\det(\boldsymbol{D}_g)|$ and thus the minimum QEP bound of BICM-ID.

Finally, the EF bound of BEP under network coding is examined. From the analysis of $\bar{\boldsymbol{\Psi}}^k_{\boldsymbol{X}_g}$ for BEP under network coding in Section 5.4, one can see that error events are all type-1 or type-2 errors. This means $\bar{\boldsymbol{\Psi}}^k_{\boldsymbol{X}_{g,3}}$ is an empty set. As an example, suppose that the label of $\boldsymbol{X}_g$ is [0 0 0 0]. Then the label set of $\bar{\boldsymbol{\Psi}}^1_{\boldsymbol{X}_g}$ consists of $\{[1\ 0\ 0\ 0], [2\ 0\ 0\ 0]\}$. If the label of $\hat{\boldsymbol{X}}_g$ is [1 0 0 0], one has $\boldsymbol{s}_{1,g} = \hat{\boldsymbol{s}}_{1,g}$, which means $\boldsymbol{X}_g \to \hat{\boldsymbol{X}}_g$ is a type-2 error. If label of $\hat{\boldsymbol{X}}_g$ is [2 0 0 0], one has $\boldsymbol{s}_{2,g} = \hat{\boldsymbol{s}}_2$, which means $\boldsymbol{X}_g \to \hat{\boldsymbol{X}}_g$ is a type-1 error. In addition, Theorem 1 proves that DLCP does not influence the PEP performance under type-1 and type-2 errors. Based on Theorem 1 and the fact that $\bar{\boldsymbol{\Psi}}^k_{\boldsymbol{X}_{g,3}}$ is an empty set, one concludes that there is no benefit in applying or designing DLCP for a TWRC system when BICM-ID is used and when the objective is to minimize the BEP under network coding. This is a major difference as compared to the case of BICM. In essence, in addition to channel fading, the MAI can also be effectively handled by BICM-ID under the error-free feedback assumption.

5.6 Simulation Results

This section provides various simulation results to evaluate the performance of different schemes and validate the analysis presented in the previous sections. In all simulations, all nodes use a rate-1/2, 4-state convolutional code with generator polynomials $\boldsymbol{g} = (5, 7)$ and random interleaver of length 512 bits. Both Rayleigh and Rician ($K_f = 10$) fading channels are simulated with unit variance ($\sigma_h^2 = 1$), i.e., the average power gains of all channels are unity.

5.6.1 TWRC with BICM

For the case of BICM, QPSK with Gray mapping [14] is adopted as the modulation format at all nodes. As for the precoder blocks in Fig. 5.1, four designs are considered: (i) No-DLCP, (ii) DLCP with $\varphi = 0$, (iii) DSTC in [39], and (iv) DLCP with optimal φ.

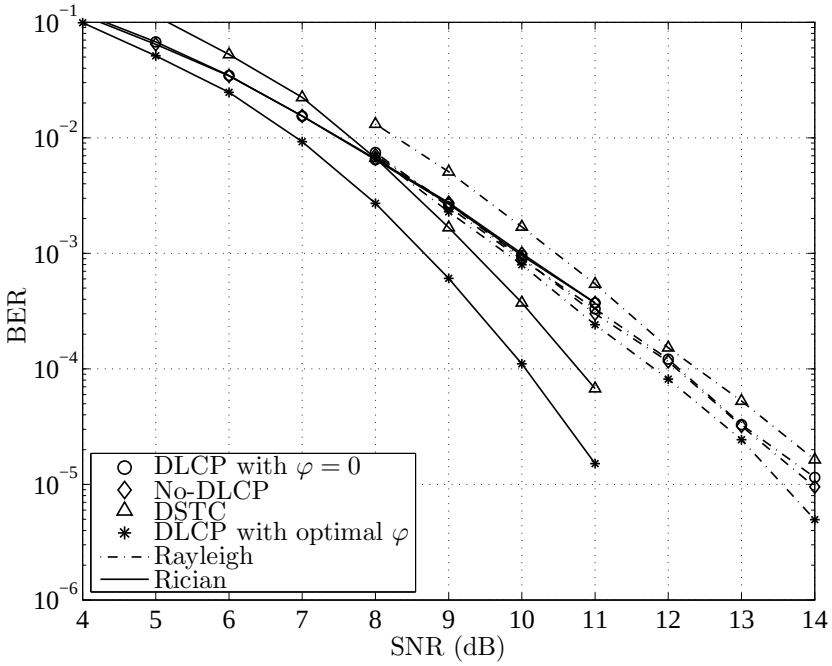

Figure 5.6 QER performance under Rayleigh and Rician fading channels.

Fig. 5.6 presents the quaternary-digit error rate (QER) performance under Rayleigh and Rician fading channels. It can be seen that in both cases of fading channels, $\varphi = 0$ yields the same QER performance as with "No-DLCP" design. This phenomenon is explained as follows. DLCP is designed to alleviate the influence of MAI by achieving cooperative diversity gain under type-3 errors. On the other hand, it is proved in [64] that using $\varphi = 0$ cannot obtain the cooperative diversity. Since DLCP does not affect the performance due to type-1 and type-2 errors as proved in Theorem 1, DLCP with $\varphi = 0$ has no performance advantage as compared to the "No-DLCP" scheme. To realize the performance advantage of DLCP, φ needs to be carefully selected.

From the QER results under Rayleigh fading channels, it can be seen that with high SNR values, the DLCP scheme with optimal φ achieves the best performance and clearly outperforms the scheme with $\varphi = 0$. With low and moderate SNR values, the DLCP scheme with optimal φ has similar performance compared to the scheme with $\varphi = 0$. The simulation results are consistent with Fig. 5.4 which shows in low and moderate SNR values, $\varphi = 0$ minimizes $\gamma_{\text{up},3}$.

For the QER results under Rician fading channels, the DLCP scheme with optimal φ achieves the best performance over the whole SNR region. It also results in a higher diversity gain over the "No-DLCP" scheme and the DLCP scheme with $\varphi = 0$ when compared to the case of Rayleigh fading. The reason for this is that under Rician fading, the probability of a deep fade is lower but the probability of experiencing MAI is the same as in the case of Rayleigh fading. In such a situation, type-3 errors become the dominant type of errors and the higher diversity gain under type-3 errors provided by DLCP can be seen clearer. The DSTC scheme can achieve the same diversity gain as the DLCP scheme with the optimal φ and therefore its performance curve has the same slope as that of the DLCP scheme with optimal φ. However, in the case of Rayleigh fading, type-3 errors are not the dominant errors since the probability of a deep fade is still high. The higher diversity gain under type-3 errors achieved by DSTC cannot effectively enhance the overall performance and in fact it performs even worse than the "No-DLCP" scheme as can be seen in performance curves under Rayleigh fading channels.

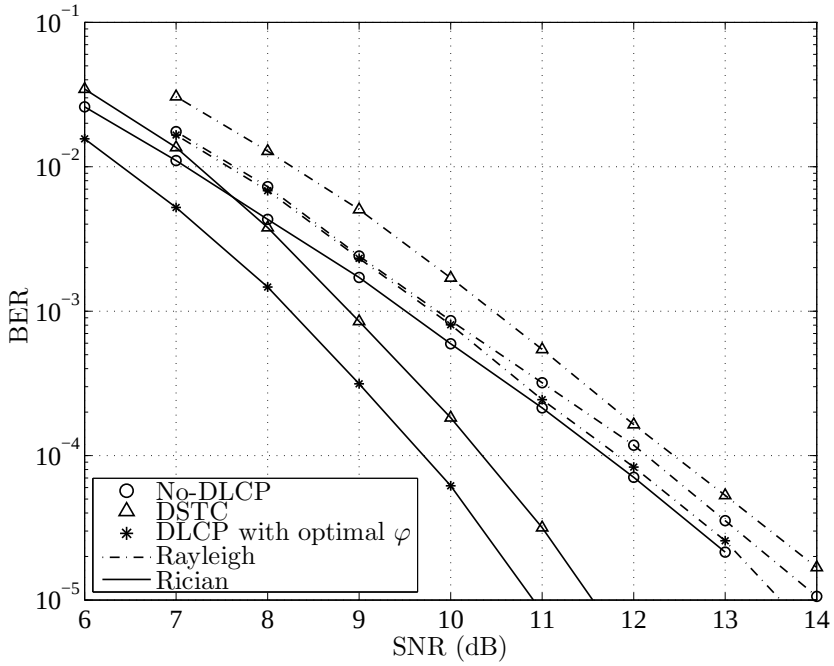

Figure 5.7 Terminal-to-terminal BER performance under Rayleigh and Rician ($K_f = 10$) fading channels.

Furthermore, the terminal-to-terminal bit error rate (BER) curves are plotted in Fig. 5.7,

which means that both MA and BC phases are included in the system simulation. As explained before, for the BC phase, the signal processing is the same as in the point-to-point communication system. For better clarity of different curves, since the DLCP scheme with $\varphi = 0$ has the same performance as the "No-DLCP" scheme, its performance is not explicitly included in the figure. It can be observed that all the BER performance curves have the same trend as QER performance curves investigated in the MA phase alone.

5.6.2 TWRC with BICM-ID

To achieve the performance gain through iterative decoding with BICM-ID, QPSK with anti-Gray mapping is adopted at all nodes. To evaluate the performance of BICM-ID in the MA phase of TWRC systems, the BER under network coding in the MA phase is plotted in Figs. 5.8 and 5.9 for Rayleigh and Rician ($K_f = 10$) fading channels, respectively. Two iterative decoding strategies are evaluated: (i) directly decoding the XOR code as given in [74], and (ii) decoding based on quaternary code representation as introduced in this paper. Specifically, shown in the figures are the BER curves after 1, 2, 3 and 9 iterations for both decoding strategies. From these two figures, it can be seen that iterative decoding using quaternary code representation significantly outperforms the direct decoding strategy. The reason is that the "XOR" method uses a reduced trellis[2] and therefore loses the useful information for decoding. This also explains why the "quaternary" decoding method obtains a larger gain through iterations than the "XOR" decoding method since the more useful information delivered in the iterations, the greater improvement can be obtained with iterative decoding.

To validate the conclusion in Section 5.5.2 that using BICM-ID can eliminate the influence of MAI on the BER under networking coding, and hence DLCP is not needed, four schemes are considered in the MA phase: (i) No-DSTC/DLCP, (ii) DSTC in [39], (iii) DLCP with optimal parameter for BICM, (iv) DLCP with $\beta = -1$ (recall that $\beta = -1$ minimizes the EF bound of QEP under BICM-ID). Fig. 5.10 presents the BER performance under network coding with 9 iterations under Rayleigh and Rician fading channels. For the all schemes

[2]The reduced trellis is shown in reference [68].

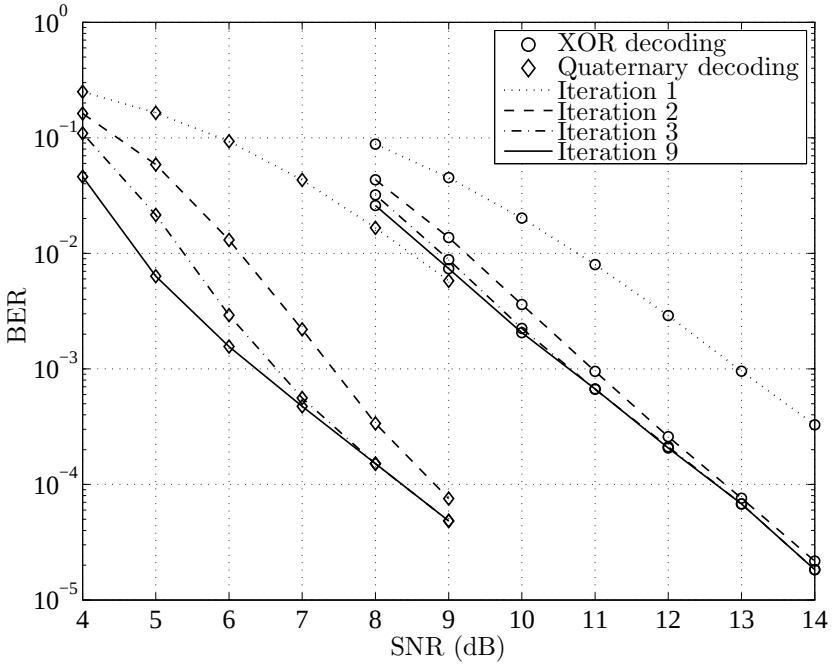

Figure 5.8 BER under XOR network coding with different iterations under Rayleigh fading channels.

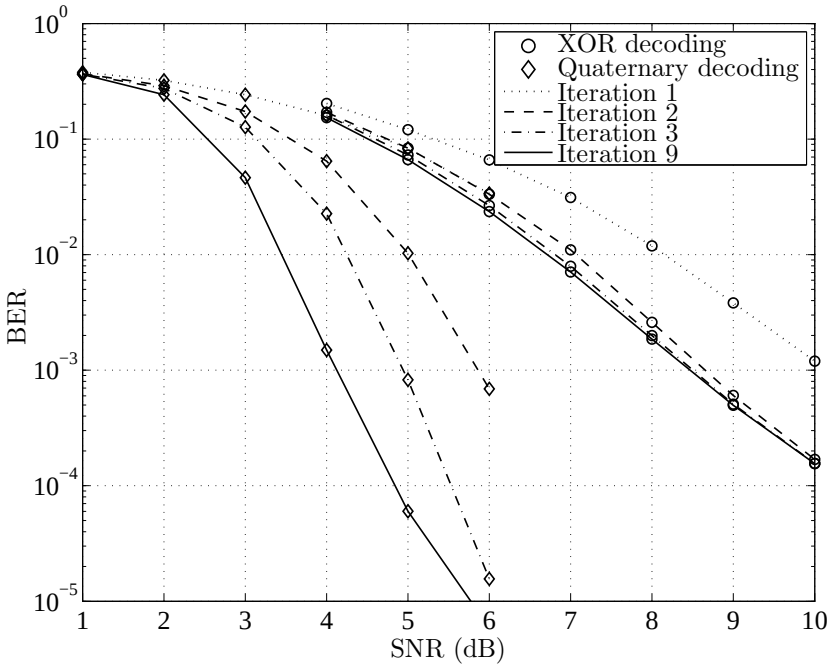

Figure 5.9 BER under XOR network coding with different iterations under Rician fading channels.

under Rician channels, they show different performance in the low SNR region but the same performance in the high SNR region. The reason is that in the low SNR region, a lot of feedback information in the iterative decoding process is erroneous and obviously the EF bound cannot be approached. But in the high SNR, through successful iterative decoding, the error-free assumption holds and the influence of MAI is eliminated and thus all schemes show the same performance. On the other hand, under Rayleigh channels, all schemes with 9 iterations show the same performance over the whole SNR region. As discussed in [64,75], fading is the more dominant factor causing errors than MAI. Therefore, in the low SNR region, although MAI is not totally eliminated, the probability of errors caused by MAI is much smaller than the probability of errors caused by fading so that it is negligible when evaluating the BER performance.

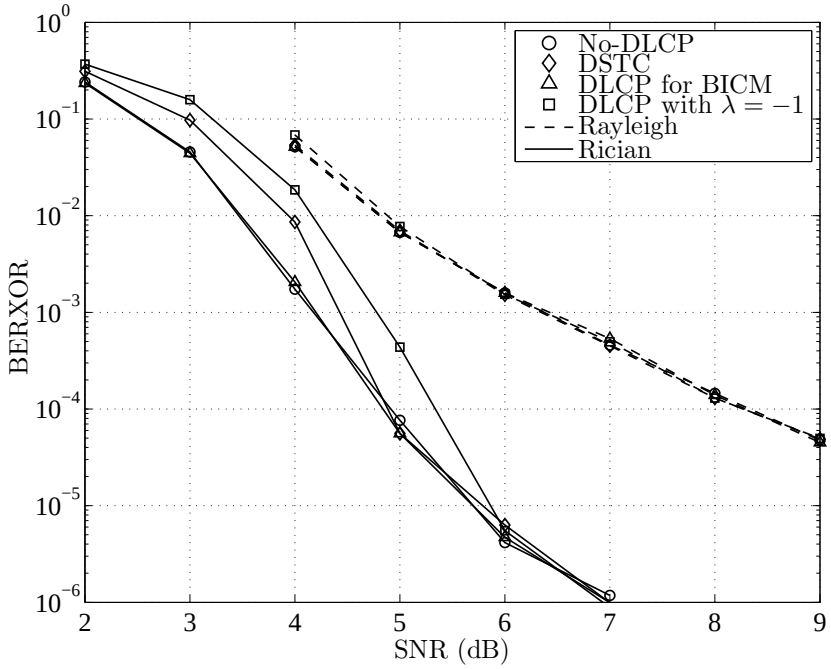

Figure 5.10 BER under XOR network coding for DLCP: Rayleigh and Rician fading channels.

For completeness, the QER of the four schemes under Rayleigh and Rician fading channels are also shown in Fig. 5.11. It is seen that all schemes have the same QER performance under Rayleigh fading channels, which validates the conclusion that after 9 iterations, the errors caused by MAI are eliminated. Under Rician fading channels, different schemes show

different performance in all SNR regions. The reason is that in Rician fading channels, even with successful iterative decoding in high SNR, MAI still impacts the QER performance. However, as shown in Section 5.5.2 using the EF bound, all the remaining errors caused by MAI can be eliminated through XOR-based network coding. As expected, in the high SNR region, the DLCP designed with $\beta = -1$ for BICM-ID achieves the best QER performance.

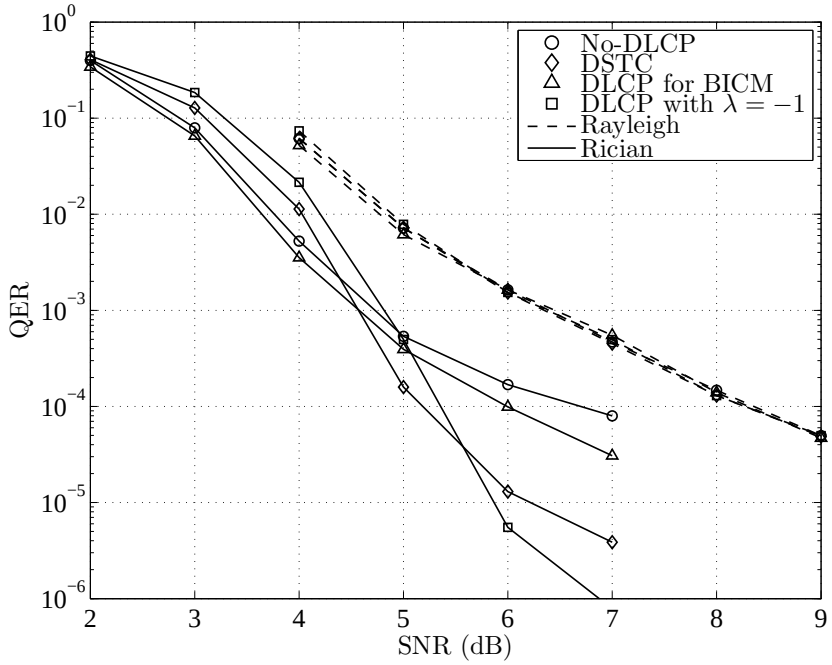

Figure 5.11 QER for DLCP under Rayleigh and Rician fading channels.

Finally, the terminal-to-terminal BER curves under Rayleigh and Rician fading channels are plotted in Fig. 5.12. For these simulation results, both the MA and BC phases are included and both phases adopt iterative decoding with 9 iterations. Five schemes are evaluated and compared, including four schemes using decoding with quaternary code representation and one with direct decoding of the XOR code. It can be observed that all the terminal-to-terminal BER performance curves have the same trend as the BER performance curves under network coding investigated in the MA phase alone. Specifically, all the schemes employing decoding based on quaternary code representation achieve much better performance than directly decoding the XOR version. Furthermore, with successful iterative decoding and XOR-based network coding, the influence of MAI is eliminated since all the schemes employing decoding based on quaternary code representation achieve the same

performance in high SNR region.

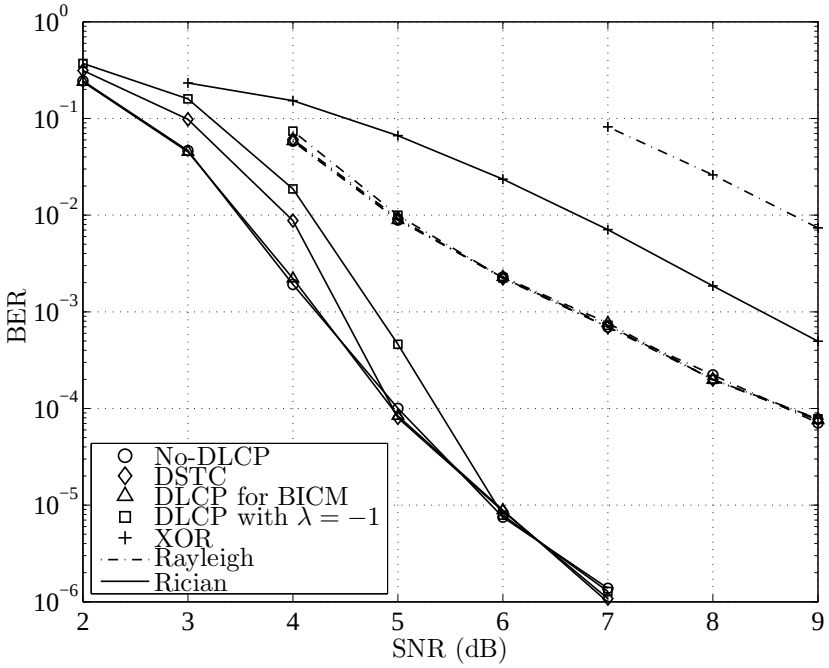

Figure 5.12 Terminal-to-terminal BER under Rayleigh and Rician fading channels.

5.7 Conclusions

The application of distributed linear constellation precoding (DLCP) in TWRC systems in conjunction with BICM and BICM-ID has been studied in this paper. An (iterative) decoding strategy based on quaternary code representation is developed for the multiple access phase. The union bounds and the EF bounds on the QEP and BEP under XOR-based network coding with BICM and BICM-ID are derived, respectively. Based on these bounds, performance metrics to search for the optimal parameters of DLCP are obtained. For the case of BICM, analysis and simulation results show that both the proposed decoding strategy and the properly-designed DLCP help to significantly improve the system performance. On the other hand, for the case of BICM-ID with enough iterations, analysis and simulation results demonstrate that there is no benefit to apply DLCP and the proposed decoding strategy combined with XOR network coding at the relay can successfully eliminate MAI in the MA phase of a TWRC system.

5.A Proof that $\gamma_{\text{up},3}$ is symmetric around $\varphi = \pi$

Theorem 1 shows that for type-1 and type-2 errors, all values of φ result in the same contribution to the upper bound of error probability. Therefore proving γ_{up} is symmetric around $\varphi = \pi$ is equivalent to proving $\gamma_{\text{up},3}$ is symmetric around $\varphi = \pi$. Since $\beta = \exp(j\varphi)$, the task is to show $\gamma_{\text{up}}(\beta) = \gamma_{\text{up}}(\beta^*)$. From (5.20), it can be observed that γ_{up} is the average of a set of PEP upper bounds $\zeta_{\text{up}}\left(\boldsymbol{X}_g \to \hat{\boldsymbol{X}}_g\right)$. Using the definition given in Section 5.2, each error event $\boldsymbol{X}_g \to \hat{\boldsymbol{X}}_g$ corresponds to $\boldsymbol{c}_{q,g} \to \hat{\boldsymbol{c}}_{q,g}$ where $\boldsymbol{X}_g$ and $\hat{\boldsymbol{X}}_g$ are 2×2 complex matrices and $\boldsymbol{c}_{q,g}$ and $\hat{\boldsymbol{c}}_{q,g}$ are vectors with $2K$ quaternary digits. For convenience, in the following, $\boldsymbol{c}_{q,g} \to \hat{\boldsymbol{c}}_{q,g}$ is used to denote an error event. By mapping the quaternary digits into binary vectors as:

$$0 \to \begin{pmatrix} 0 \\ 0 \end{pmatrix}, \quad 1 \to \begin{pmatrix} 0 \\ 1 \end{pmatrix}, \quad 2 \to \begin{pmatrix} 1 \\ 0 \end{pmatrix}, \quad 3 \to \begin{pmatrix} 1 \\ 1 \end{pmatrix}, \tag{5.31}$$

one can transfer $\boldsymbol{c}_{q,g}$ and $\hat{\boldsymbol{c}}_{q,g}$ into $2K \times 2$ matrices $\boldsymbol{C}_g$ and $\hat{\boldsymbol{C}}_g$, respectively. Let $\boldsymbol{S}_g = [\boldsymbol{s}_{1,g} \;\; \boldsymbol{s}_{2,g}]^T$ and $\hat{\boldsymbol{S}}_g = [\hat{\boldsymbol{s}}_{1,g} \;\; \hat{\boldsymbol{s}}_{2,g}]^T$ and obtain

$$\begin{aligned} \boldsymbol{S}_g(i,j) &= \mathcal{M}\left(\boldsymbol{C}(i,(j-1)K+1:jK)\right) \\ \hat{\boldsymbol{S}}_g(i,j) &= \mathcal{M}\left(\hat{\boldsymbol{C}}(i,(j-1)K+1:jK)\right) \end{aligned} \tag{5.32}$$

where $\mathcal{M}$ is a rule that maps K bits into a constellation symbol.

All error events $\boldsymbol{c}_{q,g} \to \hat{\boldsymbol{c}}_{q,g}$ can be categorized into two types:

(A) $\boldsymbol{c}_{q,g}$ and $\hat{\boldsymbol{c}}_{q,g}$ do not contain "1" or "2";

(B) In $\boldsymbol{c}_{q,g}$ and $\hat{\boldsymbol{c}}_{q,g}$, at least one of them contains "1" or "2".

For the type-A error events, the elements in the first row and second row of $\boldsymbol{C}_g$ and $\hat{\boldsymbol{C}}_g$ are identical: $\boldsymbol{C}_g(1,j) = \boldsymbol{C}_g(2,j)$ and $\hat{\boldsymbol{C}}_g(1,j) = \hat{\boldsymbol{C}}_g(2,j)$. Furthermore, since the same mapping rule is used, one has

$$\boldsymbol{S}_g(1,j) = \boldsymbol{S}_g(2,j), \quad \hat{\boldsymbol{S}}_g(1,j) = \hat{\boldsymbol{S}}_g(2,j). \tag{5.33}$$

By defining

$$\boldsymbol{y}_i = \begin{pmatrix} \boldsymbol{S}_g(i,1) - \hat{\boldsymbol{S}}_g(i,1) \\ \boldsymbol{S}_g(i,2) - \hat{\boldsymbol{S}}_g(i,2),\ i = 1,2 \end{pmatrix} \tag{5.34}$$

and using (5.33) one has

$$\boldsymbol{y}_1 = \boldsymbol{y}_2. \tag{5.35}$$

Define the vectors in the LCP matrix as:

$$\boldsymbol{\alpha}_1 = \frac{1}{\sqrt{2}} \begin{pmatrix} 1 & \mathrm{e}^{-j\frac{\pi}{4}} \end{pmatrix}, \quad \boldsymbol{\alpha}_2 = \frac{1}{\sqrt{2}} \begin{pmatrix} 1 & \mathrm{e}^{-j\frac{5\pi}{4}} \end{pmatrix}. \tag{5.36}$$

Then when parameter β is used in the design, the matrix $\boldsymbol{D}_g$ can be expressed as:

$$\boldsymbol{D}_g(\beta) = \begin{pmatrix} \boldsymbol{\alpha}_1\boldsymbol{y}_1 & \boldsymbol{\alpha}_2\boldsymbol{y}_1 \\ \boldsymbol{\alpha}_1\boldsymbol{y}_2 & \beta\boldsymbol{\alpha}_2\boldsymbol{y}_2 \end{pmatrix} \begin{pmatrix} \boldsymbol{y}_1^H\boldsymbol{\alpha}_1^H & \boldsymbol{y}_2^H\boldsymbol{\alpha}_1^H \\ \boldsymbol{y}_1^H\boldsymbol{\alpha}_2^H & \beta^*\boldsymbol{y}_2^H\boldsymbol{\alpha}_2^H \end{pmatrix}. \tag{5.37}$$

Using (5.35), $\boldsymbol{D}_g(\beta)$ becomes

$$\boldsymbol{D}_g(\beta) = \begin{pmatrix} |\boldsymbol{\alpha}_1\boldsymbol{y}_1|^2 + |\boldsymbol{\alpha}_2\boldsymbol{y}_1|^2 & |\boldsymbol{\alpha}_1\boldsymbol{y}_1|^2 + \beta^*|\boldsymbol{\alpha}_2\boldsymbol{y}_1|^2 \\ |\boldsymbol{\alpha}_1\boldsymbol{y}_1|^2 + \beta|\boldsymbol{\alpha}_2\boldsymbol{y}_1|^2 & |\boldsymbol{\alpha}_1\boldsymbol{y}_1|^2 + |\boldsymbol{\alpha}_2\boldsymbol{y}_1|^2 \end{pmatrix}. \tag{5.38}$$

For the same error event, if β^* is used in the design, the corresponding matrix is:

$$\boldsymbol{D}_g(\beta^*) = \begin{pmatrix} |\boldsymbol{\alpha}_1\boldsymbol{y}_1|^2 + |\boldsymbol{\alpha}_2\boldsymbol{y}_1|^2 & |\boldsymbol{\alpha}_1\boldsymbol{y}_1|^2 + \beta|\boldsymbol{\alpha}_2\boldsymbol{y}_1|^2 \\ |\boldsymbol{\alpha}_1\boldsymbol{y}_1|^2 + \beta^*|\boldsymbol{\alpha}_2\boldsymbol{y}_1|^2 & |\boldsymbol{\alpha}_1\boldsymbol{y}_1|^2 + |\boldsymbol{\alpha}_2\boldsymbol{y}_1|^2 \end{pmatrix}. \tag{5.39}$$

From (5.38) and (5.39) it can be seen that $\boldsymbol{D}_g(\beta^*) = \boldsymbol{D}_g^T(\beta)$. Therefore $\boldsymbol{D}_g(\beta^*)$ and $\boldsymbol{D}_g(\beta)$ have the same singular values. Referring to the derivations given in Section 5.4, one can conclude that if $\boldsymbol{c}_{q,g} \to \hat{\boldsymbol{c}}_{q,g}$ is a type-A error, using β or β^* achieves the same PEP upperbound: $\zeta_{\mathrm{up}}(\boldsymbol{c}_{q,g} \to \hat{\boldsymbol{c}}_{q,g}, \beta) = \zeta_{\mathrm{up}}(\boldsymbol{c}_{q,g} \to \hat{\boldsymbol{c}}_{q,g}, \beta^*)$.

Now, for each type-B error $\boldsymbol{c}_{q,g} \to \hat{\boldsymbol{c}}_{q,g}$, one can find one error in the set which is obtained by replacing "1" by "2" and "2" by "1" in both $\boldsymbol{c}_{q,g}$ and $\hat{\boldsymbol{c}}_{q,g}$. For example, if $\boldsymbol{c}_{q,g} = \begin{pmatrix} 1 & 1 & 3 & 2 \end{pmatrix}$ and $\hat{\boldsymbol{c}}_{q,g} = \begin{pmatrix} 2 & 1 & 2 & 0 \end{pmatrix}$, then the corresponding paired error is $\bar{\boldsymbol{c}}_{q,g} = \begin{pmatrix} 2 & 2 & 3 & 1 \end{pmatrix}$ and $\bar{\hat{\boldsymbol{c}}}_{q,g} = \begin{pmatrix} 1 & 2 & 1 & 0 \end{pmatrix}$. Then it follows that $\boldsymbol{C}_g(1,j) = \bar{\boldsymbol{C}}_g(2,j)$,

$\boldsymbol{C}_g(2,j) = \bar{\boldsymbol{C}}_g(1,j)$, $\hat{\boldsymbol{C}}_g(1,j) = \bar{\hat{\boldsymbol{C}}}_g(2,j)$ and $\hat{\boldsymbol{C}}_g(2,j) = \bar{\hat{\boldsymbol{C}}}_g(1,j)$. Using the definition in (5.34), one has

$$\boldsymbol{y}_1 = \bar{\boldsymbol{y}}_2, \quad \boldsymbol{y}_2 = \bar{\boldsymbol{y}}_1. \tag{5.40}$$

Then for error event $\boldsymbol{c}_{q,g} \to \hat{\boldsymbol{c}}_{q,g}$, if β is used, the matrix $\boldsymbol{D}_g$ is

$$\boldsymbol{D}_g(\beta) = \begin{pmatrix} |\boldsymbol{\alpha}_1\boldsymbol{y}_1|^2 + |\boldsymbol{\alpha}_2\boldsymbol{y}_1|^2 & \boldsymbol{\alpha}_1\boldsymbol{y}_1\boldsymbol{y}_2^H\boldsymbol{\alpha}_1^H + \beta^*\boldsymbol{\alpha}_2\boldsymbol{y}_1\boldsymbol{y}_2^H\boldsymbol{\alpha}_2^H \\ \boldsymbol{\alpha}_1\boldsymbol{y}_2\boldsymbol{y}_1^H\boldsymbol{\alpha}_1^H + \beta\boldsymbol{\alpha}_2\boldsymbol{y}_2\boldsymbol{y}_1^H\boldsymbol{\alpha}_2^H & |\boldsymbol{\alpha}_1\boldsymbol{y}_2|^2 + |\boldsymbol{\alpha}_2\boldsymbol{y}_2|^2 \end{pmatrix}. \tag{5.41}$$

On the other hand, for the error event $\bar{\boldsymbol{c}}_{q,g} \to \bar{\hat{\boldsymbol{c}}}_{q,g}$, using β^*, one has

$$\bar{\boldsymbol{D}}_g(\beta^*) = \begin{pmatrix} |\boldsymbol{\alpha}_1\boldsymbol{y}_2|^2 + |\boldsymbol{\alpha}_2\boldsymbol{y}_2|^2 & \boldsymbol{\alpha}_1\boldsymbol{y}_2\boldsymbol{y}_1^H\boldsymbol{\alpha}_1^H + \beta\boldsymbol{\alpha}_2\boldsymbol{y}_2\boldsymbol{y}_1^H\boldsymbol{\alpha}_2^H \\ \boldsymbol{\alpha}_1\boldsymbol{y}_1\boldsymbol{y}_2^H\boldsymbol{\alpha}_1^H + \beta^*\boldsymbol{\alpha}_2\boldsymbol{y}_1\boldsymbol{y}_2^H\boldsymbol{\alpha}_2^H & |\boldsymbol{\alpha}_1\boldsymbol{y}_1|^2 + |\boldsymbol{\alpha}_2\boldsymbol{y}_1|^2 \end{pmatrix}. \tag{5.42}$$

It can be observed that:

$$\bar{\boldsymbol{D}}_g(\beta^*) = \begin{pmatrix} 0 & 1 \\ 1 & 0 \end{pmatrix} \boldsymbol{D}_g(\beta) \begin{pmatrix} 0 & 1 \\ 1 & 0 \end{pmatrix}. \tag{5.43}$$

Therefore $\boldsymbol{D}_g(\beta^*)$ and $\bar{\boldsymbol{D}}_g(\beta^*)$ have the same singular values and thus one has $\zeta_{\text{up}}(\boldsymbol{c}_{q,g} \to \hat{\boldsymbol{c}}_{q,g}, \beta) = \zeta_{\text{up}}\left(\bar{\boldsymbol{c}}_{q,g} \to \bar{\hat{\boldsymbol{c}}}_{q,g}, \beta^*\right)$. Performing similar derivations, it can also be shown that $\zeta_{\text{up}}\left(\bar{\boldsymbol{c}}_{q,g} \to \bar{\hat{\boldsymbol{c}}}_{q,g}, \beta\right) = \zeta_{\text{up}}(\boldsymbol{c}_{q,g} \to \hat{\boldsymbol{c}}_{q,g}, \beta^*)$.

Since γ_{up} is obtained by averaging over all error events, combining the derivations for type-A and type-B errors, one can conclude that $\gamma_{\text{up}}(\beta) = \gamma_{\text{up}}(\beta^*)$.

6. Summary and Suggestions for Further Study

6.1 Summary

This thesis focuses on developing and analyzing several novel transmission and detection/decoding schemes to improve the performance of two-way relaying communication (TWRC) systems. Different from the conventional point-to-point communications, TWRC has to handle to the problem caused by multiple access interference in the MA phase. This is in addition to deal with familiar challenges such as fading and multipath dispersion faced in wireless communications. In particular, the studies in this thesis make the following contributions:

- In Chapter 3, a TWRC system with OFDM operating over multipath fading channels was studied. Adaptive PNC was investigated to handle the MAI problem. First, the error event in the MA phase was analyzed and approximations of the error probability under different channel fade states were given. It is well known that the OFDM technique can transform the (multipath) frequency-selective fading channel into a set of parallel flat fading channels. Since different parallel channels have different responses, implementing adaptive PNC may require a large overhead to convey the denoising maps in the BC phase. Based on the derived error probabilities, three methods were proposed to find a common denoising map for adaptive PNC with OFDM. Through simulation results and analysis, the method which achieves the best trade-off among performance, overhead and complexity was selected.

- In Chapter 4, the design of distributed precoding in TWRC using OFDM was studied. A general framework of a TWRC-OFDM system adopting distributed precoding was first developed and the corresponding error probability was analyzed. To aid in the design of pre-

coding, all error events were categorized into three types and it is pointed out that different types of error events were caused by different factors (fading, MAI). Conventional schemes, known as frequency-grouped linear constellation precoding (F-GLCP) and distributed space time coding (DSTC), were examined using the definitions of three types of errors. It was found that these two conventional schemes are not able to achieve the maximum diversity gains under type-3 errors. Based on the analysis, frequency-time grouped linear constellation precoding (FT-GLCP) was then proposed and demonstrated to achieve the maximum diversity gains under all three types of errors. Simulation results obtained under different fading channels verified the theoretical analysis and demonstrated the impressive performance advantage of the proposed FT-GLCP over other schemes.

- In Chapter 5, a TWRC system with BICM/BICM-ID using distributed linear constellation precoding (DLCP) was studied. First, the (iterative) decoding based on the quaternary code representation in the MA phase was developed. Different from the point-to-point communications, quaternary-digit error probability (QEP) and bit error probability (BEP) under network coding were used to evaluate the performance of BICM/BICM-ID in the MA phase of TWRC. DLCP was adopted in the MA phase to handle the MAI problem. Through analysis, the design problem was simplified to find the optimal parameter of DLCP. Two cases were analyzed: BICM without iterative decoding and BICM-ID with enough iterations and can be assumed to have error-free feedback. For BICM without iterative decoding, union bounds of QEP and BEP under network coding are used to search the optimal parameter. For BICM-ID, optimal parameter was derived using error free bound (EF bound) of QEP. By analyzing the EF bound of BEP under network coding, it was found that with successful iterative decoding and XOR-based network coding, MAI is eliminated in the MA phase of a TWRC system. Simulation results confirmed the optimality of the obtained parameter and validated the theoretical analysis.

6.2 Suggestions for Further Study

While conducting our research, a few issues arose and are worthwhile to be investigated further. They are elaborated next.

• As noted in Chapter 3, the large number of subcarriers in an OFDM system leads to a significant overhead when adaptive PNC is adopted in TWRC. In this thesis, one denoising map is proposed for all subcarriers to reduce the overhead. However, using one denoising map causes a large performance loss, especially for channels which have severe frequency selectivity. It is known that, compared to the number of subcarriers, the number of channel taps for a multipath channel is usually smaller and thus the channel responses on neighbouring subcarriers usually have a strong correlation. Therefore, utilizing the frequency correlation is a promising idea to reduce the overhead of adaptive PNC in a TWRC-OFDM system.

• The maximum likelihood (ML) criterion is used by the relay node for detection in the MA phase in this thesis. Although the ML detection achieves the best performance, it also requires a high computation complexity, especially when linear constellation precoding is adopted at the terminal nodes. Other non-linear detection schemes such as sphere decoding [77, 78] and linear detection schemes based on the minimum mean square error (MMSE) criterion [79, 79] can be used to lower the detection complexity. It is noted that since detection is conducted under the multiple access channel, the above mentioned low-complexity detection schemes cannot be directly applied but requires proper modifications and analysis.

• Quaternary code representation is used to decode the codeword over the multiple access channel in this thesis. In TWRC, another solution in coded system is to jointly design FEC code at the terminal nodes so that the relay is able to detect its linear combination [80, 81]. It is an interesting study to apply those jointly designed codes in BICM-ID system. Specifically, the iterative decoding process and design optimization for this joint code need further investigation in TWRC systems.

• In our research, it is assumed that the terminal nodes do not know the channel response between them and to the relay node. However, if the terminal nodes are fully aware of the channel sates in the system, pre-processing can be conducted to eliminate the multiple access interference. Under this circumstance, pre-processing designs under flat or frequency-selective fading channels, with or without FEC, are worthwhile to be studied.

References

[1] R. Pabst, B. H. Walke, D.C. Schultz, P. Herhold, H. Yanikomeroglu, S. Mukherjee, H. Viswanathan, M. Lott, W. Zirwas, M. Dohler, H. Aghvami, D. D. Falconer, and G. P. Fettweis, "Relay-based deployment concepts for wireless and mobile broadband radio," *IEEE Commun. Mag.*, vol. 42, pp. 80–89, Sept. 2004.

[2] Y. Yang, H. Hu, J. Xu, and G. Mao, "Relay technologies for WiMax LTE-advanced mobile system," *IEEE Commun. Mag.*, vol. 47, pp. 100–105, Oct. 2009.

[3] 3GPP TR 36.806, "Evolved Universal Terrestrial Radio Access (E-UTRA); Relay Architecture for E-UTRA (LTE-Advanced)," *http://www.3gpp.org*.

[4] IEEE 802.16j, "Part 16: Air interface for fixed and mobile broadband wireless access system: multihop relay specification," *http://www.ieee802.org/16/relay/*.

[5] L. Hanzo, W. Webb, and T. Keller, *Single and multi-carrier quadrature amplitude modulation - Principle and applications for personal communications, WLANs and broadcasting*, John Wiley & Sons, Ltd, 2000.

[6] B. Hirosaki, "An analysis of automatic equalizer for orthogonally multiplexed QAM system," *IEEE Trans. Commun.*, vol. 28, pp. 73–83, Jan. 1980.

[7] ETSN EN 302 755, "Frame structure channel coding and modulation for a second generation digital terrestrial television broadcasting system (DVB-T2)," *https://www.dvb.org/standards*.

[8] IEEE 802.11n Standard, "802.11n," *http://grouper.ieee.org/groups/802/11/*.

[9] 3GPP TS 36.211, "Techincal Specification Group Radio Access Network: Evolved Universal Terrestrial Radio Access (E-UTRA), Release 8," *http://www.3gpp.org*.

[10] Z. Liu, Y. Xin, and G. B. Giannakis, "Linear constellation precoding for OFDM with maximum multipath diversity and coding gains," *IEEE Trans. Commun.*, vol. 51, pp. 416–427, Mar. 2003.

[11] J. Tan and G. L. Stüber, "Multicarrier delay diversity modulation for MIMO systems," *IEEE Trans. on Wireless Commun.*, vol. 3, pp. 1756–1763, May 2004.

[12] Enis Akay and Ender Ayanoglu, "Achieving full frequency and space diversity in wireless system via BICM, OFDM, STBC and Viterbi decoding," *IEEE Trans. Commun.*, vol. 54, pp. 2164–2172, Dec. 2006.

[13] E. Zehavi, "8-PSK trellis codes for a Rayleigh channel," *IEEE Trans. Commun.*, vol. 40, pp. 873–884, May 1992.

[14] G. Caire, G. Taricco, and E. Biglieri, "Bit-interleaved coded modulation," *IEEE Trans. Inform. Theory*, vol. 44, pp. 927–946, May 1998.

[15] I. Lee, A. M. Chan, and C.-E. W. Sundberg, "Space-time bit-interleaved coded modulation for OFDM systems," *IEEE Trans. Signal Process.*, vol. 52, pp. 820–825, Mar. 2004.

[16] N. Gresset, J. J. Boutros, and L. Brunel, "Multidimensional mapping for iteratively decoding BICM on multiple-antenna channels," *IEEE Trans. Inform. Theory*, vol. 51, pp. 3337–3346, Sept. 2005.

[17] J. J. Boutros, F. Boixadera, and C. Lamy, "Bit-interleaved coded modulations for multiple-input multiple-output channels," in *Proc. IEEE Int. Symp. Inform. Theory*, Parsippany, NJ, USA, Sept. 2000, pp. 123–126.

[18] Xiaodong Li and James A. Ritcey, "Bit-iterative coded modulation with iterative decoding," *IEEE Commun. Letters*, vol. 1, pp. 169–171, Nov. 1997.

[19] P. Popovski and H. Yomo, "The anti-packets can increase the achievable throuput of a wireless multi-hop network," in *Proc. IEEE Int. Conf. Commun.*, Istanbul, Turkey, June 2006, pp. 3885–3890.

[20] T. Koike-Akino, P. Popovski, and V. Tarokh, "Optimized constellations for two-way wireless relaying with physical network coding," *IEEE J. Select. Areas in Commun.*, vol. 27, pp. 773–787, June 2009.

[21] Z. Chen, H. Liu, and W. Wang, "A novel decoding-and-forward scheme with joint modulation for two-way relay channel," *IEEE Commun. Letters*, vol. 12, pp. 1149–1151, Dec. 2010.

[22] T. Koike-Akino, P. Popovski, and V. Tarokh, "Adaptive network coding in two-way relaying mimo systems," in *Proc. IEEE Global Telecommun. Conf.*, miami, USA, dec 2010, pp. 1–5.

[23] T. T. Pham, Ha H. Nguyen, and H. D. Tuan, "Power allocation in orthogonal wireless relay networks with partial channel state information," *IEEE Trans. Signal Process.*, vol. 58, pp. 810–878, Feb. 2010.

[24] T. T. Pham, Ha H. Nguyen, and H. D. Tuan, "Power allocation in MMSE relaying over frequency-selective rayleigh fading channels," *IEEE Trans. Commun.*, vol. 58, pp. 3330–3343, Nov. 2010.

[25] Z. Han, X. Zhang, and H. Vicent Poor, "High performance cooperative transmission protocols based on multiuser detection and network coding," *IEEE Trans. Wireless Commun.*, vol. 8, pp. 2352–2361, May 2009.

[26] H. Zeng, Y. Shi, Y.T. Hou, and W. Lou, "An efficient DoF scheduling algorithm for multi-hop MIMO networks," in *Proc. IEEE Int. Conf. Computer Commun.*, Turin, Italy, Apr. 2013, pp. 1554–1564.

[27] H. Zeng, Y. Shi, Y. T. Hou, W. Lou, R. Zhu, and S. F. Midkiff, "A scheduling algorithm for MIMO DoF allocation in multi-hop networks," *IEEE Trans. on Mobile Computing.*, vol. 15, Mar. 2015.

[28] M. R. Avendi and Ha H. Nguyen, "Performance of selection combining for differential

amplify-and-forward relaying over time-varying channels," *IEEE Trans. on Wireless Commun.*, vol. 13, pp. 4156–4166, Aug. 2014.

[29] M. R. Avendi and Ha H. Nguyen, "Differential dual-hop relaying under user mobility," *IET Proceedings - Communications*, vol. 8, pp. 3161–3169, Aug. 2014.

[30] L. Li, Y. Jing, and H. Jafarkhani, "Interference Cancellation at the Relay for Multi-User Wireless Cooperative Networks," *IEEE Trans. Wireless Commun.*, vol. 10, pp. 930–939, 2011.

[31] D. Xu, Z. Bai, A. Waadt, G. H.Bruck, and P. Jung, "Combining MIMO with network coding: a viable means to provide multiplexing and diversity in wireless relay networks," in *Proc. IEEE Int. Conf. Commun.*, Cape Town, South Africa, May 2010, pp. 1–5.

[32] H. Gao, X. Su, T. Lv, and Z. Zhang, "Joint relay antenna selection and zero-forcing spatial multiplexing for MIMO two-way relay with physical-layer network coding," in *Proc. IEEE Global Telecommun. Conf.*, Houston, Texas, USA, Dec. 2011, pp. 1–6.

[33] H. Zeng, Y. Shi, Y. T. Hou, W. Lou, S. Kompella, and S. F. Midkiff, "An anlytical model for interference alignment in multi-hop MIMO networks," *IEEE Trans. on Mobile Computing.*, vol. 15, Mar. 2015.

[34] H. Zeng, Y. Shi, Y.T. Hou, W. Lou, S. Kompella, and S.F. Midkiff, "On interference alignment for multi-hop MIMo networks," in *Proc. IEEE Int. Conf. Computer Commun.*, Turin, Italy, Apr. 2013, pp. 1330–1338.

[35] T. Cui, F. Gao, T. Ho, and A. Nallanathan, "Distributed space-time coding for two-way wireless relay networks," *IEEE Trans. Signal Process.*, vol. 57, pp. 658–671, Feb. 2009.

[36] B. Rankov and A. Wittneben, "Spectral efficient protocols for half-duplex fading relay channels," *IEEE J. Select. Areas in Commun.*, vol. 25, pp. 379–389, Feb. 2007.

[37] S. Katti, H. Rahul, W. Hu, D. Katabi, M. Mëdard, and J. Crowcroft, "XORs in the Air: Practical Wireless Network coding," *IEEE/ACM Trans. Network.*, vol. 16, pp. 497–510, 2008.

[38] Vishnu Namboodiri Vijayvaradharaj T. Muralidharan and B. Sundar Rajan, "Wireless network-coded bidirectional relaying using latin squares for M-PSK modulation," *IEEE Trans. Inform. Theory*, vol. 59, pp. 6683–6711, Oct. 2013.

[39] V. T. Muralidharan and B. S. Rajan, "Distributed space time coding for wireless two-way relaying," *IEEE Trans. Signal Process.*, vol. 61, pp. 980–991, Feb. 2013.

[40] J. Boutros and E. Viterbo, "Signal space diversity: A power and bandwidth efficient diversity technique for the Rayleigh fading channel," *IEEE Trans. Inform. Theory*, vol. 44, pp. 1453–1467, July 1998.

[41] X. Giraud, E. Boutillon, and J.C. Belfiore, "Algebraic tools to build modulation schemes for fading channels," *IEEE Trans. Inform. Theory*, vol. 43, pp. 938–952, May 1997.

[42] V. Tarokh, N. Seshadri, and A. R. Calderbank, "Space-time codes for high data rate wireless communication: Performance criterion and code construction," *IEEE Trans. Inform. Theory*, vol. 44, pp. 744–765, Mar. 1998.

[43] S. Benedetto, D. Divsalar, G. Montorsi, and F. Pollara, "A soft-input soft-output APP module for iterative decoding of concatenated codes," *IEEE Commun. Letters*, vol. 1, pp. 22–24, Jan. 1997.

[44] Aik Chindapol and James A. Ritcey, "Design, analysis, and performance evaluation for BICM-ID with square QAM constellation in Rayleigh fading channels," *IEEE J. Select. Areas in Commun.*, vol. 19, pp. 944–957, May 2001.

[45] Nghi H. Tran, Ha H. Nguyen, and Tho Le-Ngoc, "Performance of BICM-ID with signal space diversity," *IEEE Trans. on Wireless Commun.*, vol. 6, pp. 1732–1742, May 2007.

[46] P. Popovski and H. Yomo, "Bi-directional amplification of throughput in a wireless multi-hop network," in *Proc. IEEE Veh. Technol. Conf.*, Melbourne, Australia, May 2006, pp. 588–593.

[47] S. Zhang, S.-C Liew, and P.P. Lam, "Hot topic: Physical-layer network coding," in *Proc. IEEE MobiComm'06*, Los Angeles, USA, Sept. 2006, pp. 358–369.

[48] S. Katti, S. Gollakota, and D. Katabi, "Embracing wireless interference: Analog network coding," in *Proc. ACM SIGCOMM'07*, Kyoto, Japan, Aug. 2007, pp. 397–408.

[49] V. Namboodiri, V. T. Muralidharan, and B. S. Rajan, "Wireless birectional relaying and latin squares," in *Proc. IEEE Wireless Commun. and Networking. Conf.*, Paris, France, Apr. 2012, pp. 1404–1409.

[50] V. T. Muralidharan, V. Namboodiri, and B. S. Rajan, "Channel quantization for physical layer network-coded two-way relaying," in *Proc. IEEE Wireless Commun. and Networking. Conf.*, Paris, France, Apr. 2012, pp. 1654–1659.

[51] V. T. Muralidharan and B. S. Rajan, "Performance analysis of adaptive physical layer network coding for wireless two-way relaying," *IEEE Trans. on Wireless Commun.*, vol. 12, pp. 1328–1339, Mar. 2013.

[52] Andrea Goldsmith, *Wireless Communications*, Cambridge University Press, 2005.

[53] S. J. Kim, P. Mitran, and V. Tarokh, "Performance bounds for bidirectional coded cooperation protocols," *IEEE Trans. Inform. Theory*, vol. 54, pp. 5235–5241, Nov. 2008.

[54] P. Popovski and H. Yomo, "Physical network coding in two-way wireless relay channels," in *Proc. IEEE Int. Conf. Commun.*, Glasgow, Scotland, 2007, pp. 707–712.

[55] R. Ahlswede, N. Cai, S. Y. R. Li, and R. W. Yeung, "Netwrok information flow," *IEEE Trans. Inform. Theory*, vol. 46, pp. 1204–1216, July 2000.

[56] Hongzhong Yan and Ha H. Nguyen, "Adaptive physical-layer network coding in two-way relaying with OFDM," in *Proc. IEEE Global Telecommun. Conf.*, Atlanta, GA, USA, Dec. 2013, pp. 4349–4354.

[57] W. Zou and Y. Wu, "COFDM: an overview," *IEEE Trans. Broadcast.*, vol. 41, pp. 1–8, Mar. 2003.

[58] N. H. Tran, H. H. Nguyen, and T. Le-Ngoc, "Subcarrier grouping for OFDM with linear constellation precoding over multipath fading channels," *IEEE Trans. Veh. Technol.*, vol. 56, pp. 3607–3613, Nov. 2007.

[59] R.G. Gallager, "A perspective on multiaccess channels," *IEEE Trans. Inform. Theory*, vol. 31, pp. 124–142, Mar. 1985.

[60] M. Gartner and H. Bolcskei, "Multiuser space-time/frequency code design," in *Proc. IEEE Int. Symp. Inform. Theory*, Seattle, USA, July 2006, pp. 2819–2823.

[61] Roger A. Horn and Charles R. Johnson, *Matrix Analysis*, Cambridge University Press, 1999.

[62] M. O. Damen, A. Tewfik, and J.-C. Belfiore, "A construction of a space-time code based on number theory," *IEEE Trans. Inform. Theory*, vol. 48, pp. 753–760, Mar. 2002.

[63] A. Berman and N. Shaked-Monderer, *Completely Positive Matrices*, World Scientific, Singapore, 2003.

[64] Hongzhong Yan, Ha H. Nguyen, and Jian Su, "Distributed precoding for OFDM in two-way relaying communications," *IEEE Trans. Veh. Technol.*, vol. 64, pp. 1930–1941, May 2015.

[65] Shengli Zhang and Soung-Chang Liew, "Channel coding and decoding in a relay system operated with physical-layer network coding," *IEEE J. Select. Areas in Commun.*, vol. 27, pp. 788–796, 2009.

[66] Tao Yang, Tao Huang, Jinhong Yuan, and Zhuo Chen, "Distance spectrum and performance of channel-coded physical-layer network coding for binary-input Gaussian two-way relay channels," *IEEE Trans. Commun.*, vol. 60, pp. 1499–1510, May 2012.

[67] D. Wübben and L. Dong, "Generalized sum-product algorithm for joint channel decoding and physical-layer network coding in two-way relay system," in *Proc. IEEE Global Telecommun. Conf.*, Miami, FL, USA, Dec. 2010, pp. 1–5.

[68] D. To and J. Choi, "Convolutional codes in two-way relay networks with physical-layer network coding," *IEEE Trans. on Wireless Commun.*, vol. 9, pp. 2724–2729, Sept. 2010.

[69] Maria Cláudia Castro, Bartolomeu F. Uchôa-Filho, Tiago T. V. Vinhoza, Mario Noronha-Neto, and Joao Barros, "Improved joint turbo decoding and physical-layer network coding," in *IEEE Information Theory Workshop*, Lausanne, Switzerland, Sept. 2012, pp. 532–536.

[70] T. Koike-Akino, P. Popovski, and V. Tarokh, "Denoising strategy for convolutionally-coded bidirectional relaying," in *Proc. IEEE Int. Conf. Commun.*, Dresden, Germany, June 2009, pp. 1–5.

[71] Jianquan Liu, Meixia Tao, and Youyun Xu, "Pairwise check decoding for LDPC coded two-way relay block fading channels," *IEEE Trans. Commun.*, vol. 60, pp. 2065–2076, Aug. 2012.

[72] Xiaodong Li, Aik Chindapol, and James A. Ritcey, "Bit-interleaved coded modulation with iterative decoding and 8PSK signaling," *IEEE Trans. Commun.*, vol. 50, pp. 1250–1257, Aug. 2002.

[73] Ao Zhan, Chen He, and Lingge Jiang, "A turbo-BICM based scheme for joint network coding and channel coding," in *Proc. IEEE Int. Conf. Commun.*, Capetown, South Africa, May 2010, pp. 1–5.

[74] Terry Ferrett, Matthew C. Valenti, and Don Torrieri, "An iterative noncoherent relay receiver for the two-way relay channel," in *Proc. IEEE Int. Conf. Commun.*, Budapest, Hungary, June 2013, pp. 5903–5908.

[75] Hongzhong Yan and Ha H. Nguyen, "Distributed space time coding for bit-interleaved coded modulation in two-way relaying communications," in *Proc. IEEE Global Telecommun. Conf.*, San Diego, CA, USA, Dec. 2015.

[76] Yan Xin, Zhengdao Wang, and Georgios B. Giannakis, "Space-time diversity systems

based on linear constellation precoding," *IEEE Trans. on Wireless Commun.*, vol. 2, pp. 294–309, Mar. 2003.

[77] H. Vikalo and B. Hassibi, "On the sphere-decoding algorithm ii. generalizations, second-order statistics, and applications to communications," *IEEE Trans. Signal Process.*, vol. 53, pp. 2819–2834, Aug. 2005.

[78] O. Damen, A. Chkeif, and J. C. Belfiore, "Lattice code decoder for space-time codes," *IEEE Commun. Letters*, vol. 4, pp. 161–163, May 2000.

[79] Ping Li, "Approximate MMSE-APP estimation for linear systems with binary inputs," *IEEE Commun. Letters*, vol. 9, pp. 172–174, Feb. 2005.

[80] O. Ordentlich, U. Erez, and B. Nazer, "The compute-and-forward transform," in *Proc. IEEE Int. Symp. Inform. Theory*, Cambridge, MA, USA, July 2012, pp. 3008–3012.

[81] B. Nazer and M. Gastpar, "Computation over multiple-access channels," *IEEE Trans. Inform. Theory*, vol. 53, pp. 3498–3516, Oct. 2007.